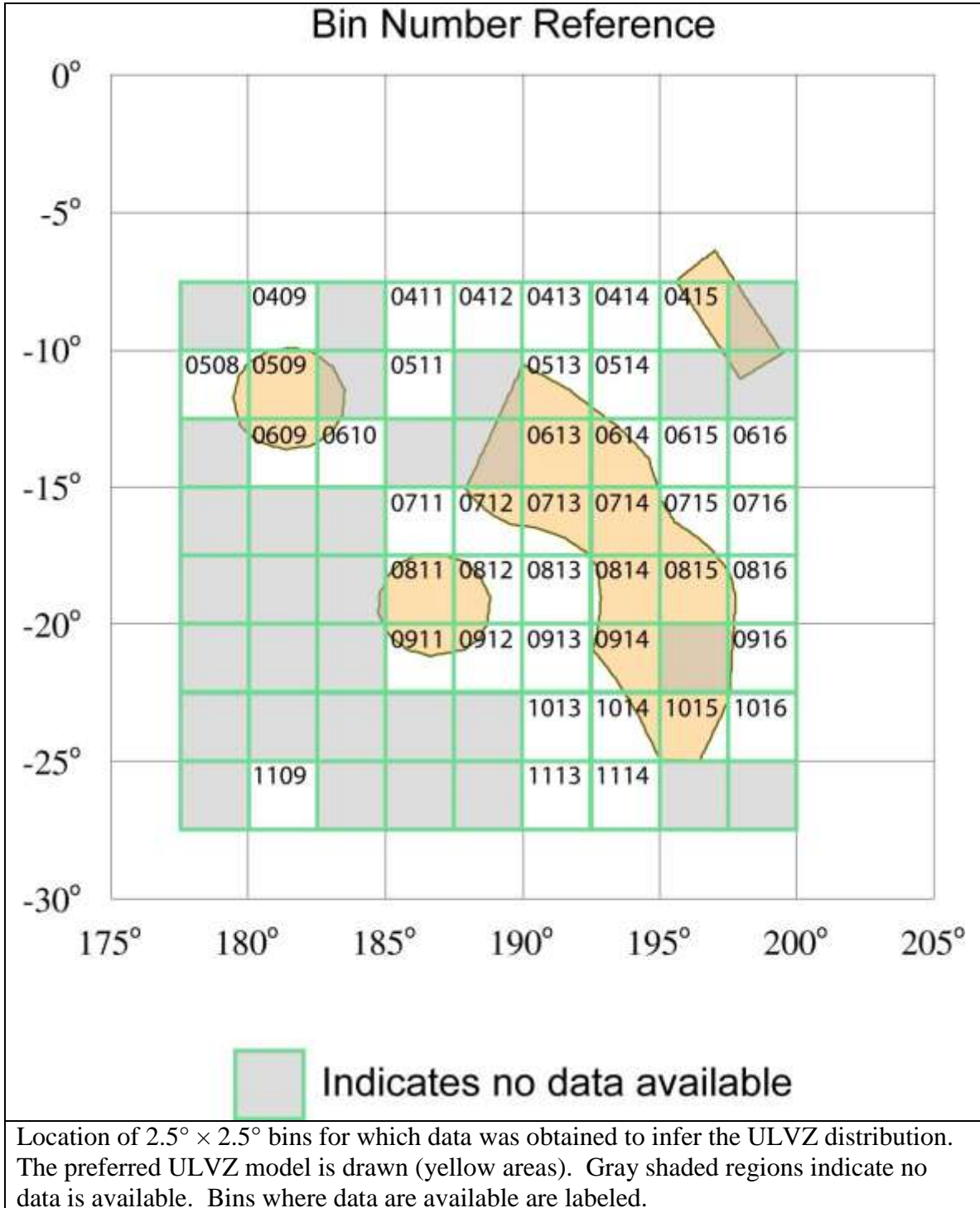


Supplementary Material

S1. Bin Location Map



S2. Data

The following plots contain show data used in this study for the numbered bins on the previous page. Each plot contains up to 5 figures as explained below:

(a) Data and Stacks. Data used in this study are shown as gray traces. These traces are all Radial component displacement seismograms aligned and normalized to unity on the SKS arrival. The PREM predicted arrival time for the SPdKS phase is shown. For comparison with synthetic seismograms data stacks are drawn with the heavy red line.

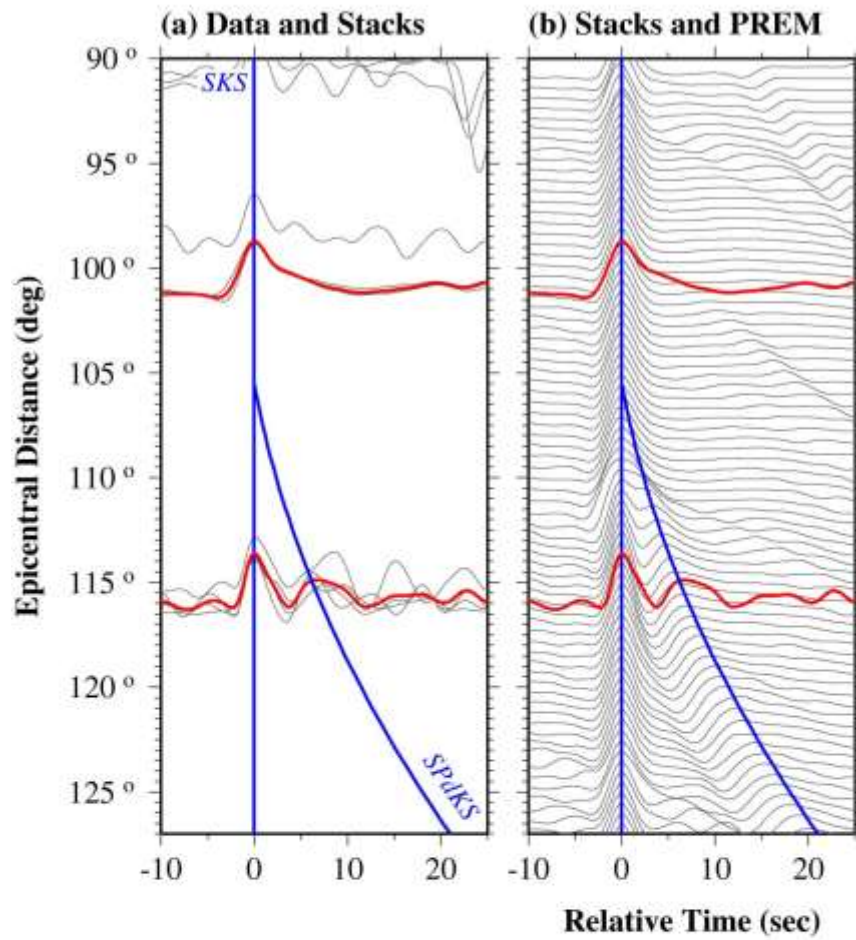
(b) Stacks and PREM. The gray traces show synthetic seismograms calculated for the PREM model. These synthetics are overlain with the stacked data (red traces).

(c) Stacks and ULVZ. The gray traces show synthetic seismograms calculated for the best-fit ULVZ model. These synthetics are overlain with the stacked data (red traces). Note: Panel (c) is not shown for bins where the data are indistinguishable from the PREM model.

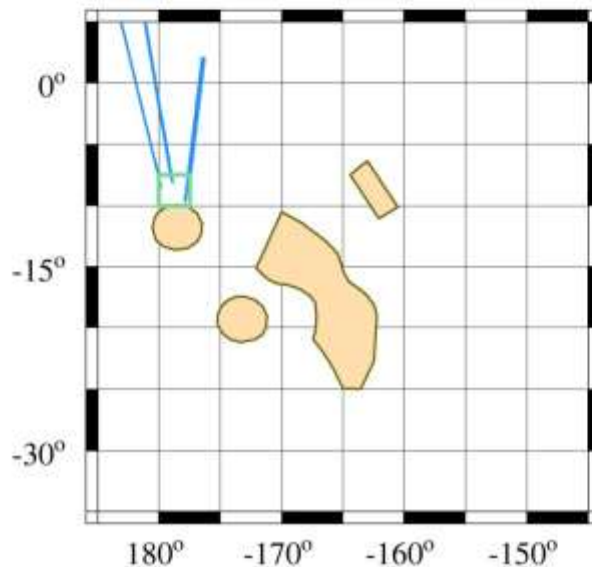
(d) Pd-Rays and Bin Location. Map showing the geographic location of the bin (green box), preferred ULVZ model (yellow regions) and the Pdiff portion of SPdKS on the CMB (blue lines).

(e) ULVZ Model Cross-Section. Shown is the cross-sectional view of the best-fit ULVZ model for the data bin. The ULVZ position and size are shown by the gray box. Ray paths for the SKS (blue) and SPdKS (red) seismic phases are drawn for an epicentral distance of 109° . Directly above the plot the parameters of the best-fit ULVZ model are displayed (i.e., δV_S , δV_P , $\delta \rho$, thickness - h , length, and edge position). Panel (e) is not shown for bins where the data are indistinguishable from the PREM model.

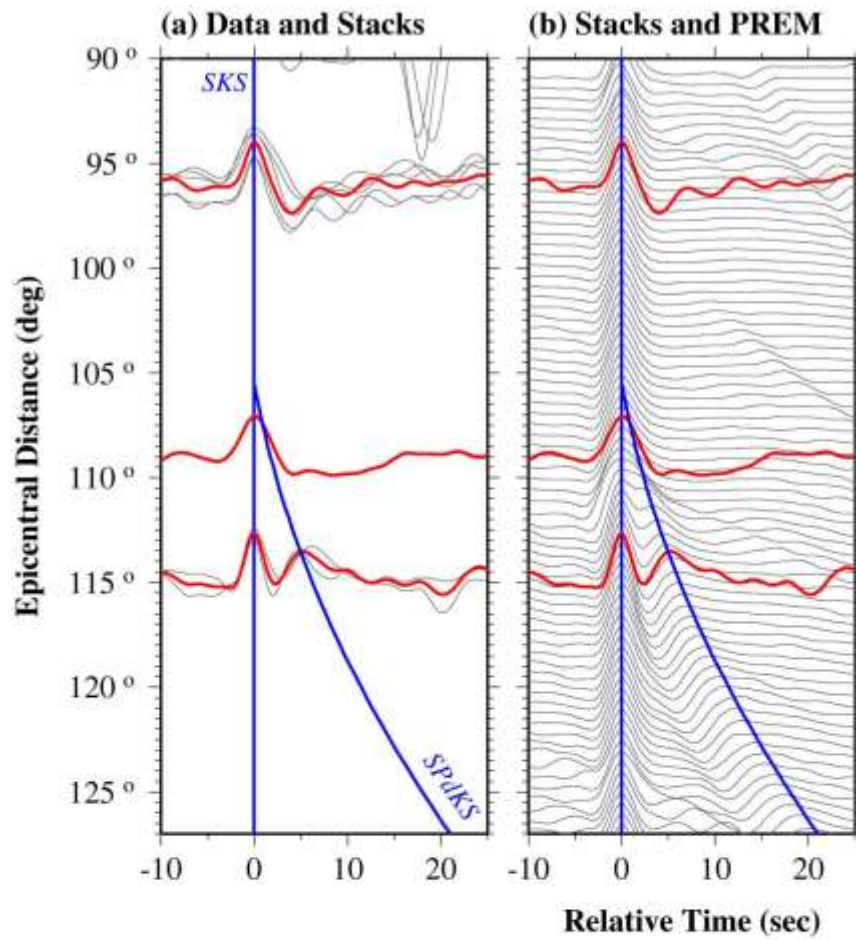
Bin: 0409
Bin Center: Lon= 181.25° Lat=-8.75°



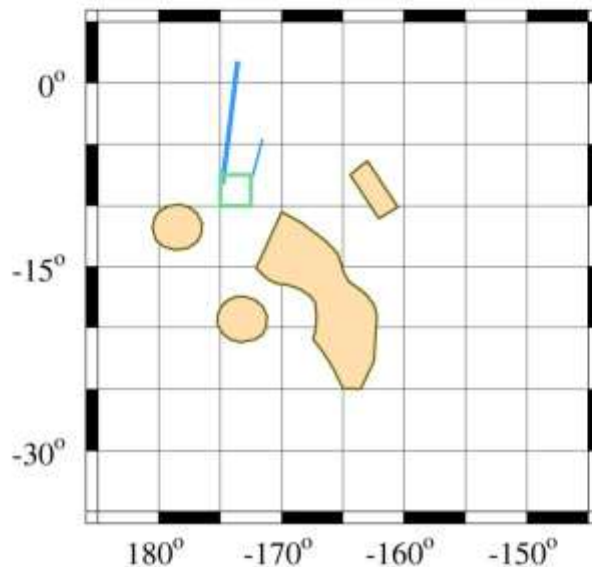
(d) Pd-Rays and Bin Location



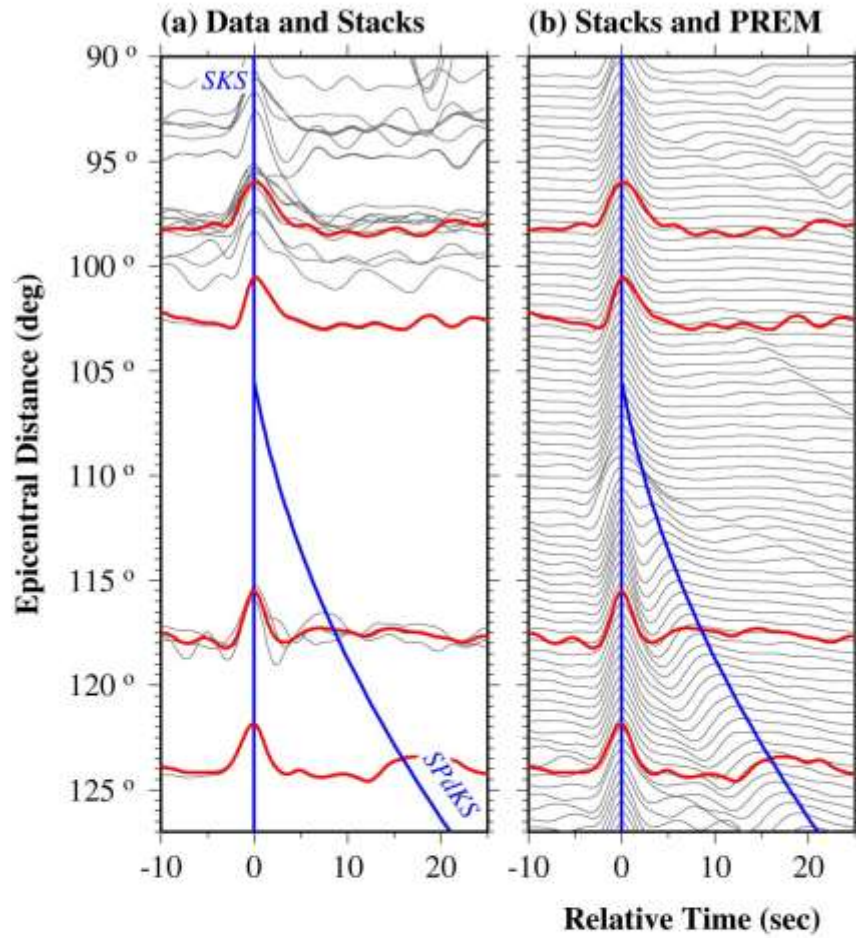
Bin: 0411
Bin Center: Lon= 186.25° Lat=-8.75°



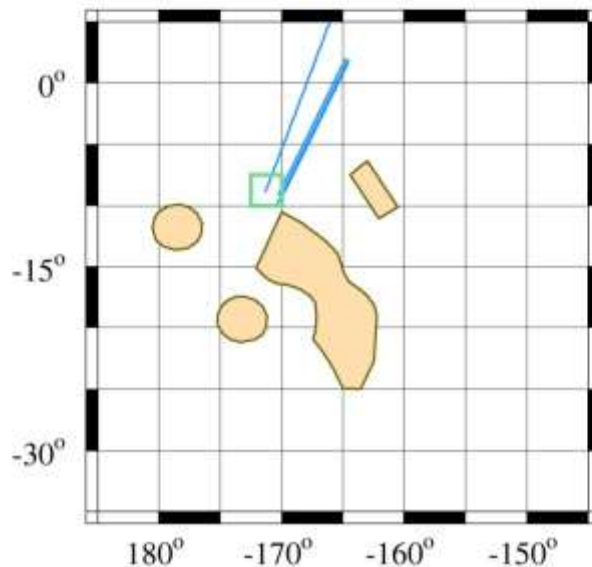
(d) Pd-Rays and Bin Location



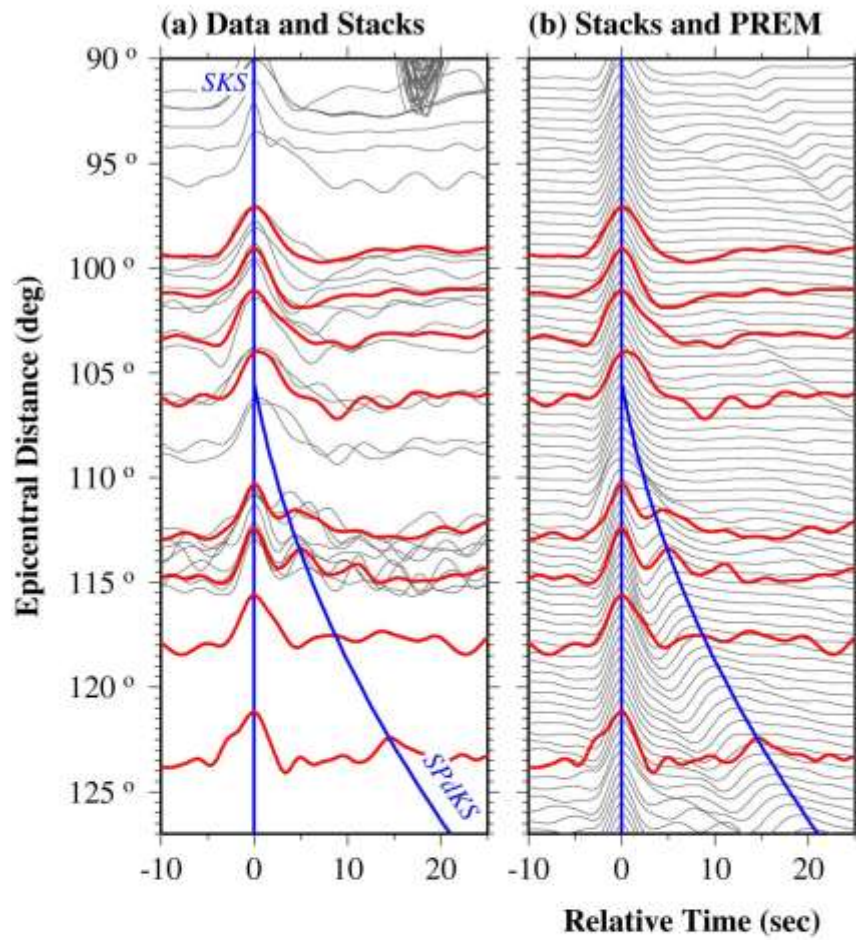
Bin: 0412
Bin Center: Lon= 188.75° Lat=-8.75°



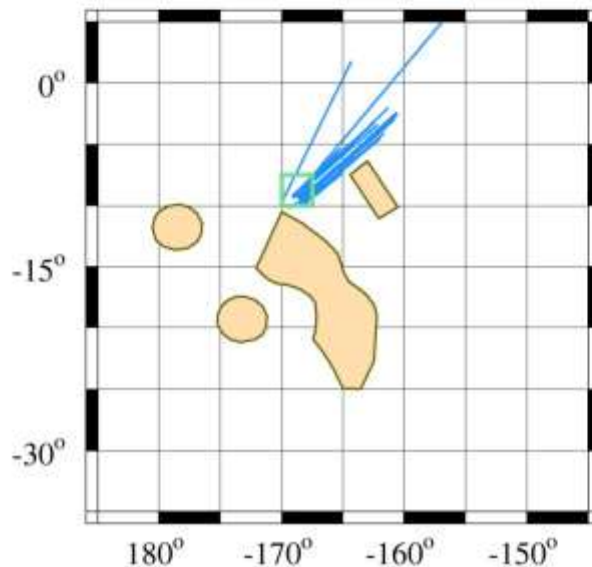
(d) Pd-Rays and Bin Location



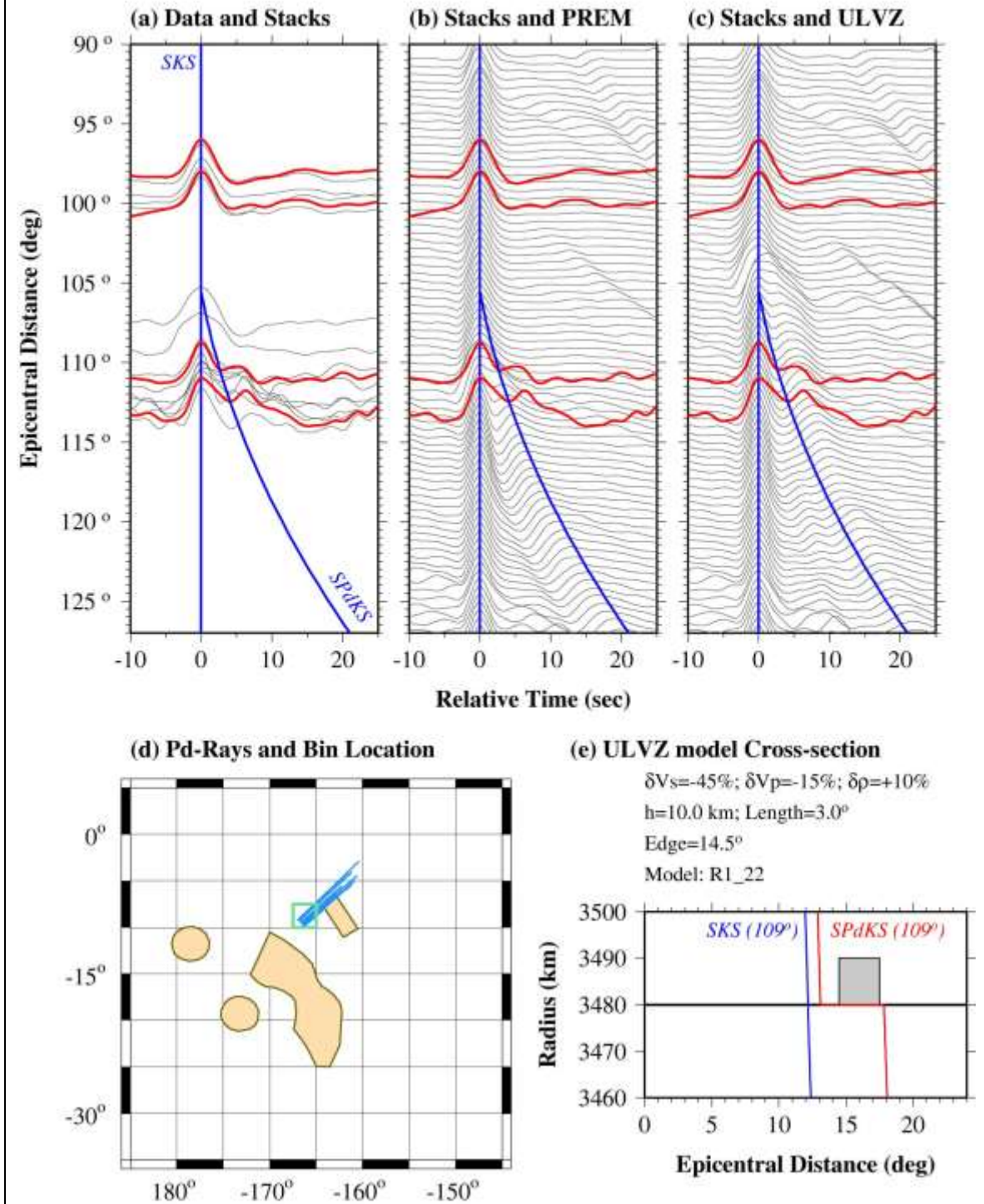
Bin: 0413
Bin Center: Lon= 191.25° Lat=-8.75°



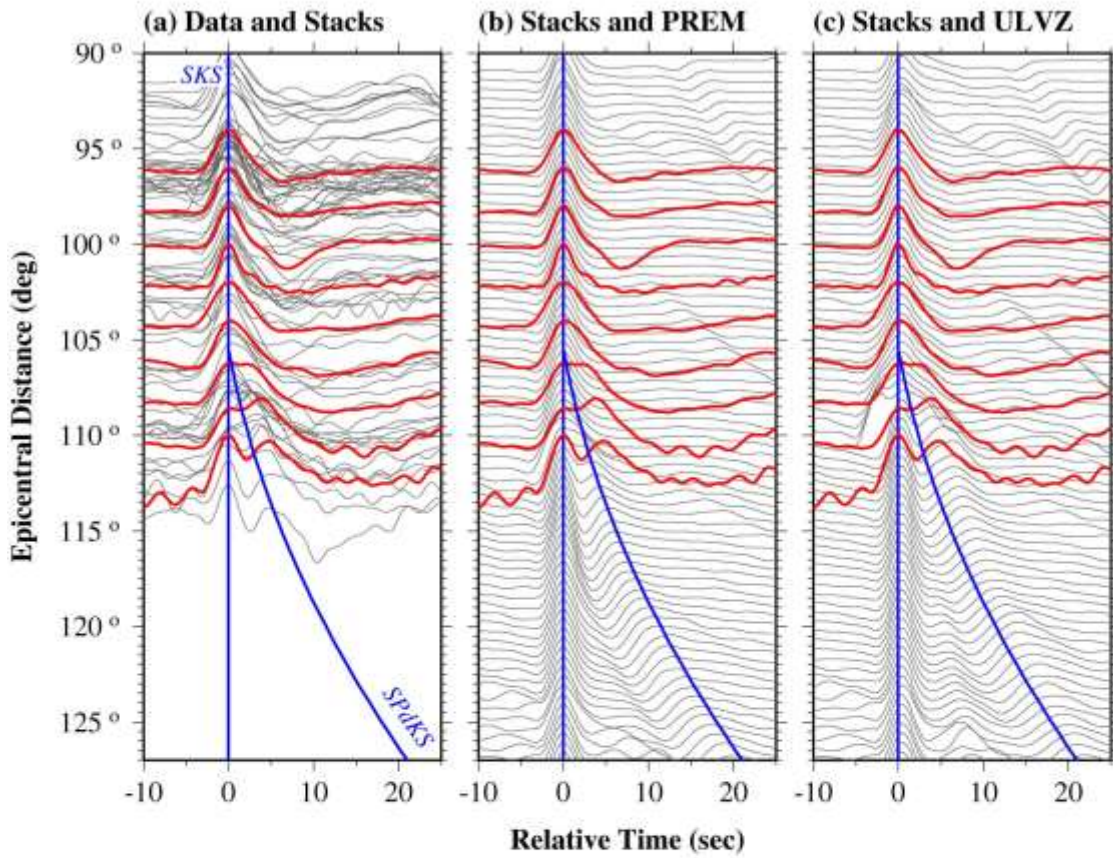
(d) Pd-Rays and Bin Location



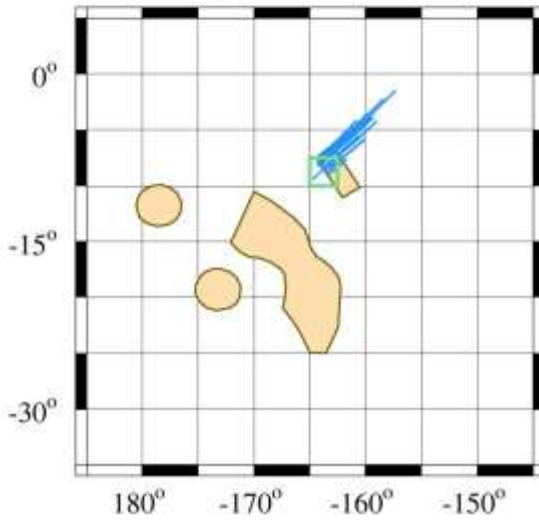
Bin: 0414
Bin Center: Lon= 193.75° Lat=-8.75°



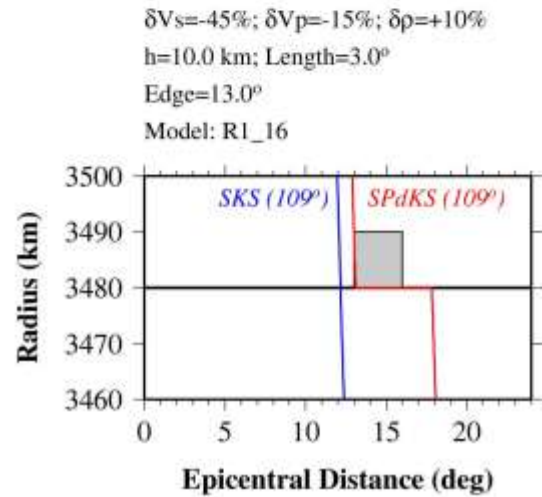
Bin: 0415
Bin Center: Lon= 196.25° Lat=-8.75°



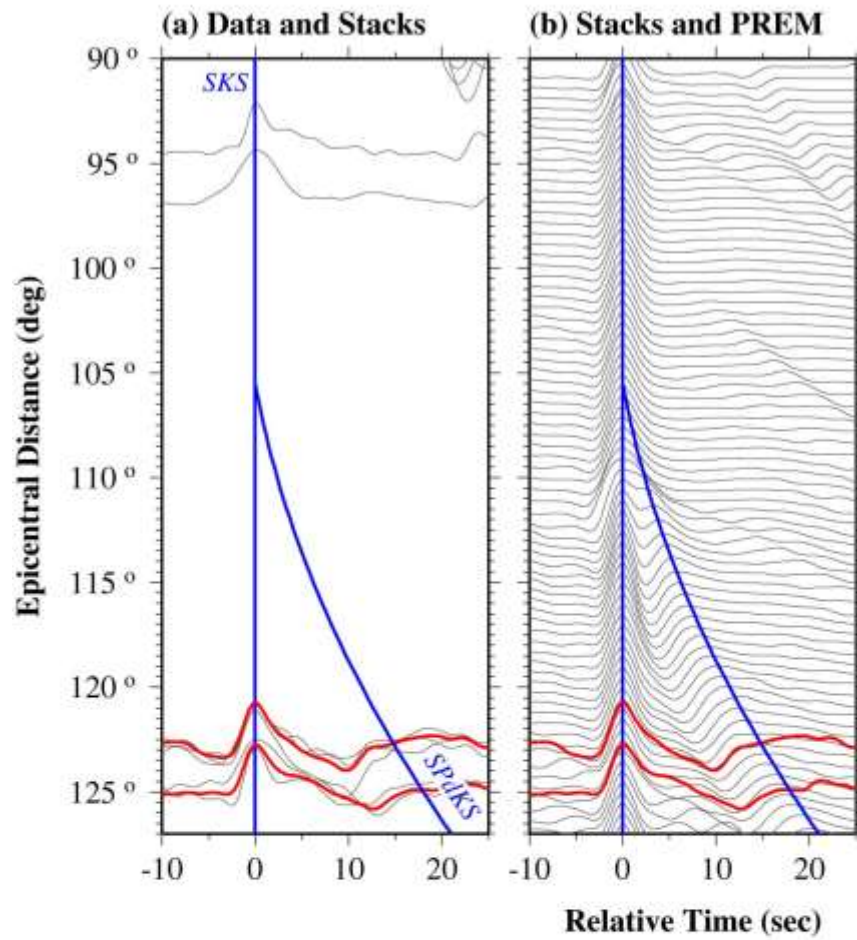
(d) Pd-Rays and Bin Location



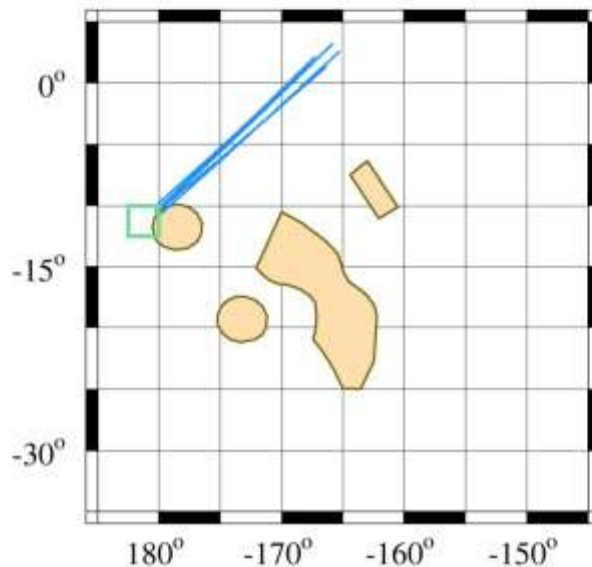
(e) ULVZ model Cross-section



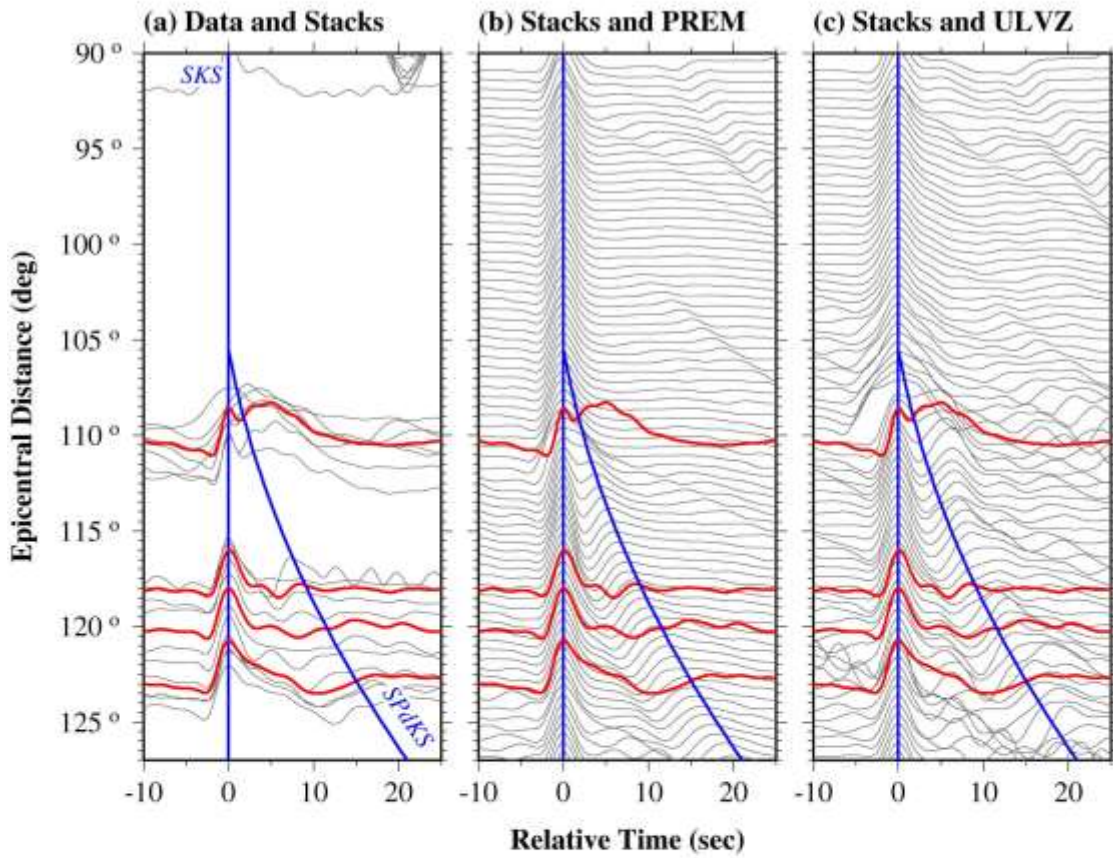
Bin: 0508
Bin Center: Lon= 178.75° Lat=-11.25°



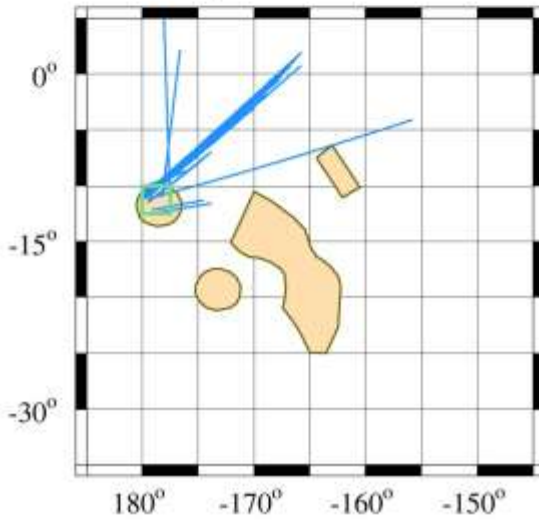
(d) Pd-Rays and Bin Location



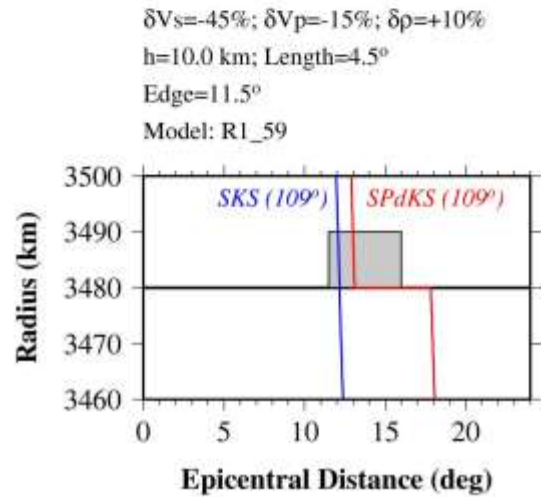
Bin: 0509
Bin Center: Lon= 181.25° Lat=-11.25°



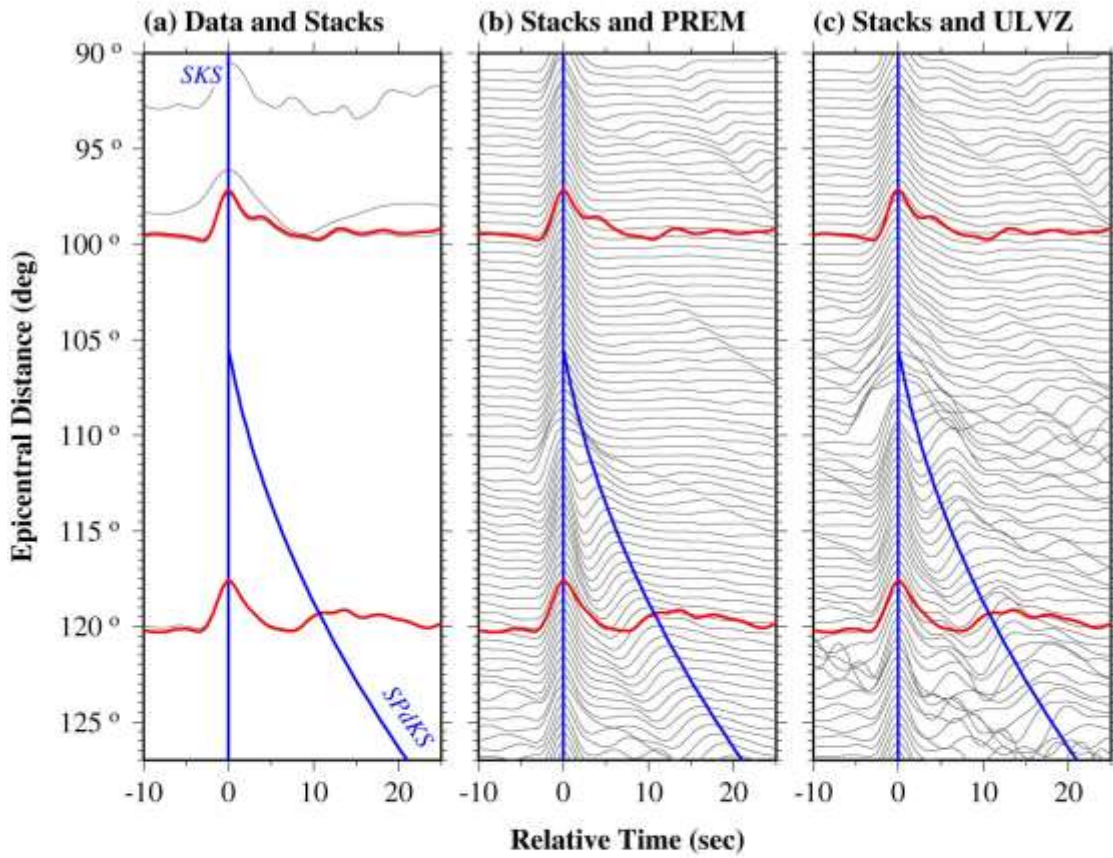
(d) Pd-Rays and Bin Location



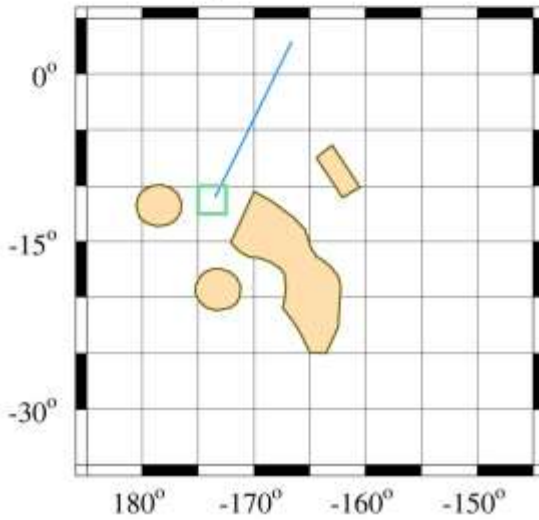
(e) ULVZ model Cross-section



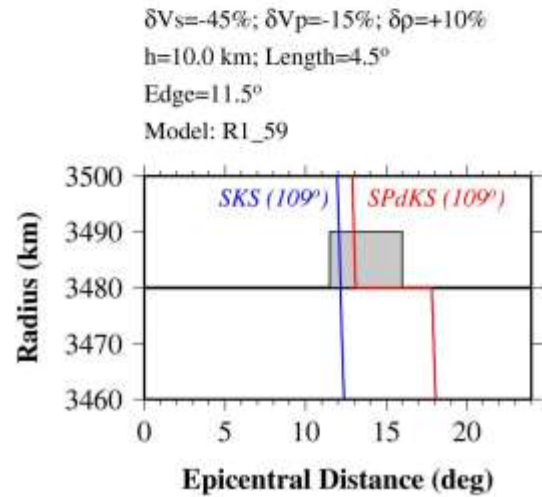
Bin: 0511
Bin Center: Lon= 186.25° Lat=-11.25°



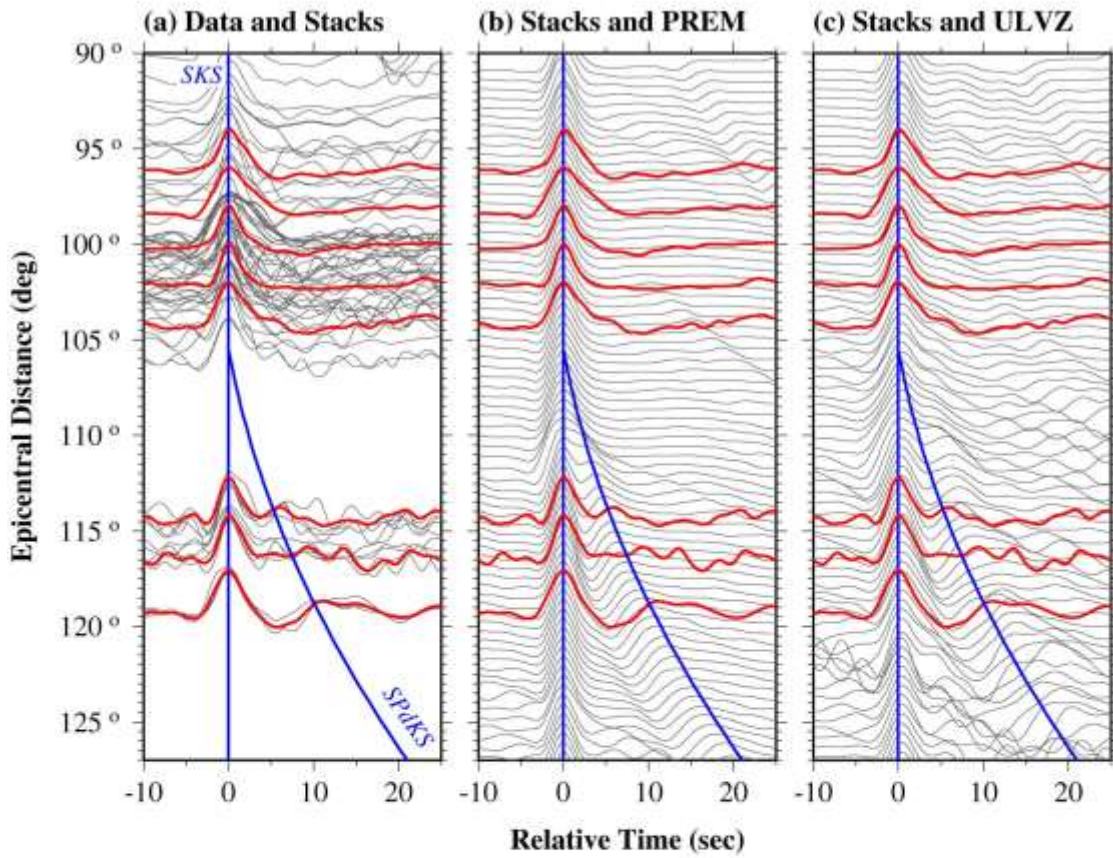
(d) Pd-Rays and Bin Location



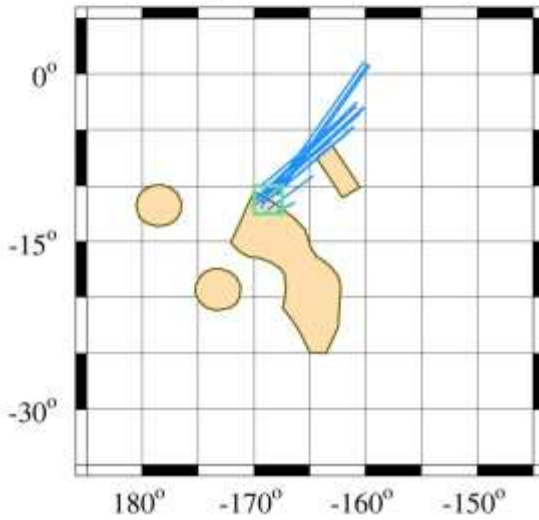
(e) ULVZ model Cross-section



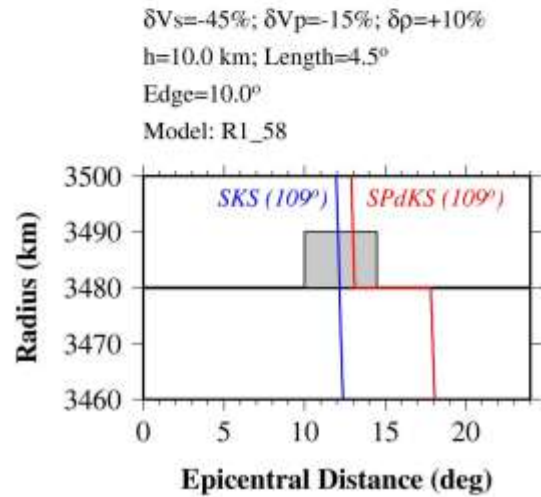
Bin: 0513
Bin Center: Lon= 191.25° Lat=-11.25°



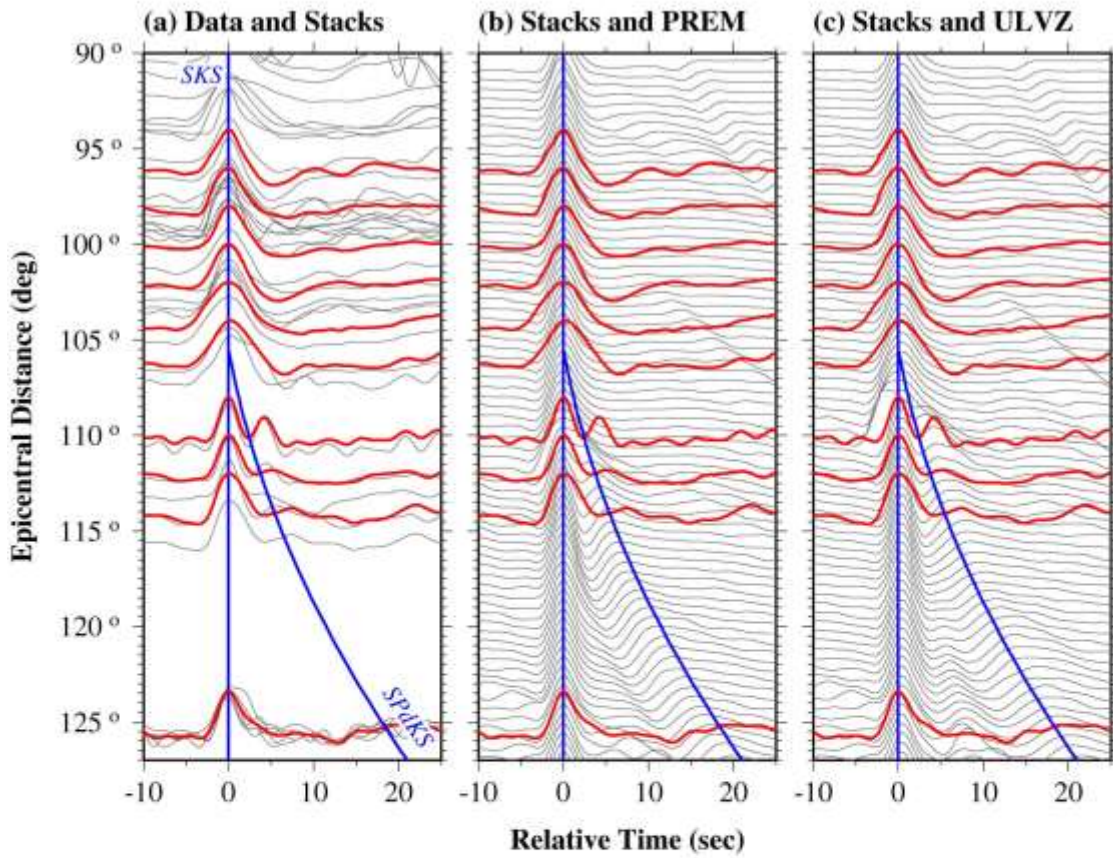
(d) Pd-Rays and Bin Location



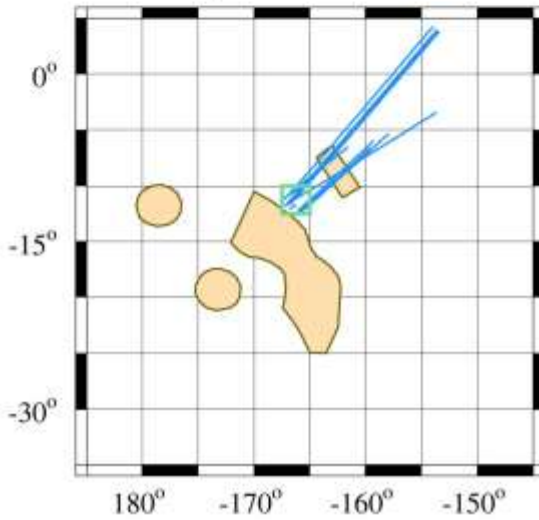
(e) ULVZ model Cross-section



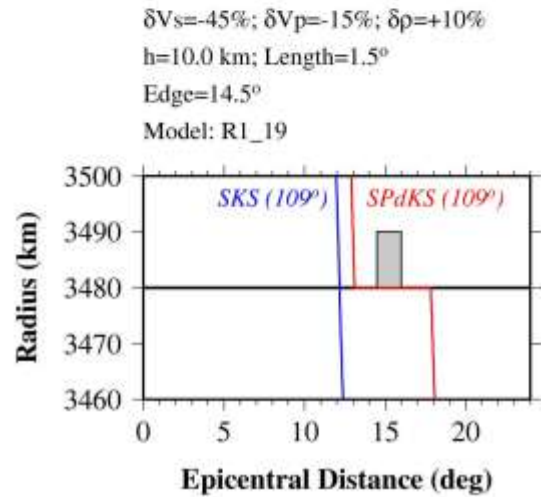
Bin: 0514
Bin Center: Lon= 193.75° Lat=-11.25°



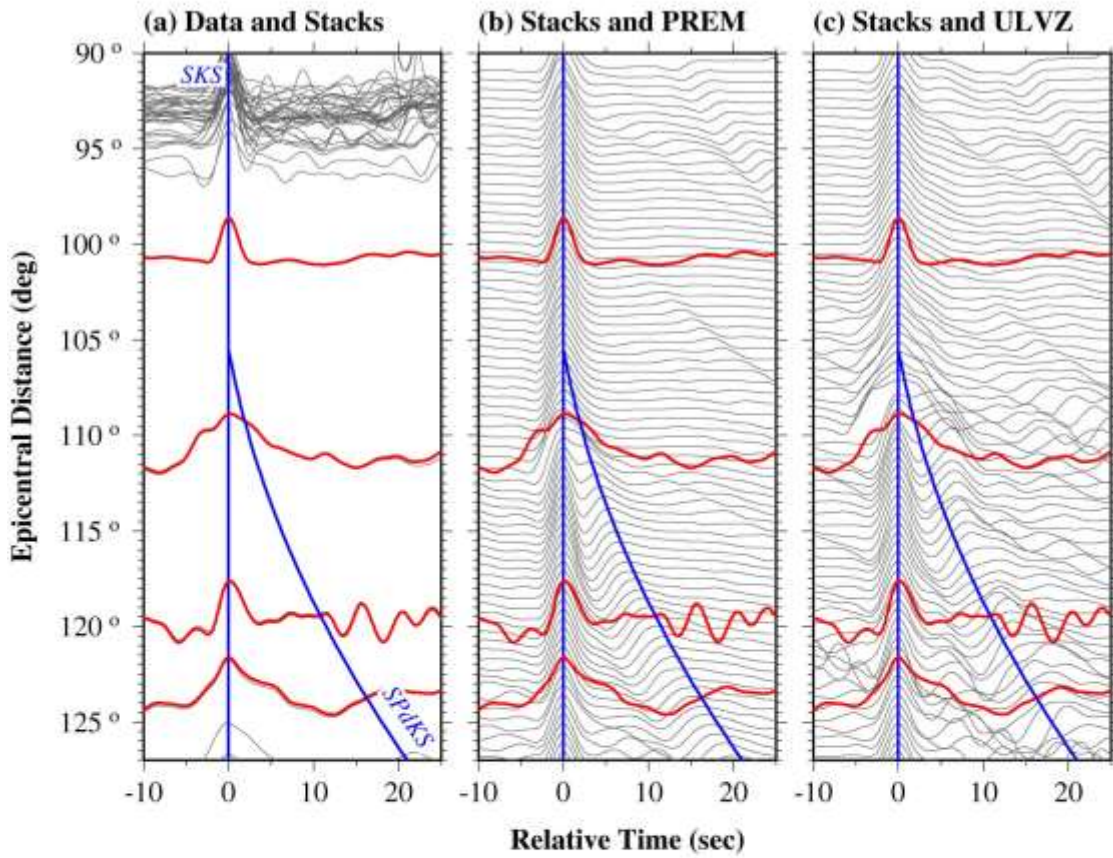
(d) Pd-Rays and Bin Location



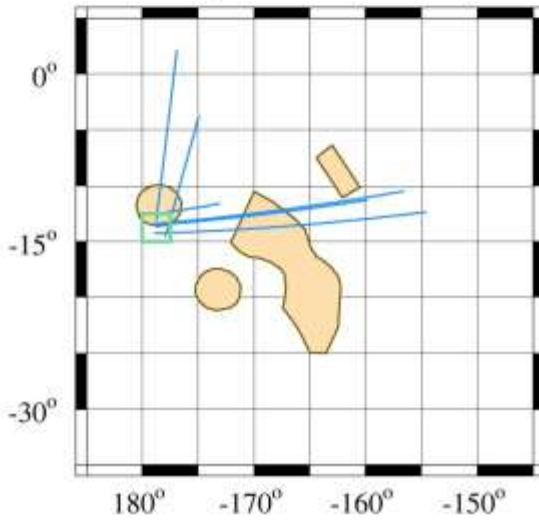
(e) ULVZ model Cross-section



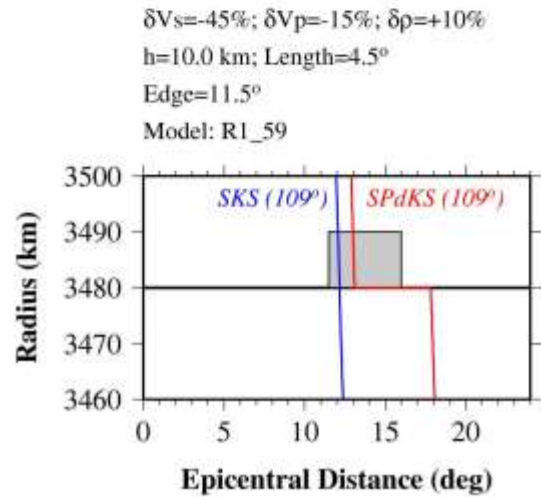
Bin: 0609
Bin Center: Lon= 181.25° Lat=-13.75°



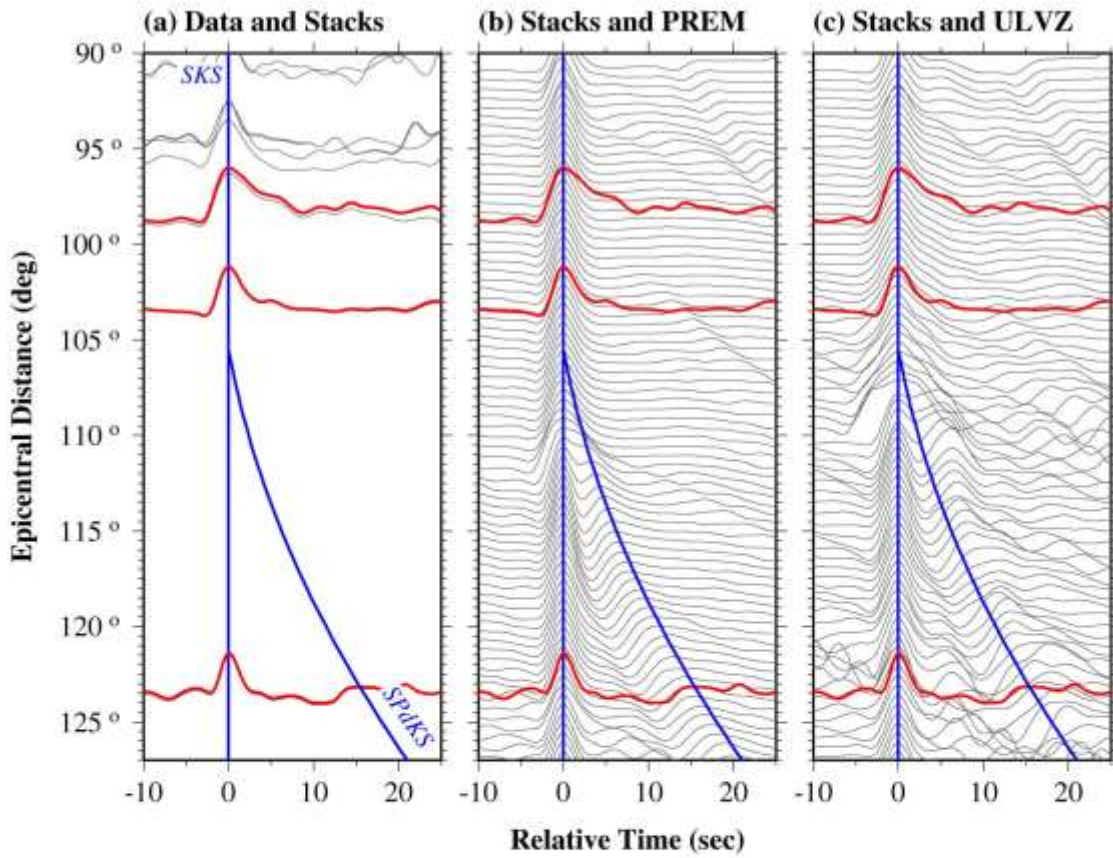
(d) Pd-Rays and Bin Location



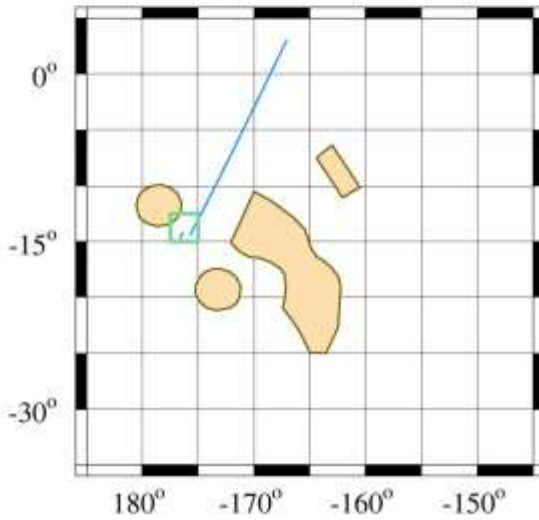
(e) ULVZ model Cross-section



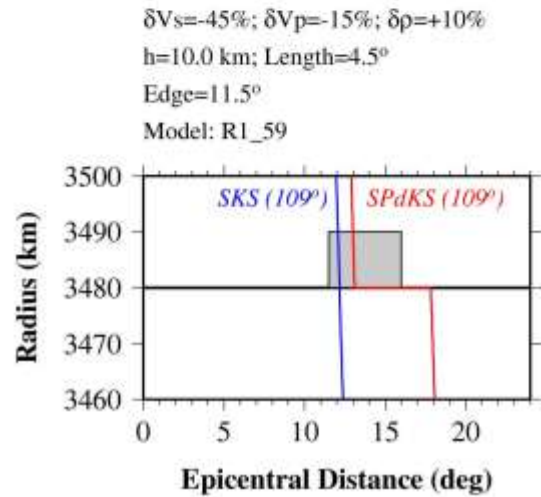
Bin: 0610
Bin Center: Lon= 183.75° Lat=-13.75°



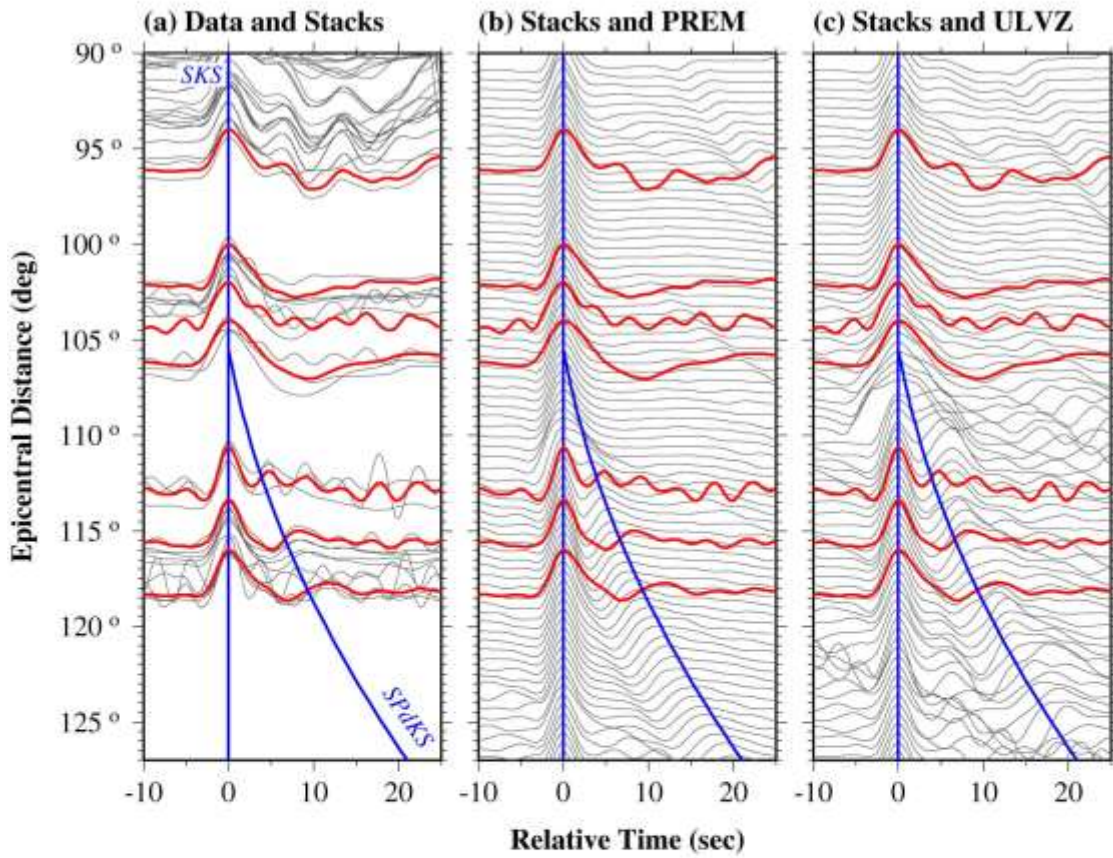
(d) Pd-Rays and Bin Location



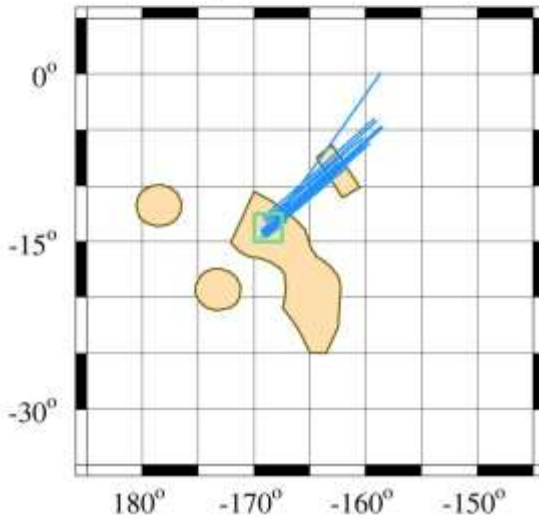
(e) ULVZ model Cross-section



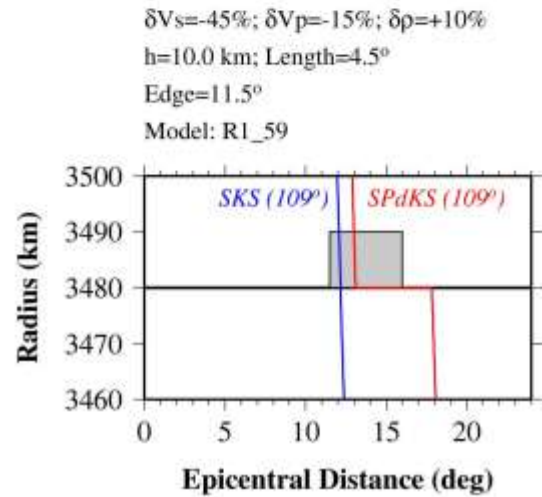
Bin: 0613
Bin Center: Lon= 191.25° Lat=-13.75°



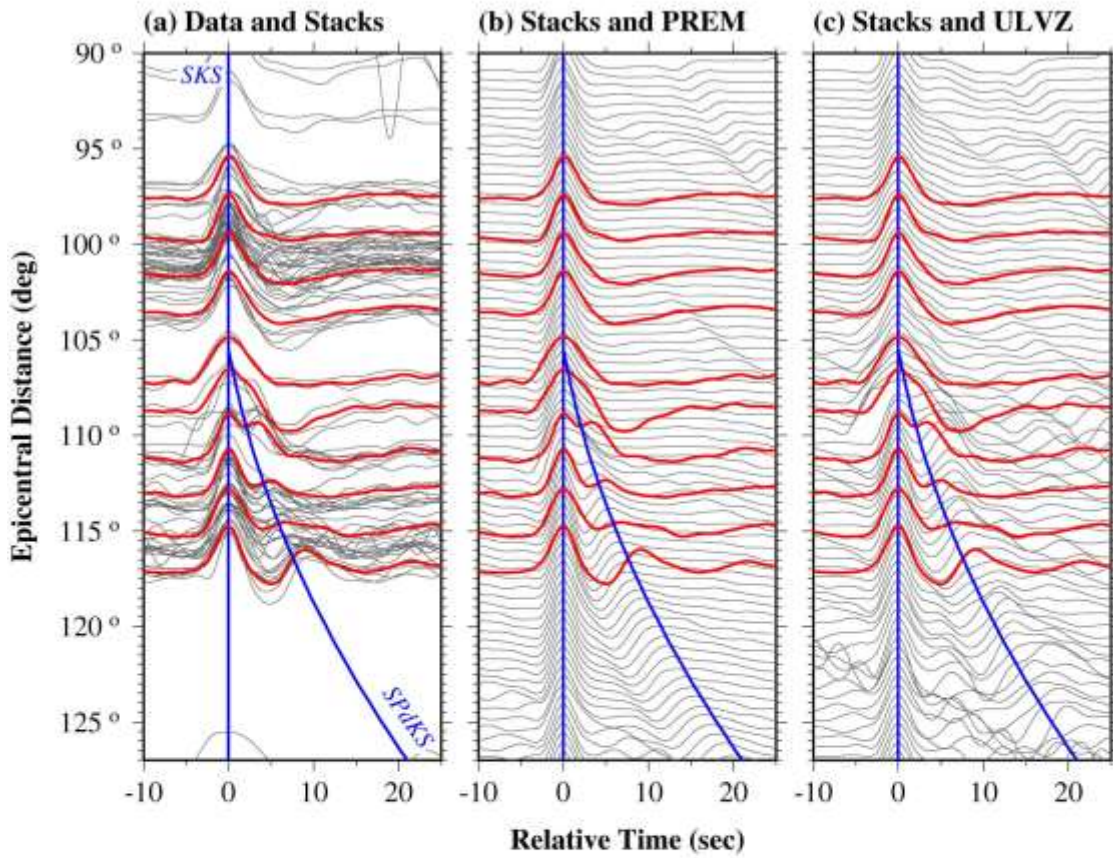
(d) Pd-Rays and Bin Location



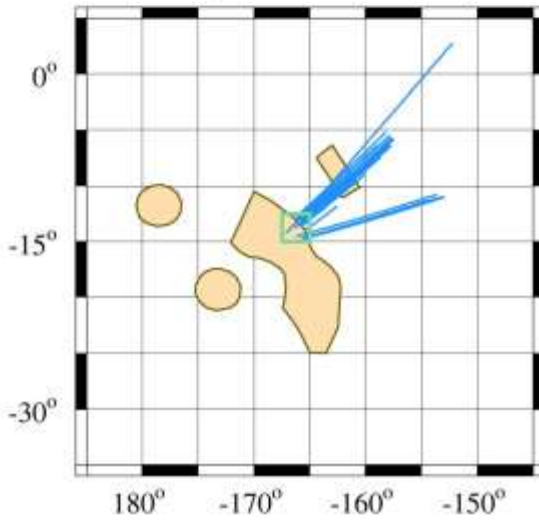
(e) ULVZ model Cross-section



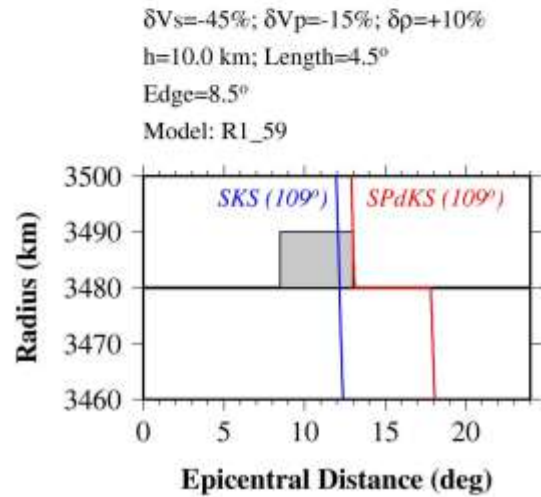
Bin: 0614
Bin Center: Lon= 193.75° Lat=-13.75°



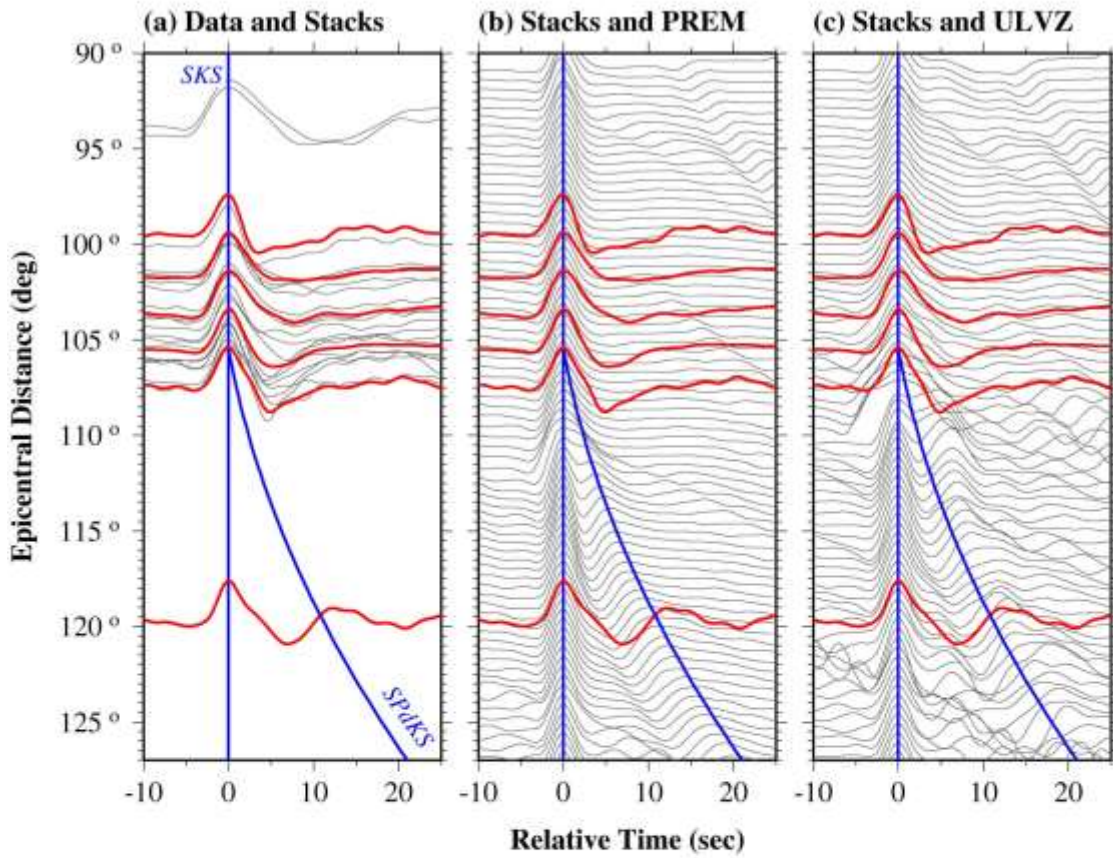
(d) Pd-Rays and Bin Location



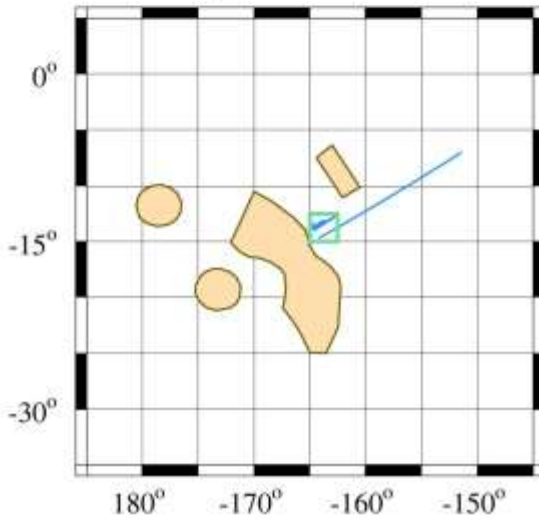
(e) ULVZ model Cross-section



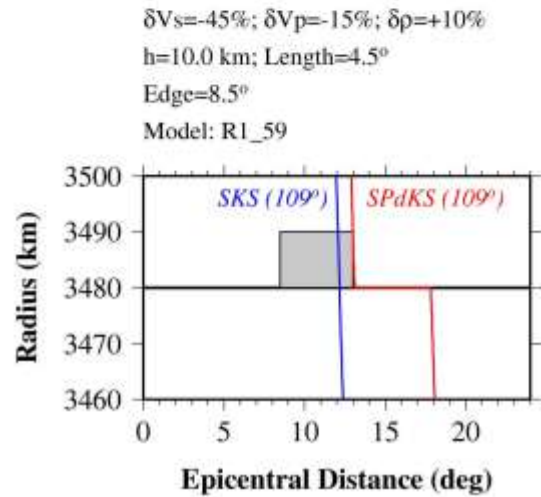
Bin: 0615
Bin Center: Lon= 196.25° Lat=-13.75°



(d) Pd-Rays and Bin Location

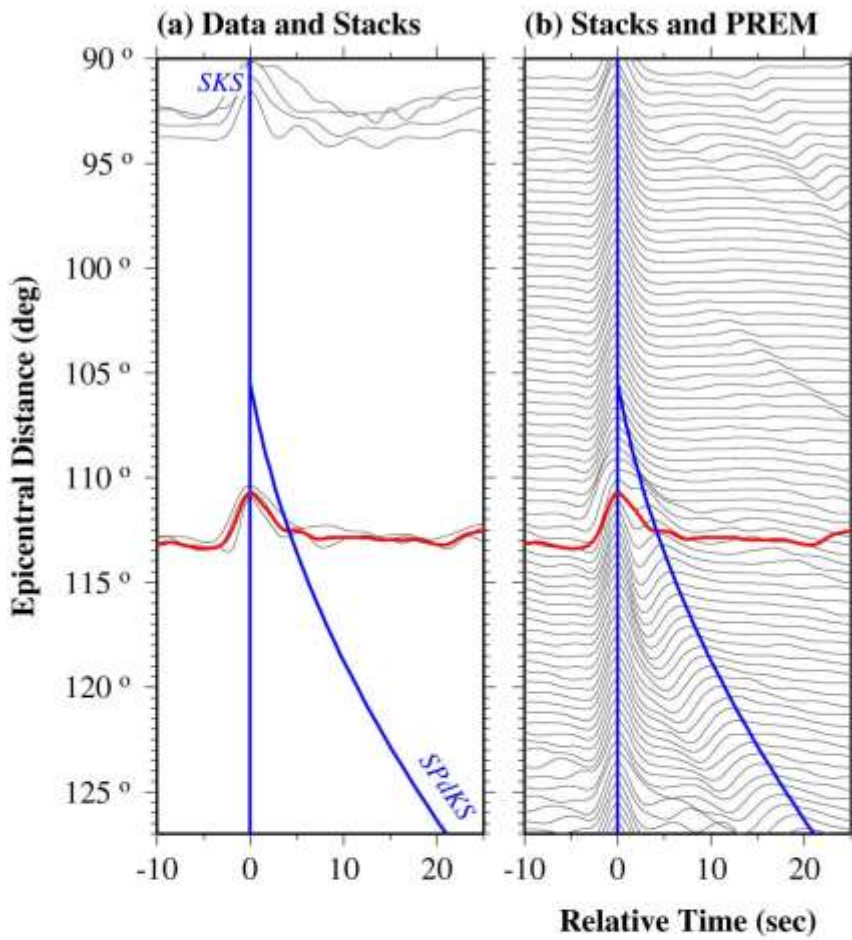


(e) ULVZ model Cross-section

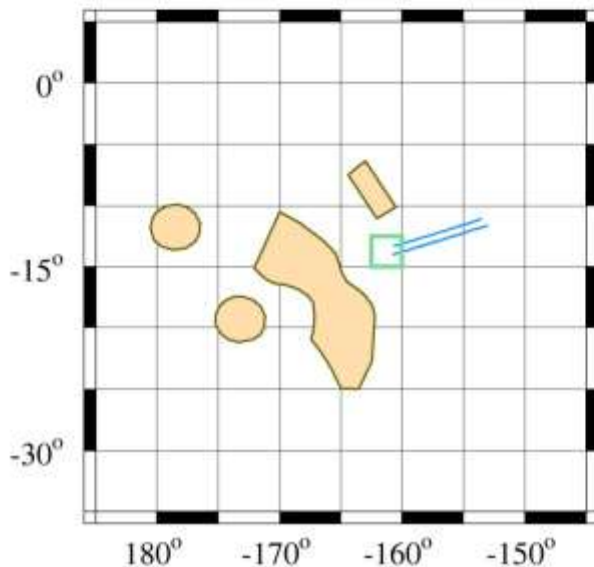


Bin: 0616

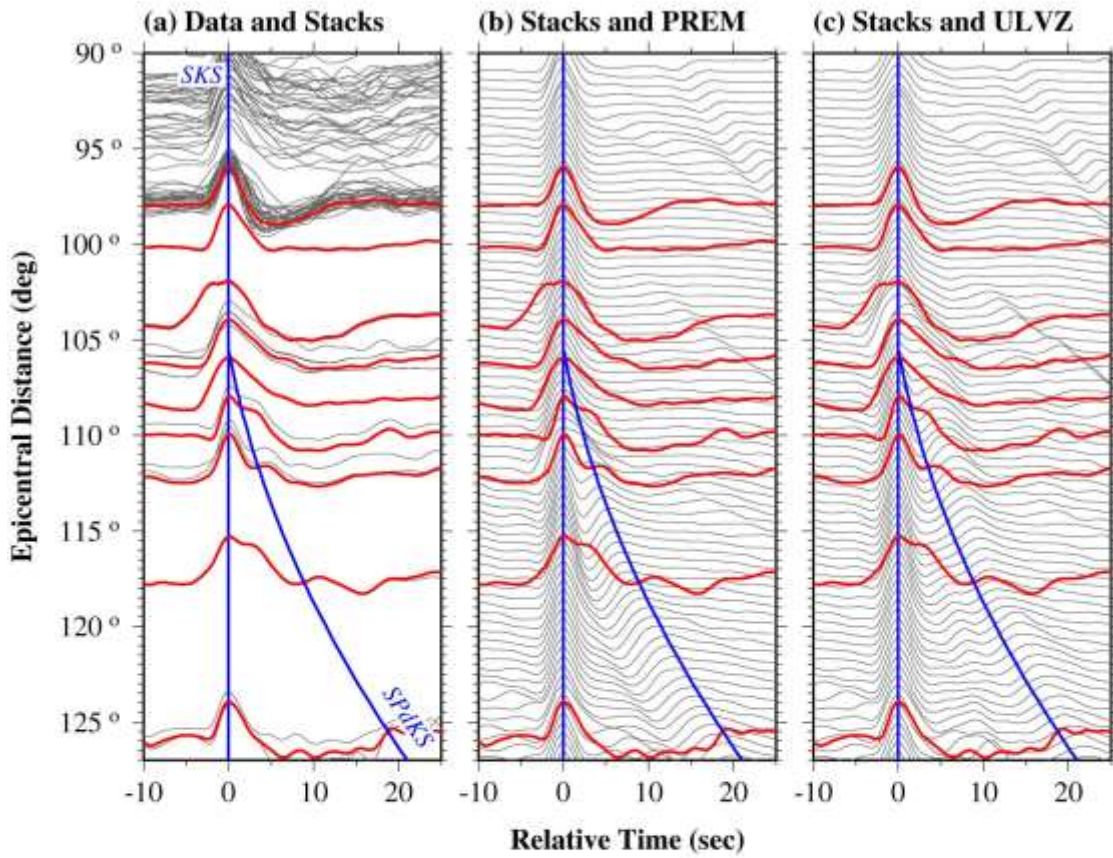
Bin Center: Lon= 198.75° Lat=-13.75°



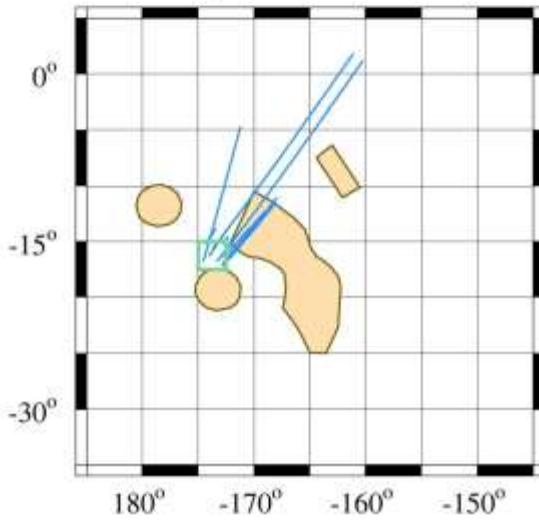
(d) Pd-Rays and Bin Location



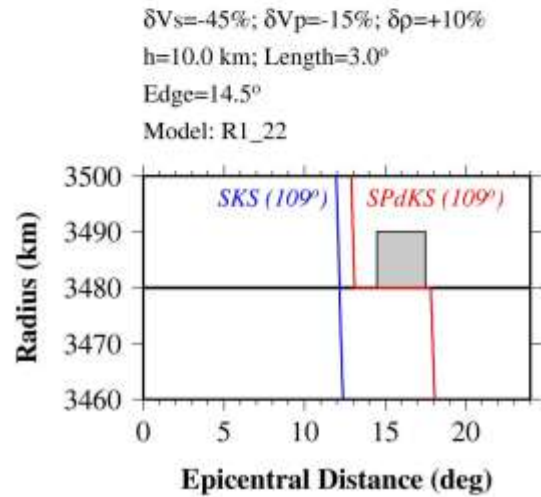
Bin: 0711
Bin Center: Lon= 186.25° Lat=-16.25°



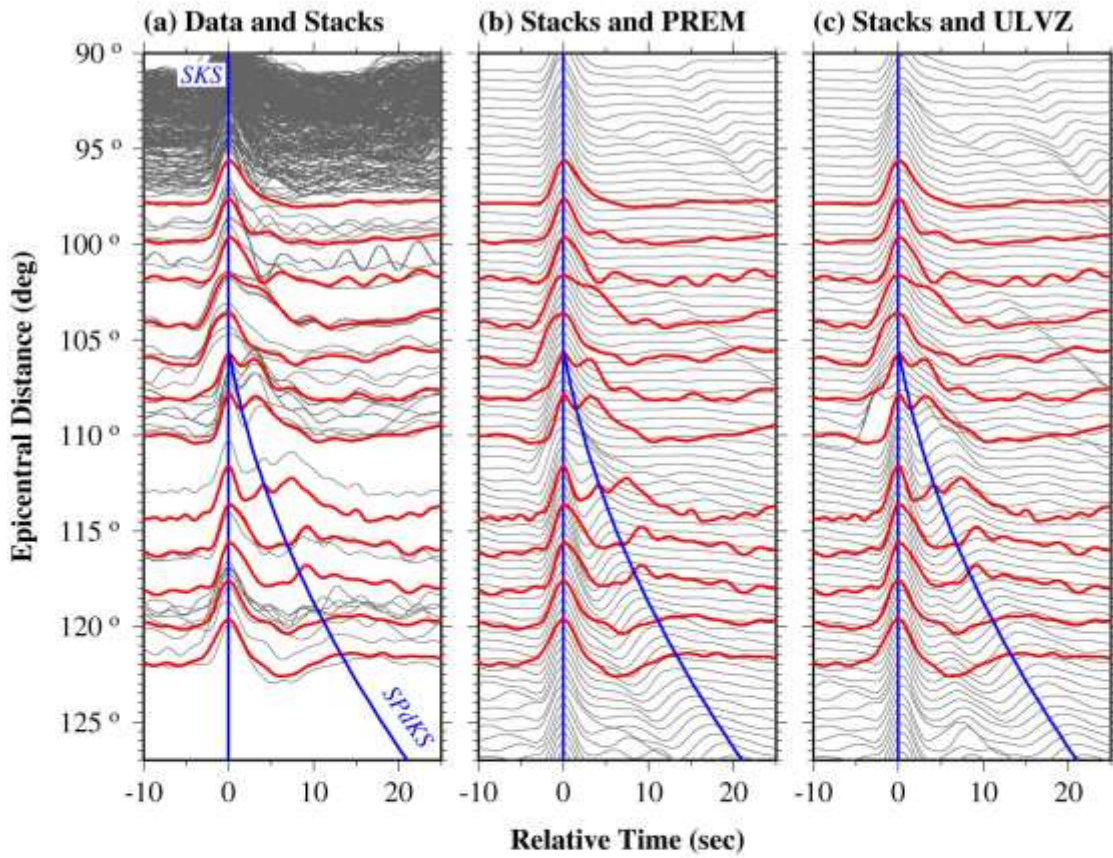
(d) Pd-Rays and Bin Location



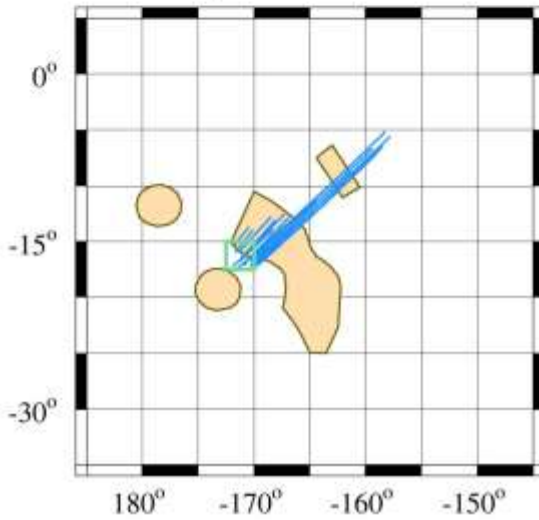
(e) ULVZ model Cross-section



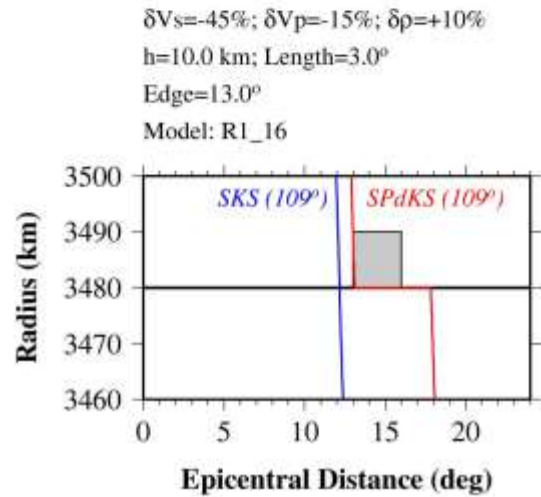
Bin: 0712
Bin Center: Lon= 188.75° Lat=-16.25°



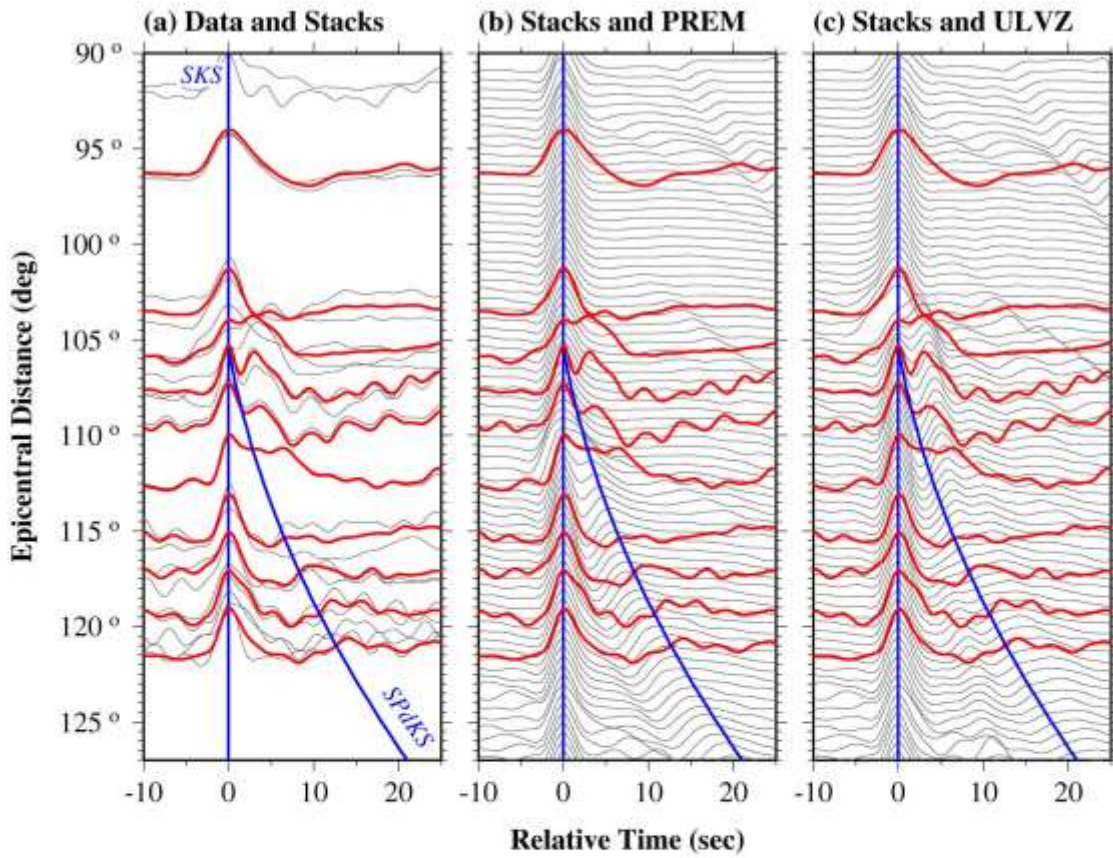
(d) Pd-Rays and Bin Location



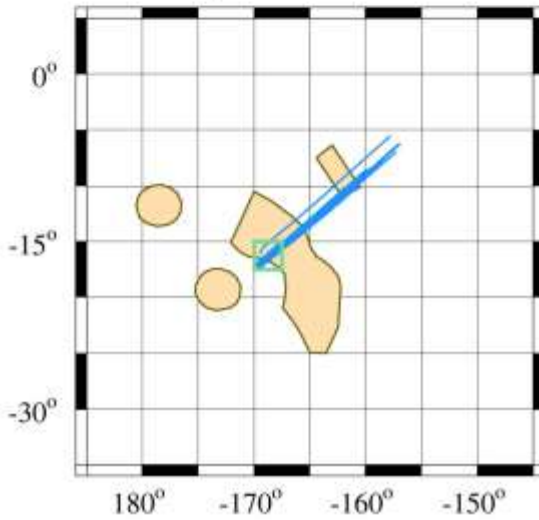
(e) ULVZ model Cross-section



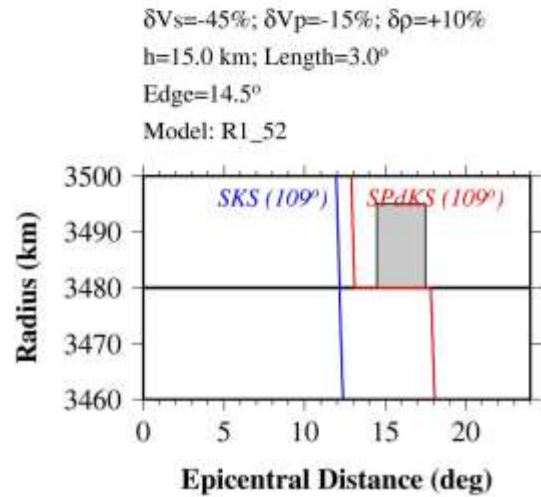
Bin: 0713
Bin Center: Lon= 191.25° Lat=-16.25°



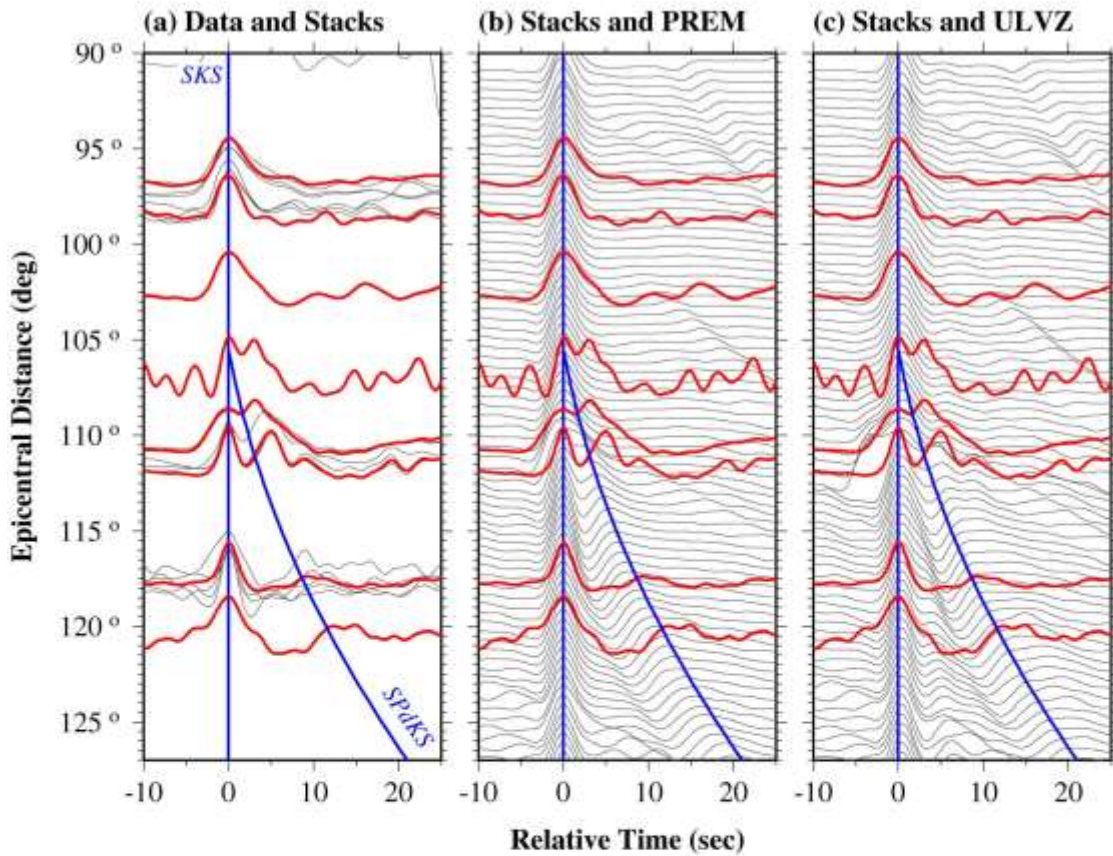
(d) Pd-Rays and Bin Location



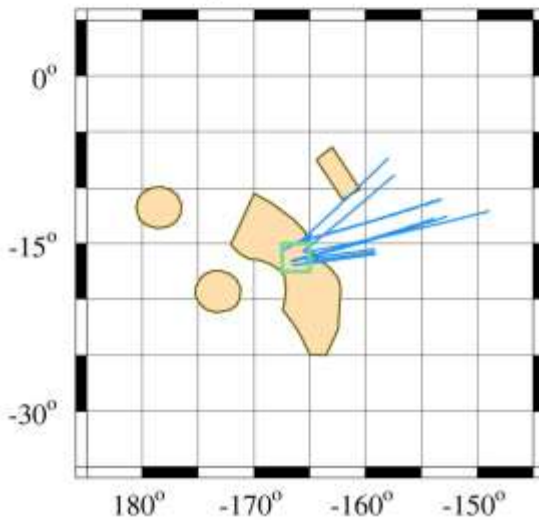
(e) ULVZ model Cross-section



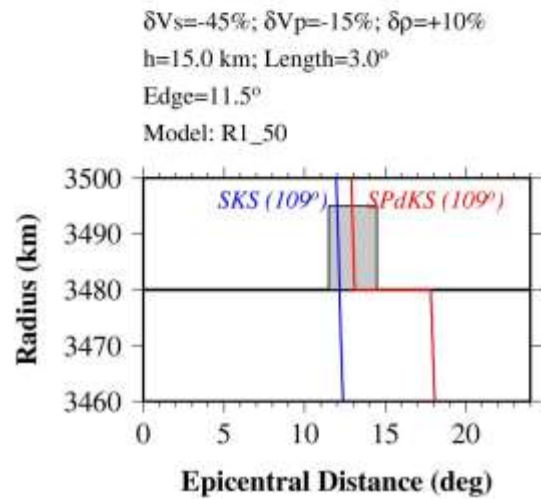
Bin: 0714
Bin Center: Lon= 193.75° Lat=-16.25°



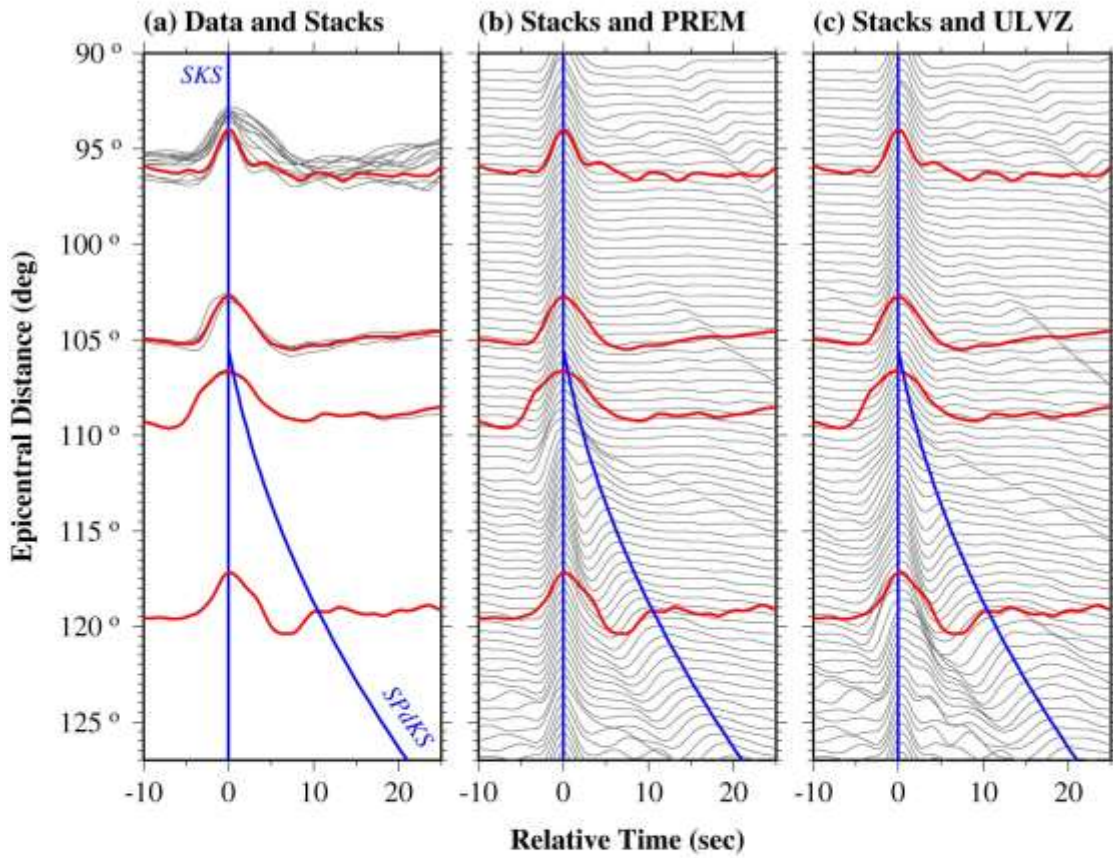
(d) Pd-Rays and Bin Location



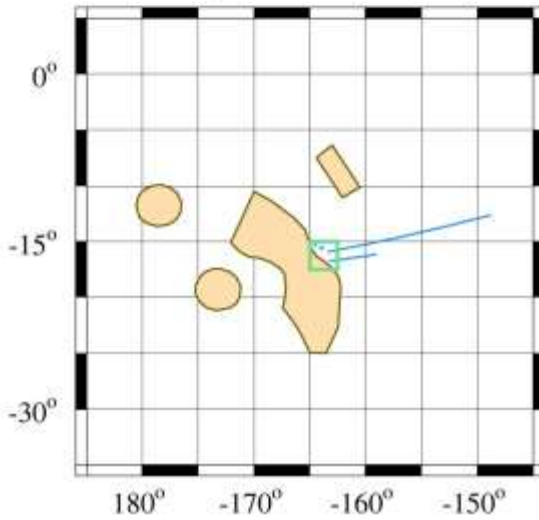
(e) ULVZ model Cross-section



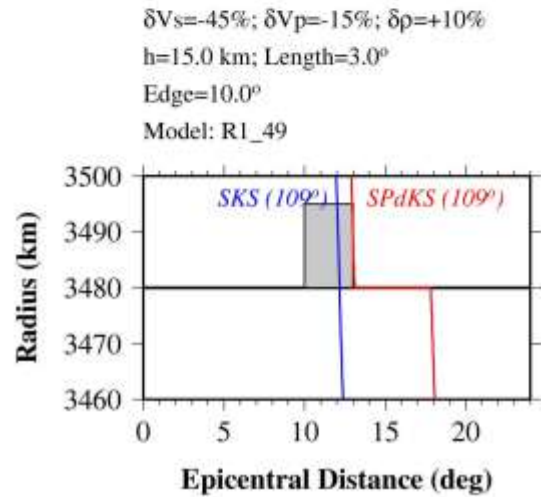
Bin: 0715
Bin Center: Lon= 196.25° Lat=-16.25°



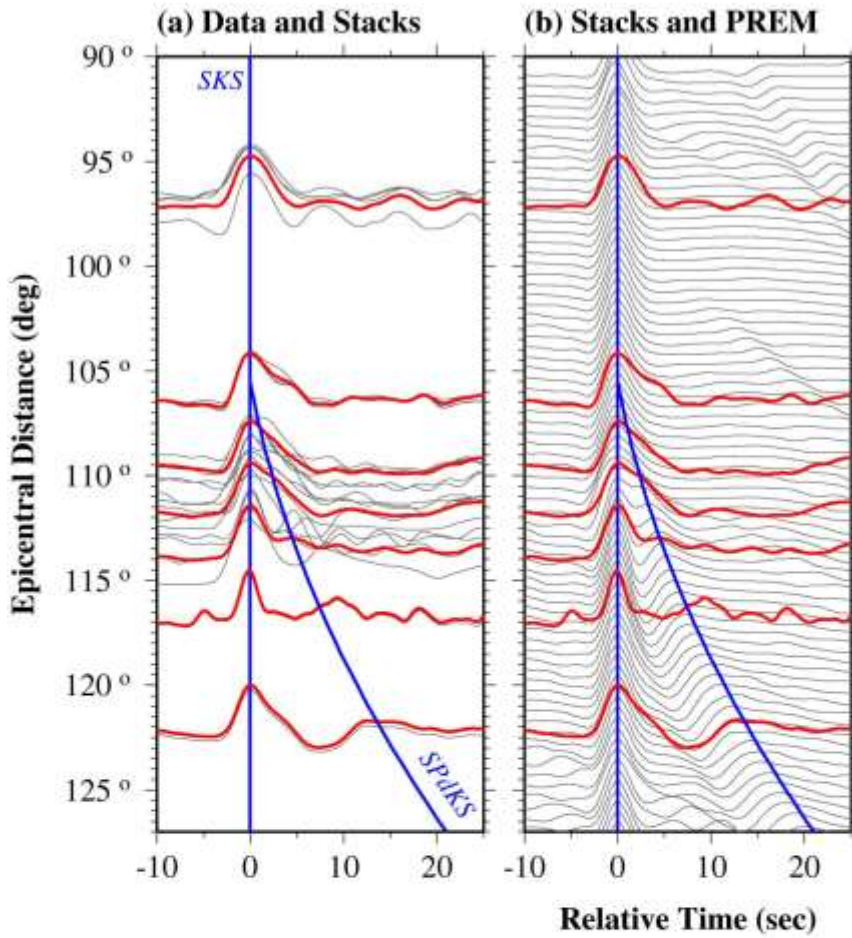
(d) Pd-Rays and Bin Location



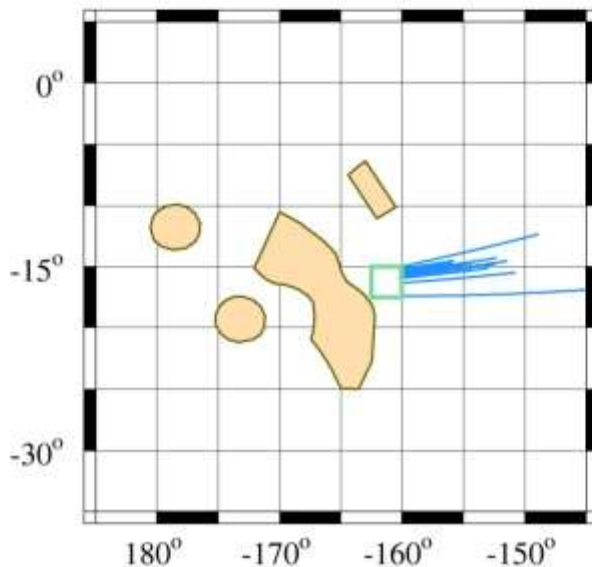
(e) ULVZ model Cross-section



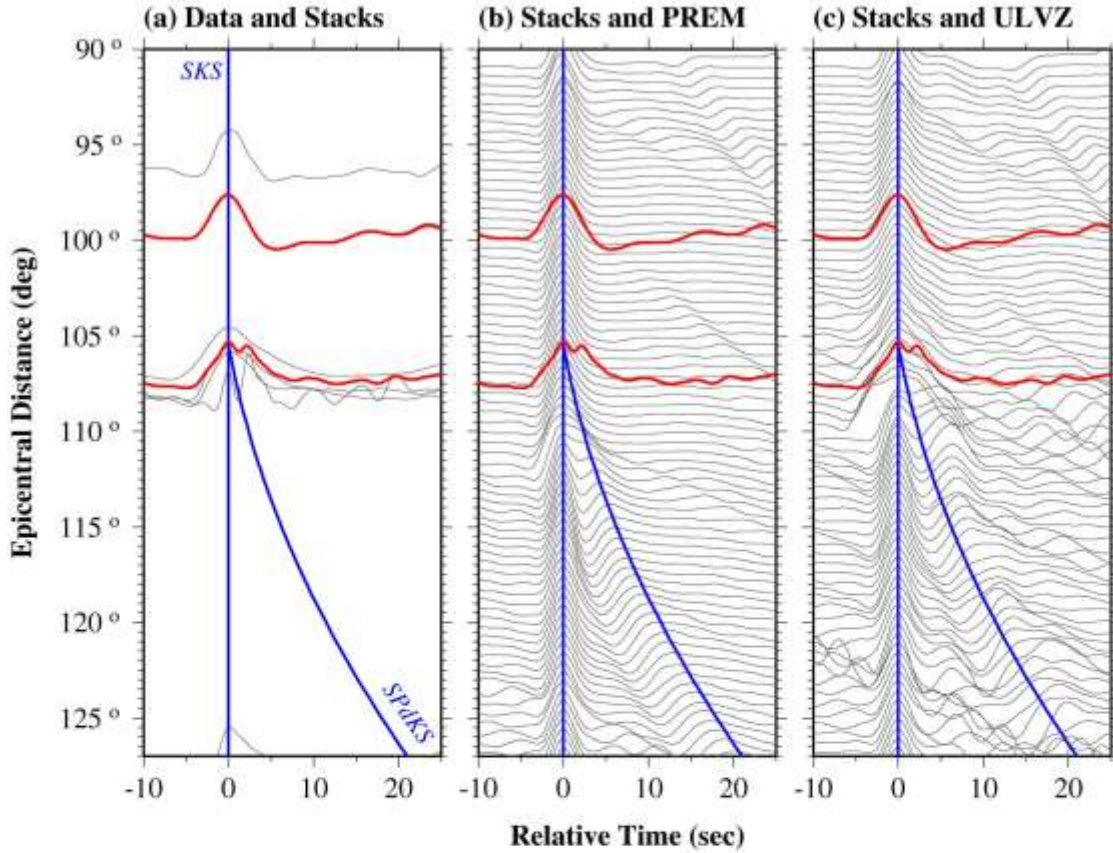
Bin: 0716
Bin Center: Lon= 198.75° Lat=-16.25°



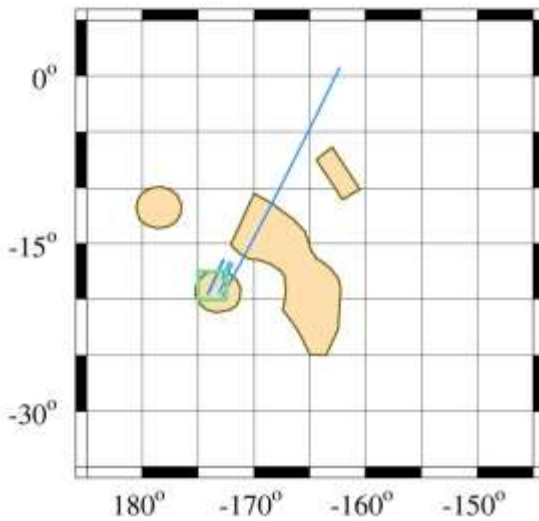
(d) Pd-Rays and Bin Location



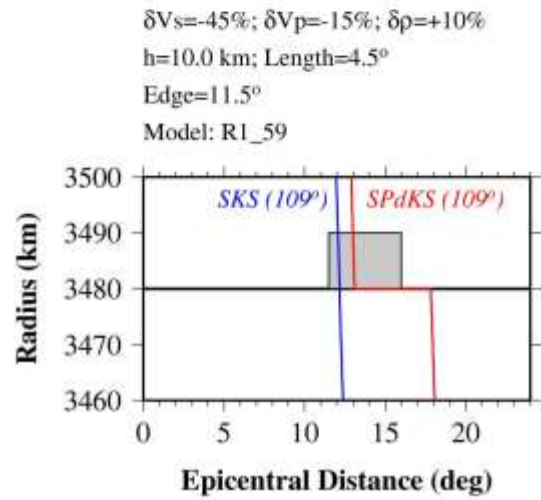
Bin: 0811
Bin Center: Lon= 186.25° Lat=-18.75°



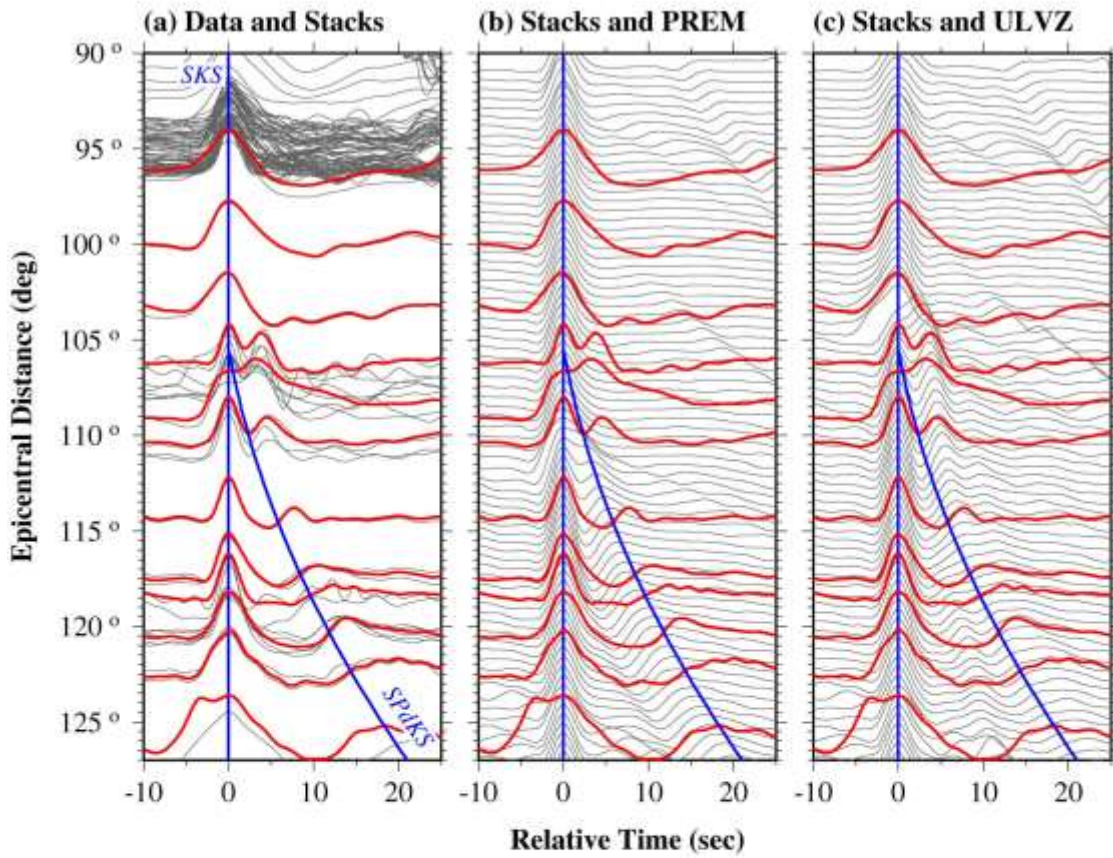
(d) Pd-Rays and Bin Location



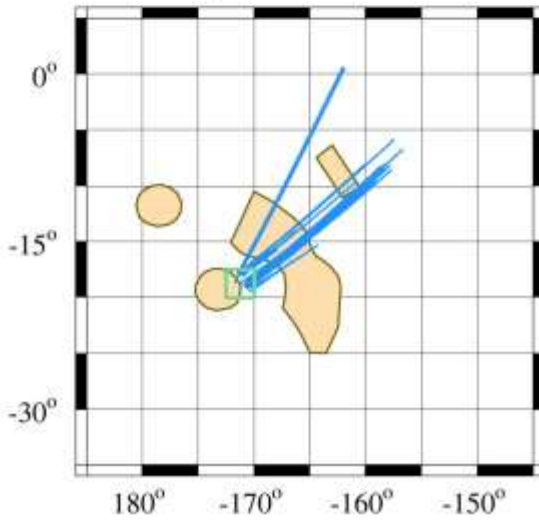
(e) ULVZ model Cross-section



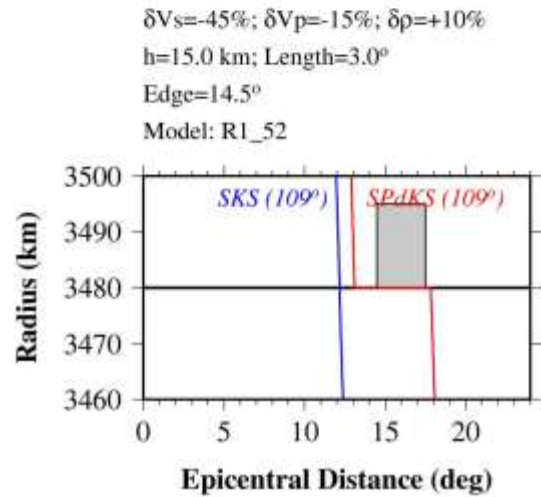
Bin: 0812
Bin Center: Lon= 188.75° Lat=-18.75°



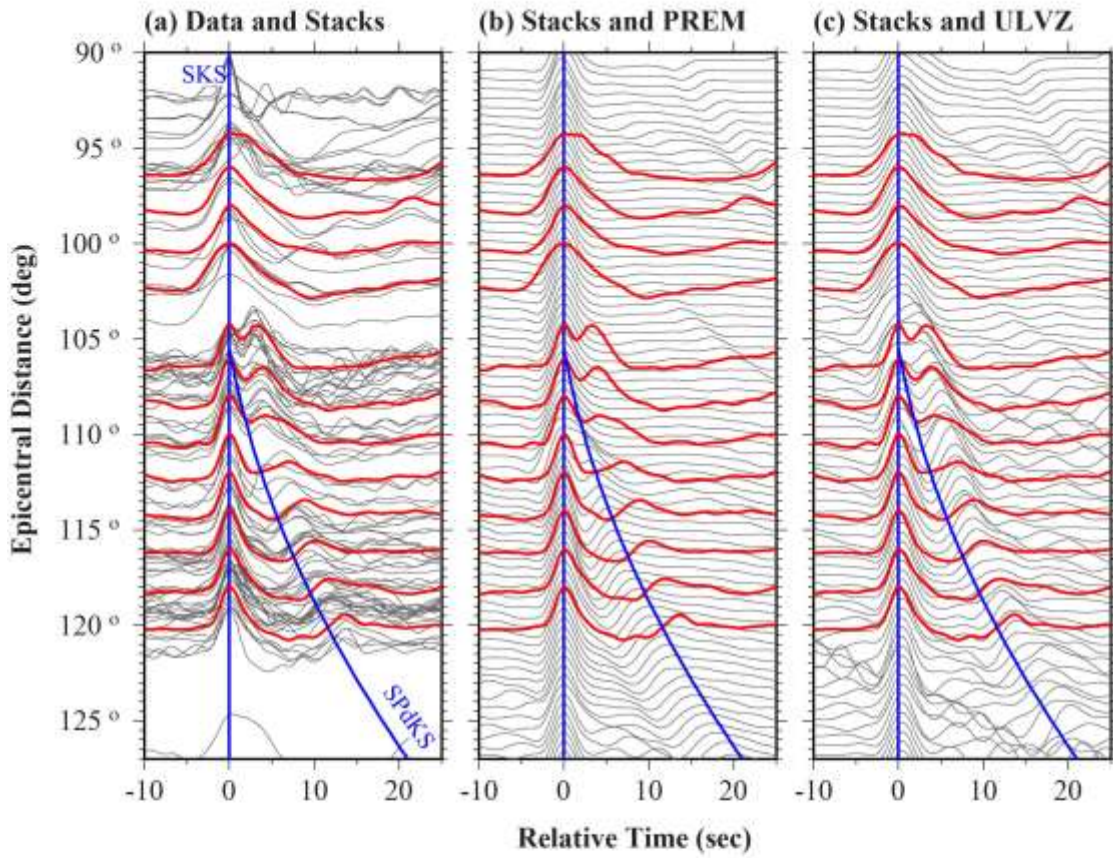
(d) Pd-Rays and Bin Location



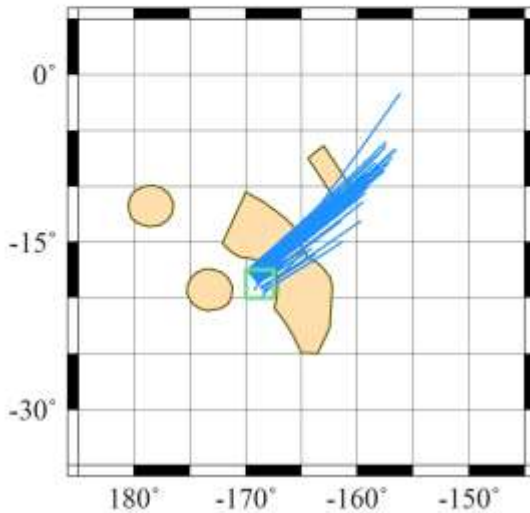
(e) ULVZ model Cross-section



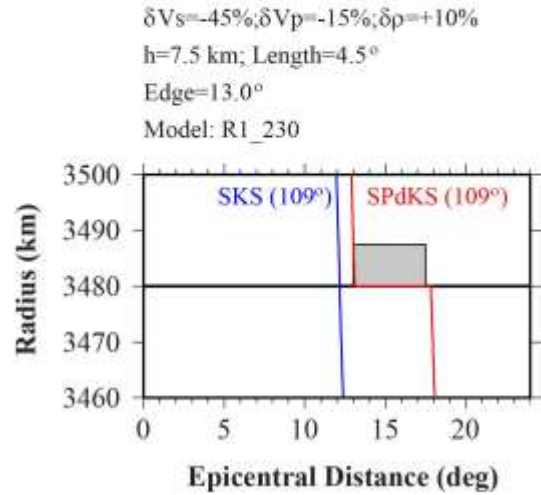
Bin: 0813
Bin Center: Lon= 191.25° Lat=-18.75°



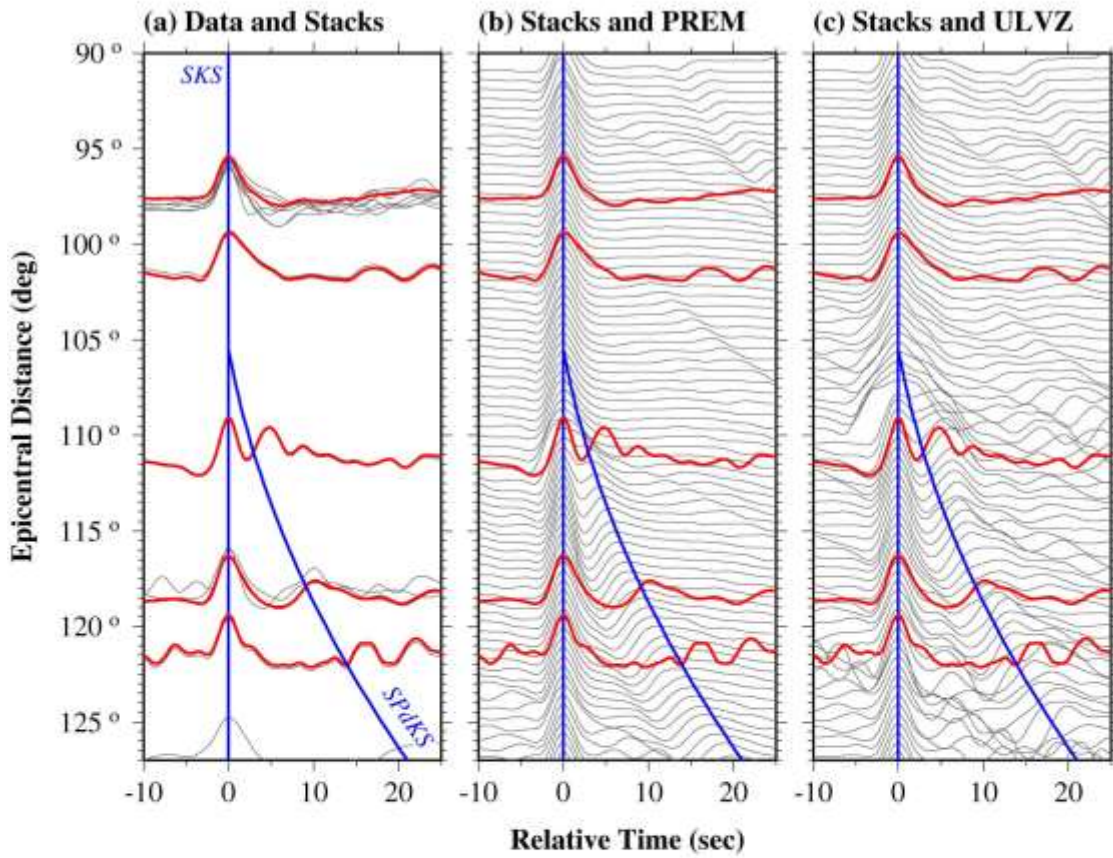
(d) Pd-Rays and Bin Location



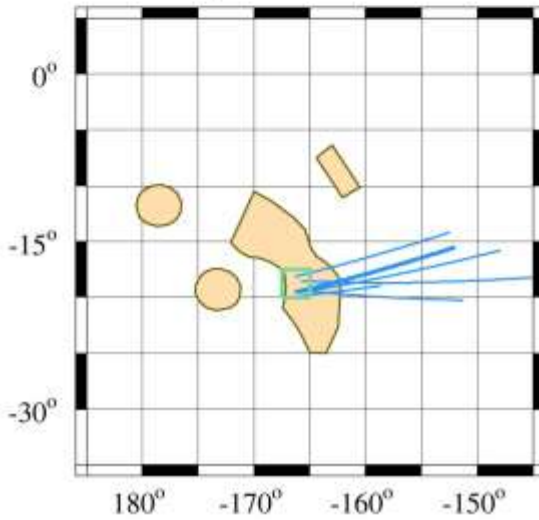
(e) ULVZ model Cross-section



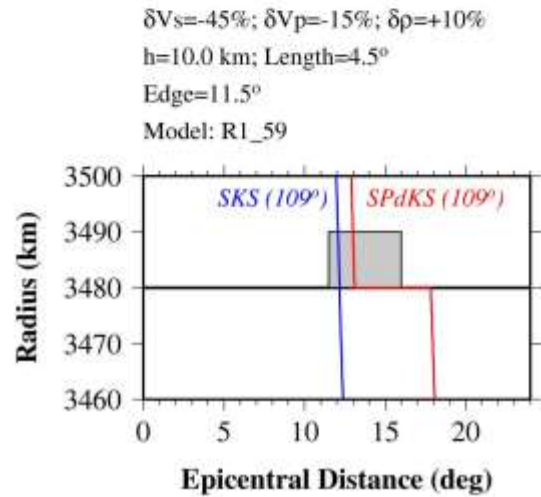
Bin: 0814
Bin Center: Lon= 193.75° Lat=-18.75°



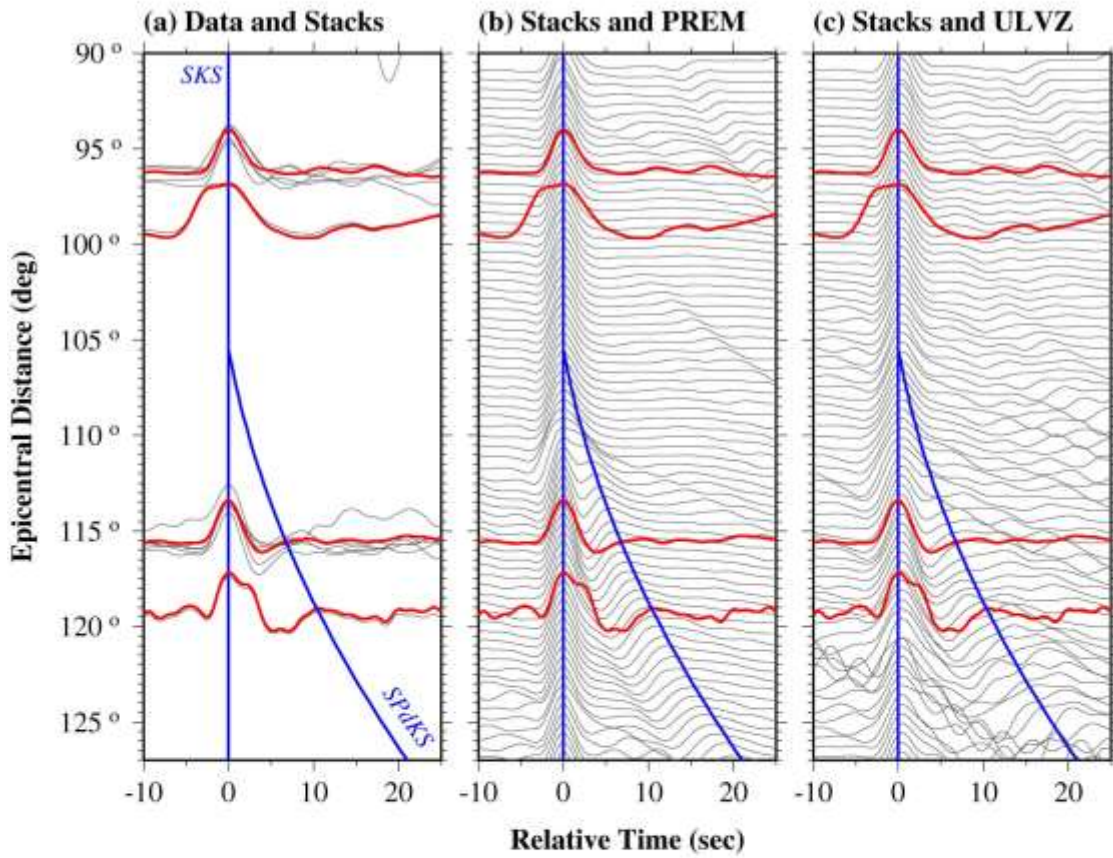
(d) Pd-Rays and Bin Location



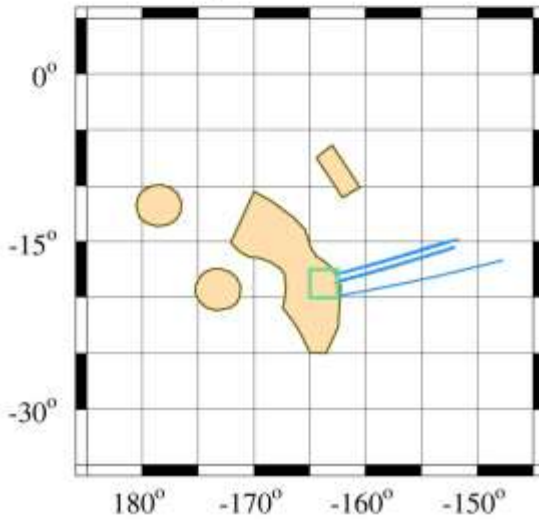
(e) ULVZ model Cross-section



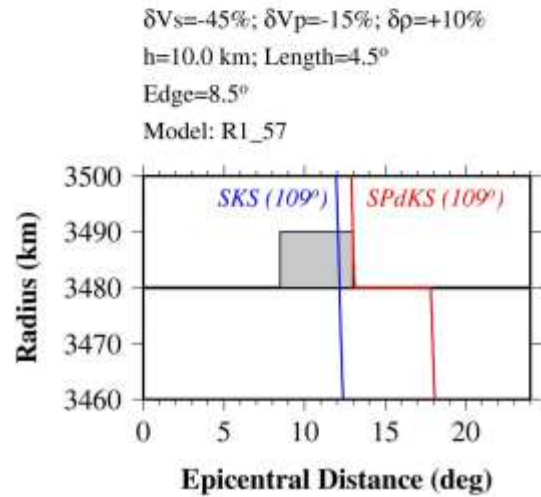
Bin: 0815
Bin Center: Lon= 196.25° Lat=-18.75°



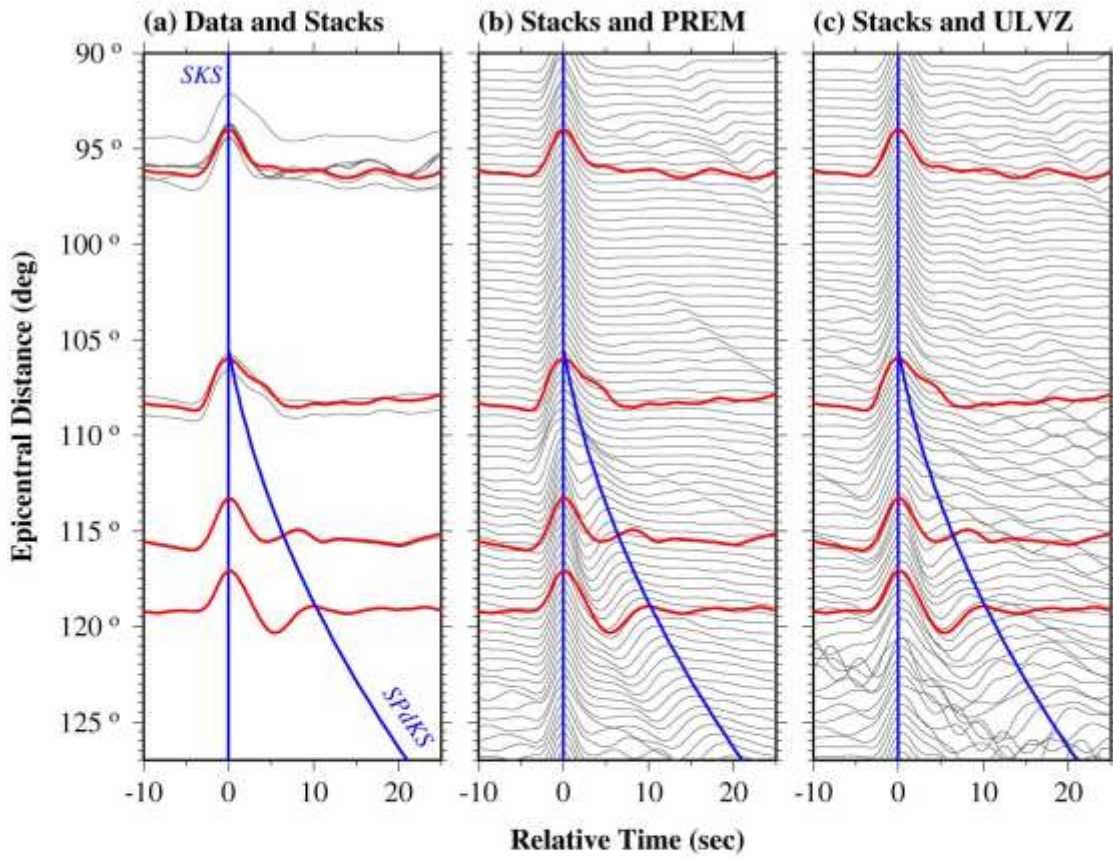
(d) Pd-Rays and Bin Location



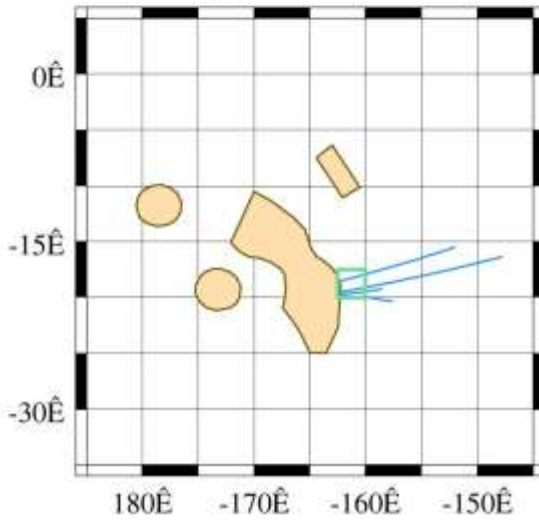
(e) ULVZ model Cross-section



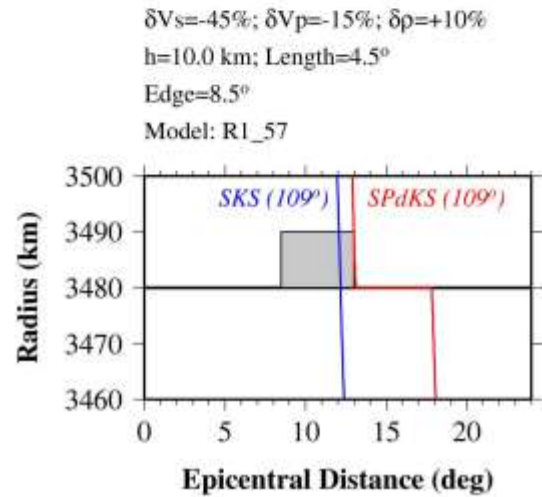
Bin: 0816
Bin Center: Lon= 198.75° Lat=-18.75°



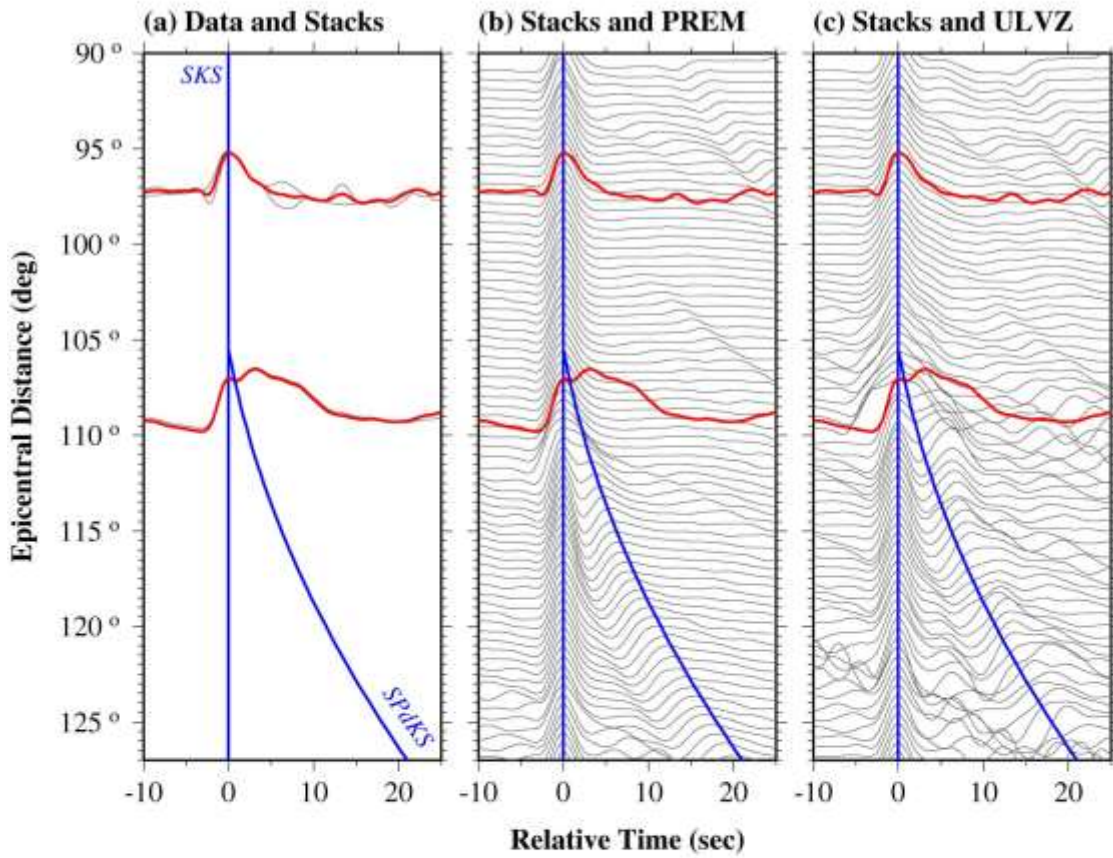
(d) Pd-Rays and Bin Location



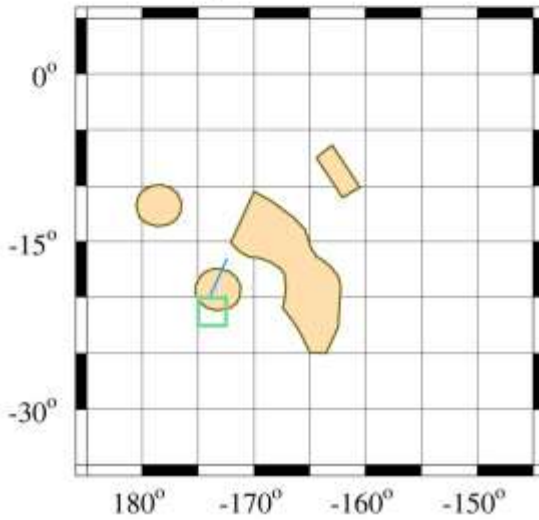
(e) ULVZ model Cross-section



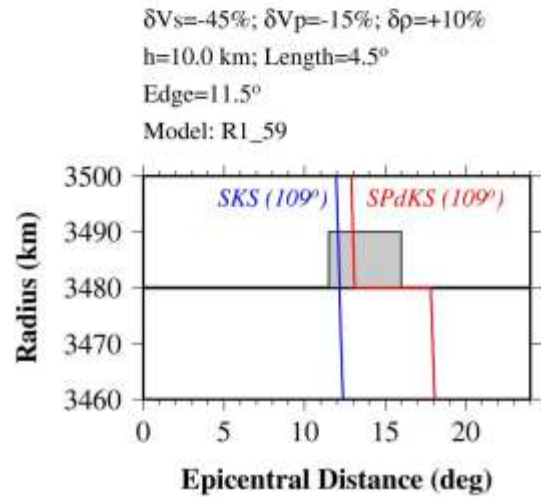
Bin: 0911
Bin Center: Lon= 186.25° Lat=-21.25°



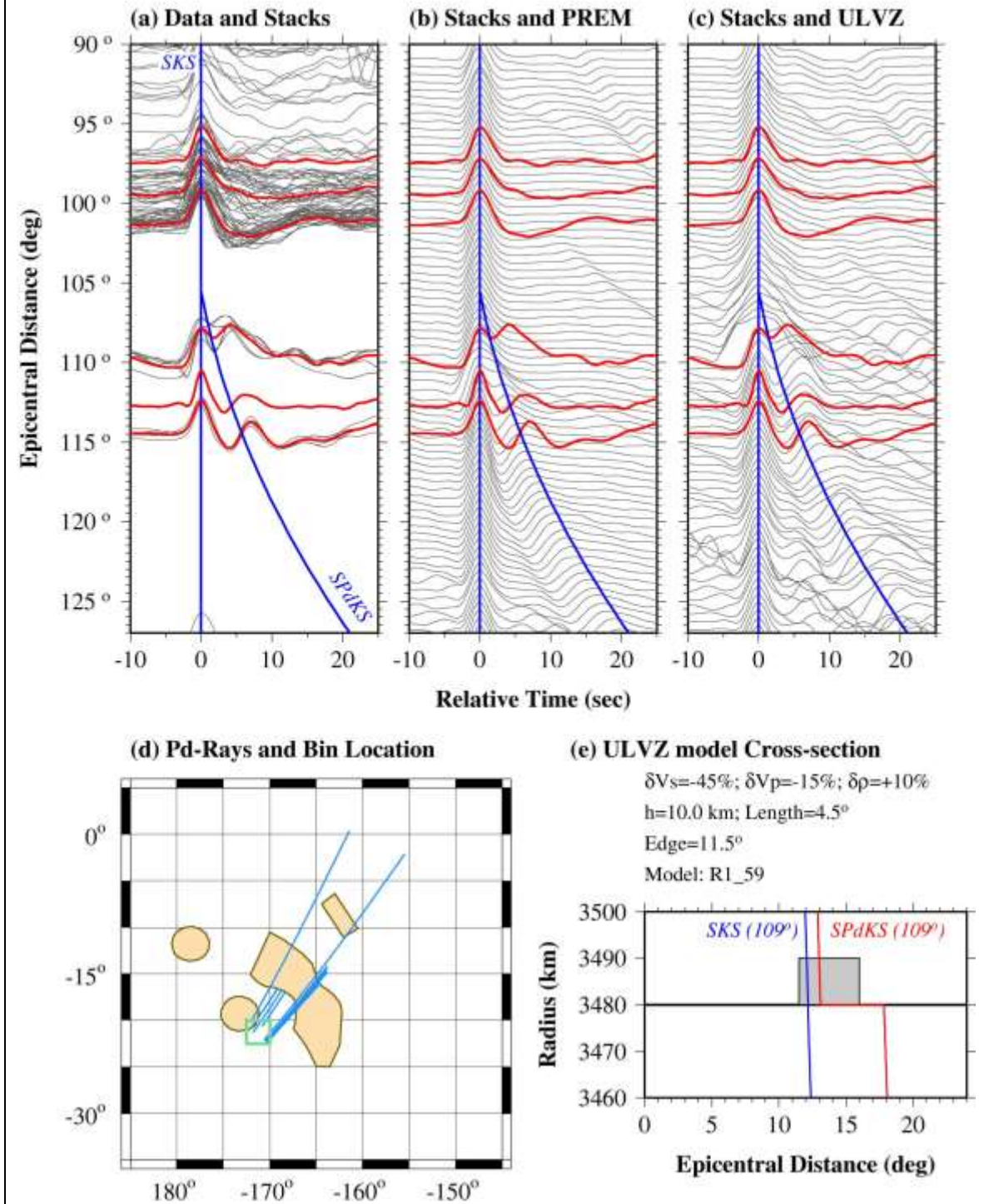
(d) Pd-Rays and Bin Location



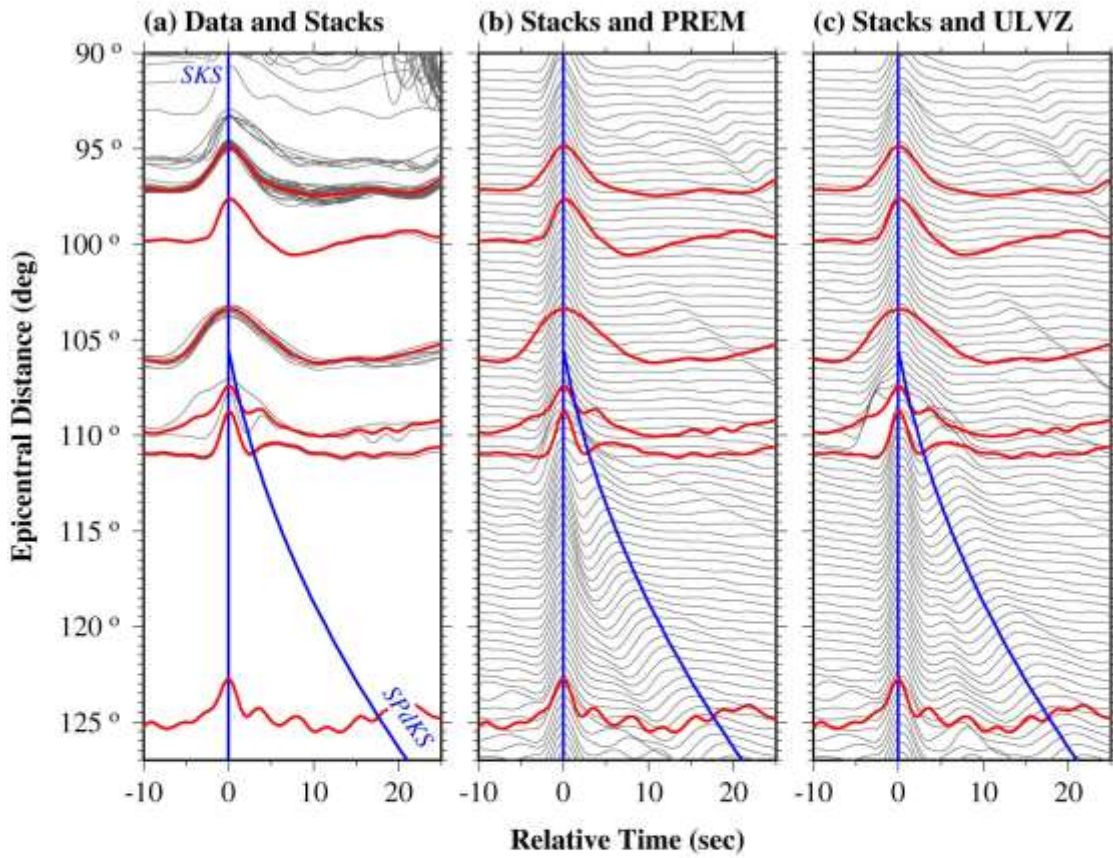
(e) ULVZ model Cross-section



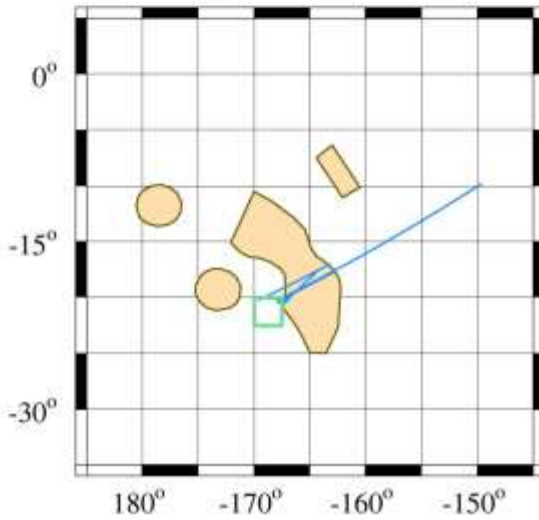
Bin: 0912
Bin Center: Lon= 188.75° Lat=-21.25°



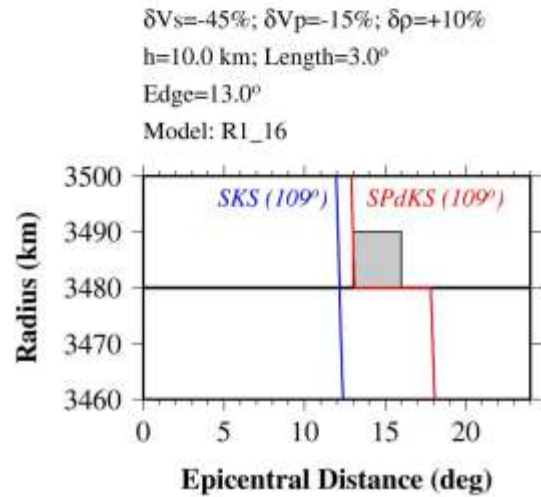
Bin: 0913
Bin Center: Lon= 191.25° Lat=-21.25°



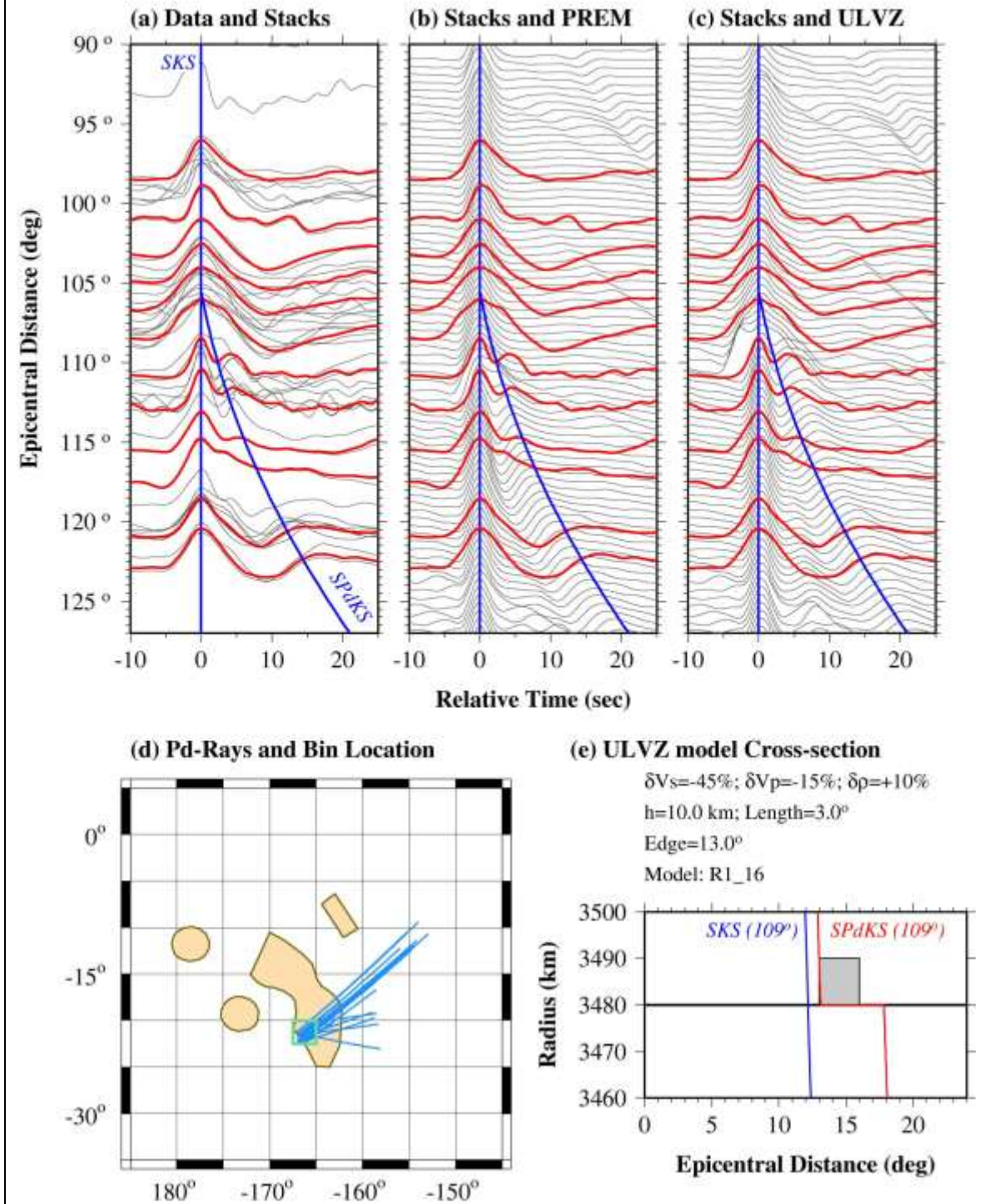
(d) Pd-Rays and Bin Location



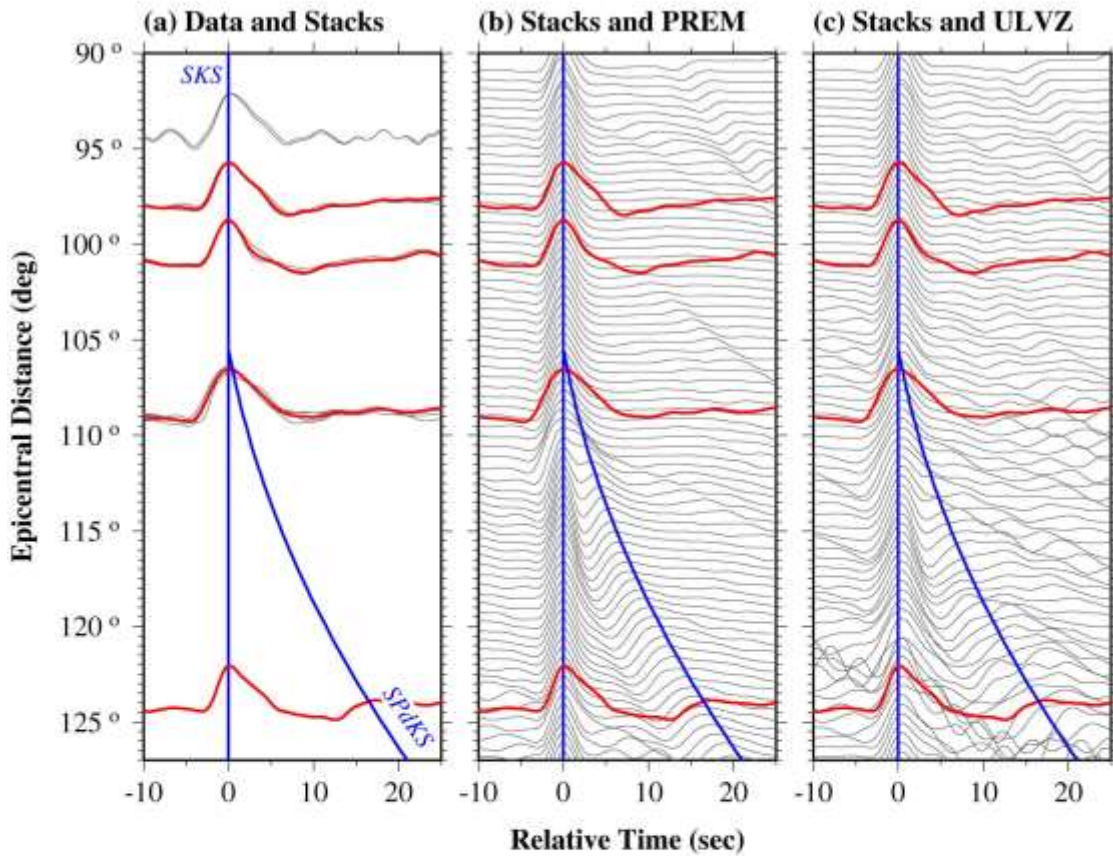
(e) ULVZ model Cross-section



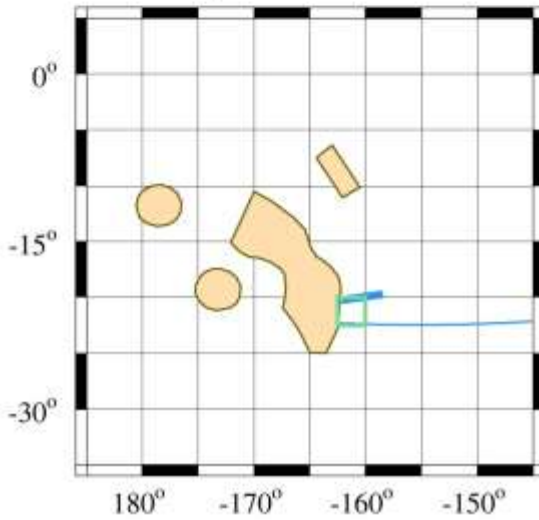
Bin: 0914
Bin Center: Lon= 193.75° Lat=-21.25°



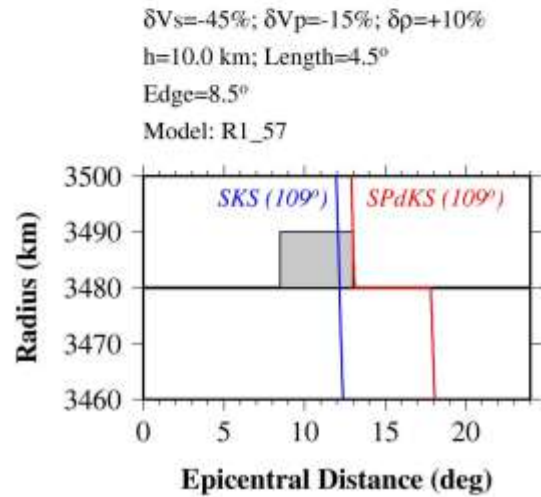
Bin: 0916
Bin Center: Lon= 198.75° Lat=-21.25°



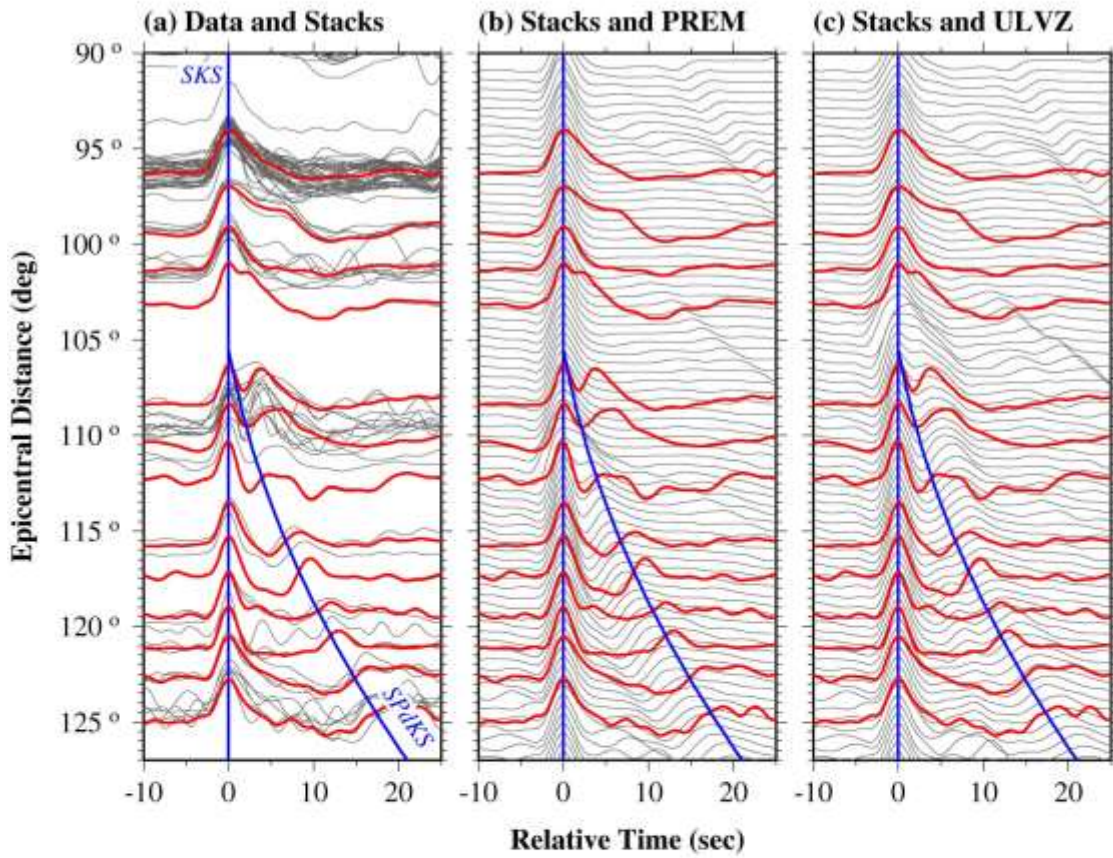
(d) Pd-Rays and Bin Location



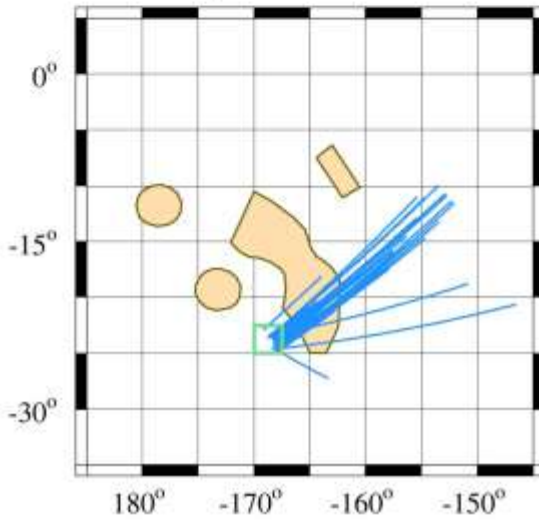
(e) ULVZ model Cross-section



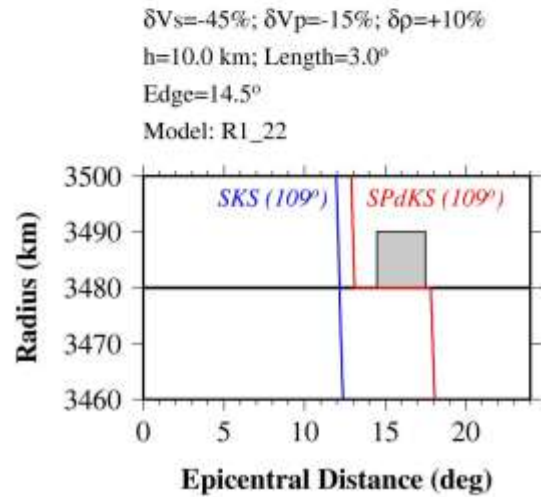
Bin: 1013
Bin Center: Lon= 191.25° Lat=-23.75°



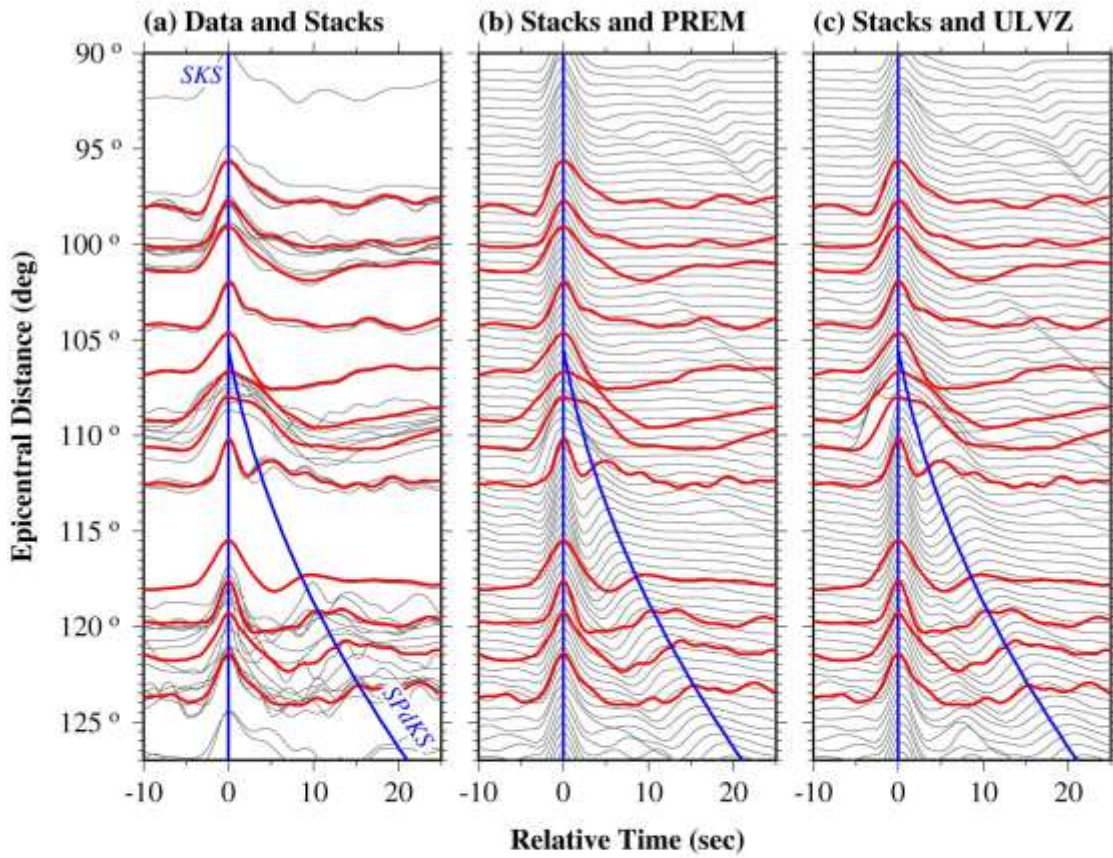
(d) Pd-Rays and Bin Location



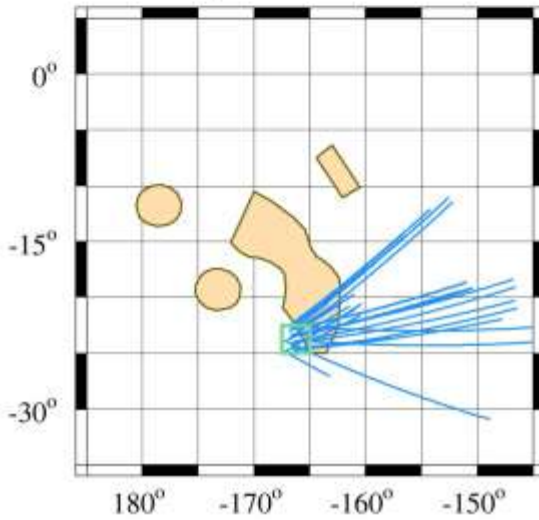
(e) ULVZ model Cross-section



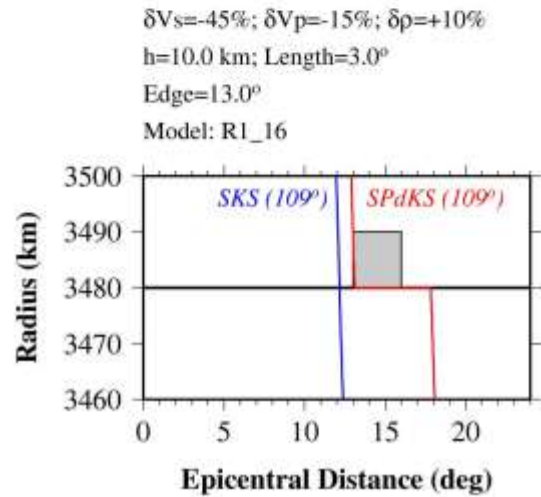
Bin: 1014
Bin Center: Lon= 193.75° Lat=-23.75°



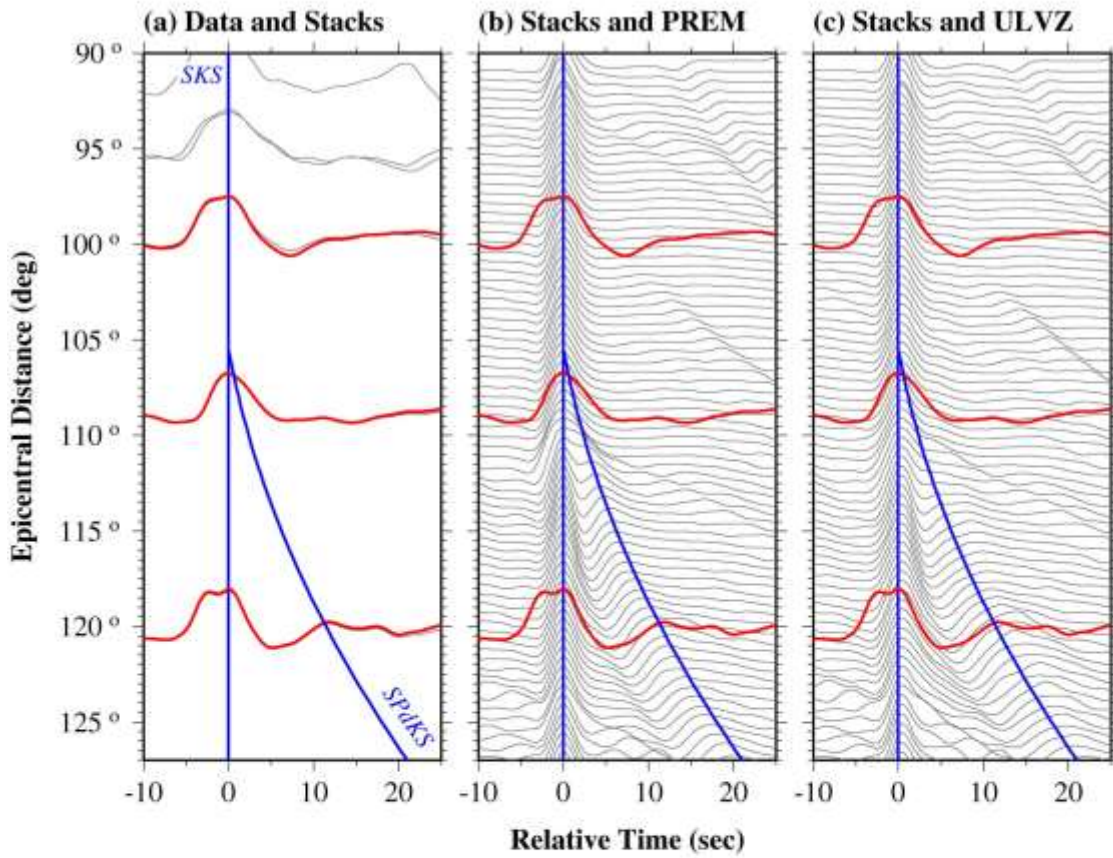
(d) Pd-Rays and Bin Location



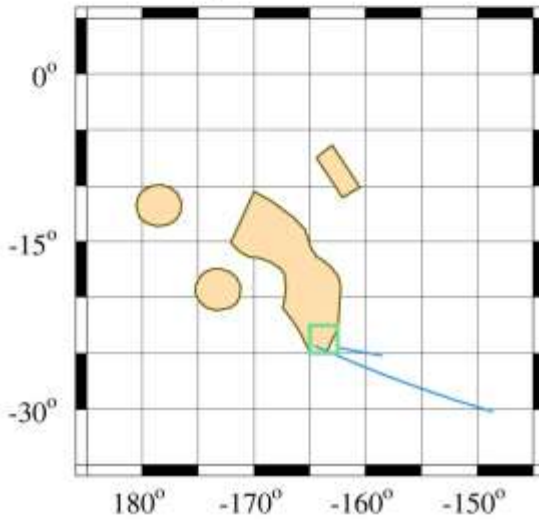
(e) ULVZ model Cross-section



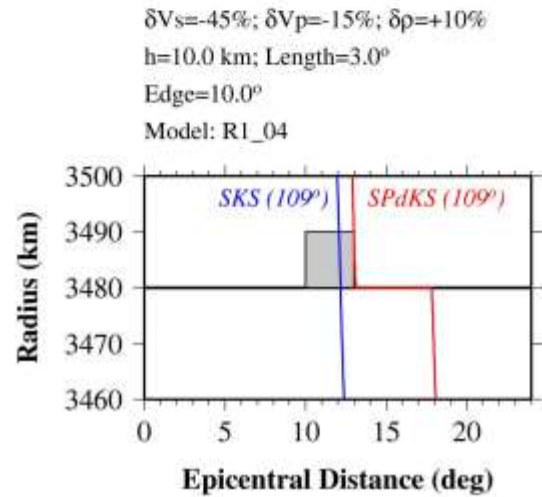
Bin: 1015
Bin Center: Lon= 196.25° Lat=-23.75°



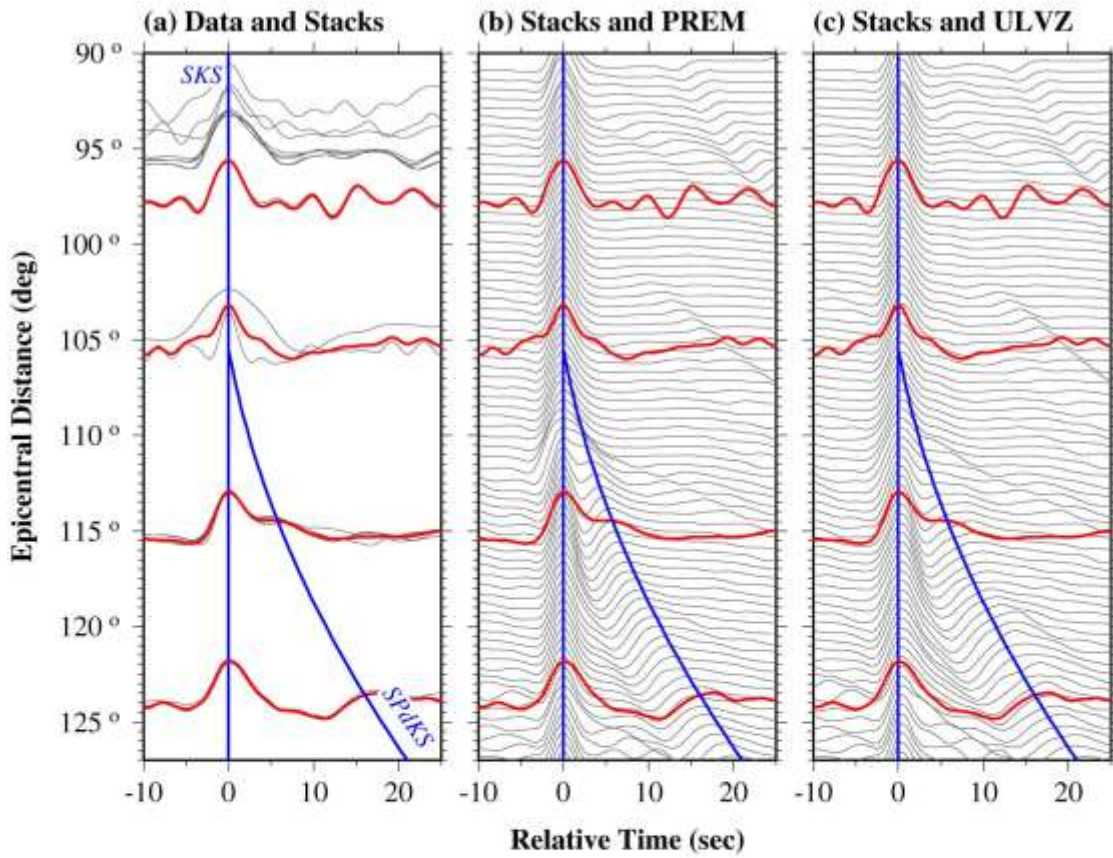
(d) Pd-Rays and Bin Location



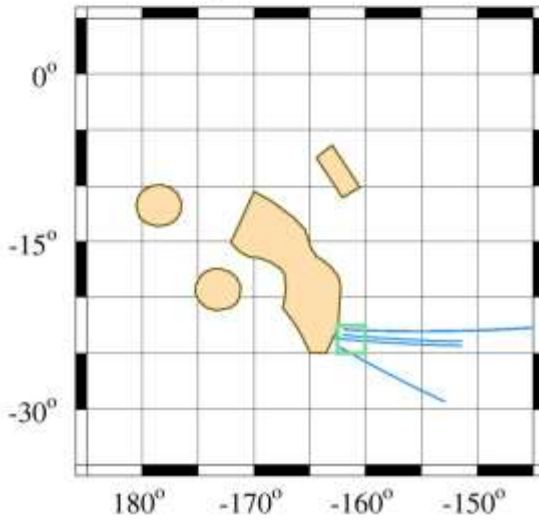
(e) ULVZ model Cross-section



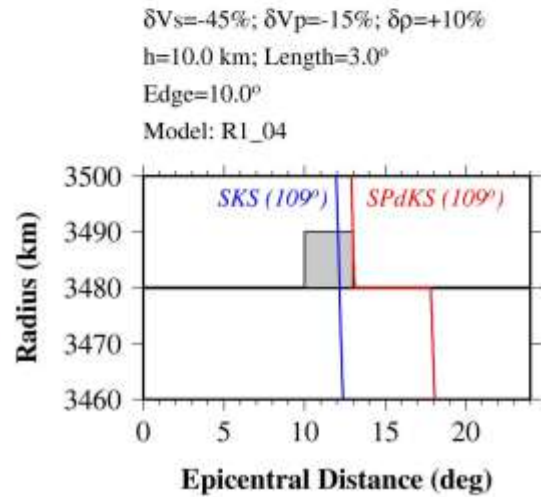
Bin: 1016
Bin Center: Lon= 198.75° Lat=-23.75°



(d) Pd-Rays and Bin Location

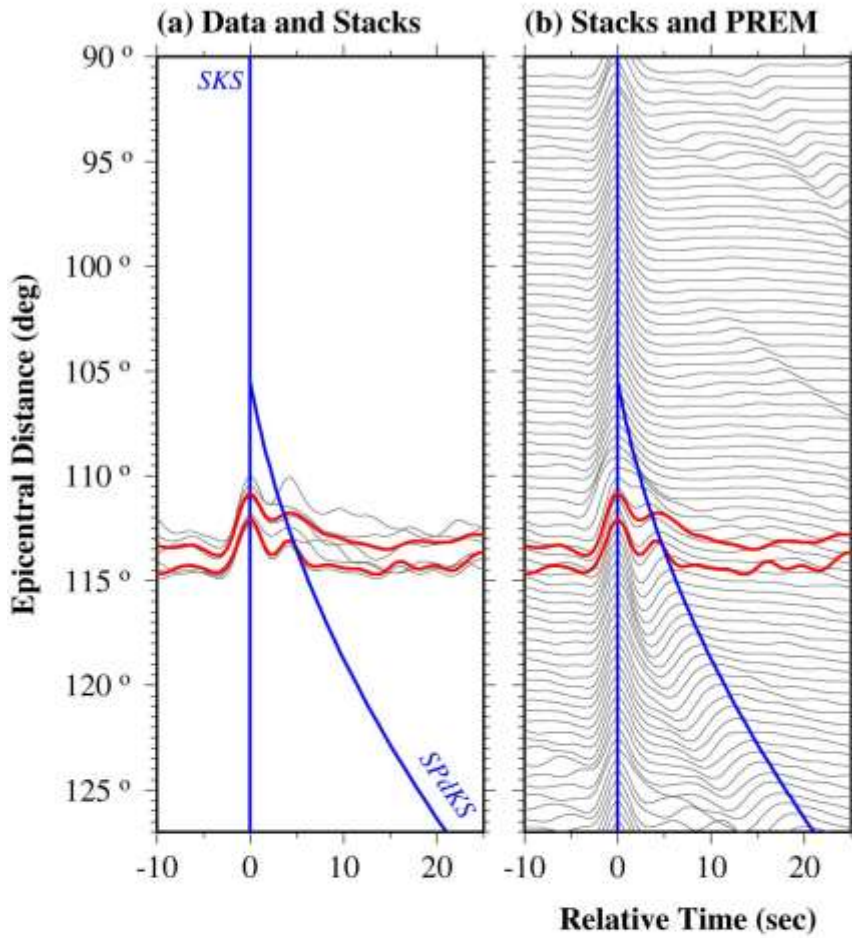


(e) ULVZ model Cross-section

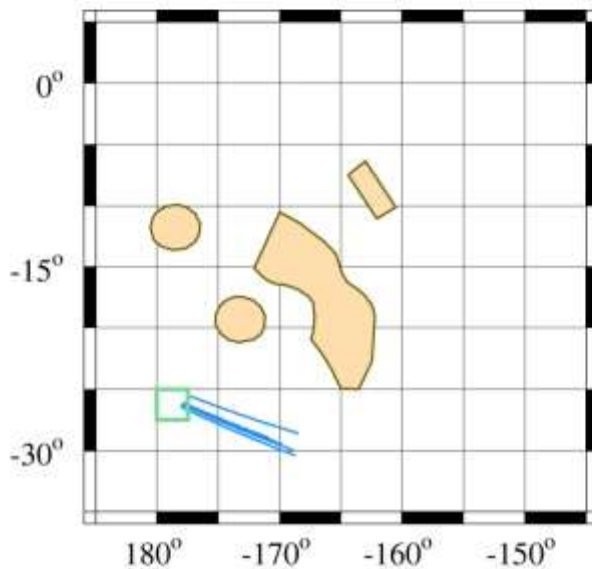


Bin: 1109

Bin Center: Lon= 181.25° Lat=-26.25°

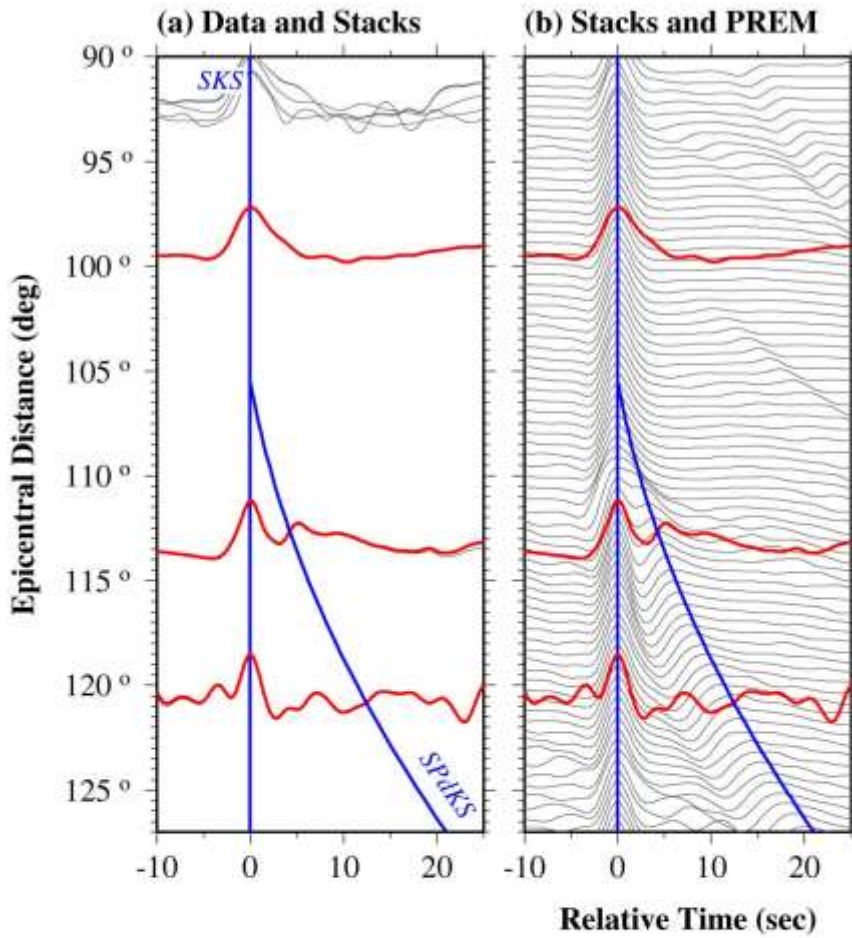


(d) Pd-Rays and Bin Location

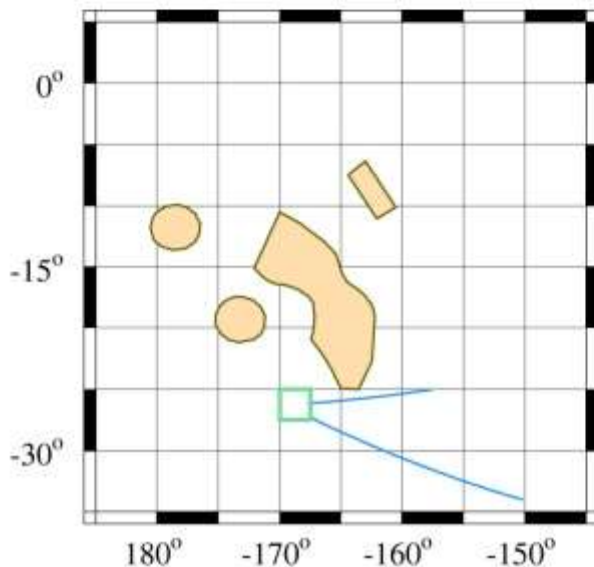


Bin: 1113

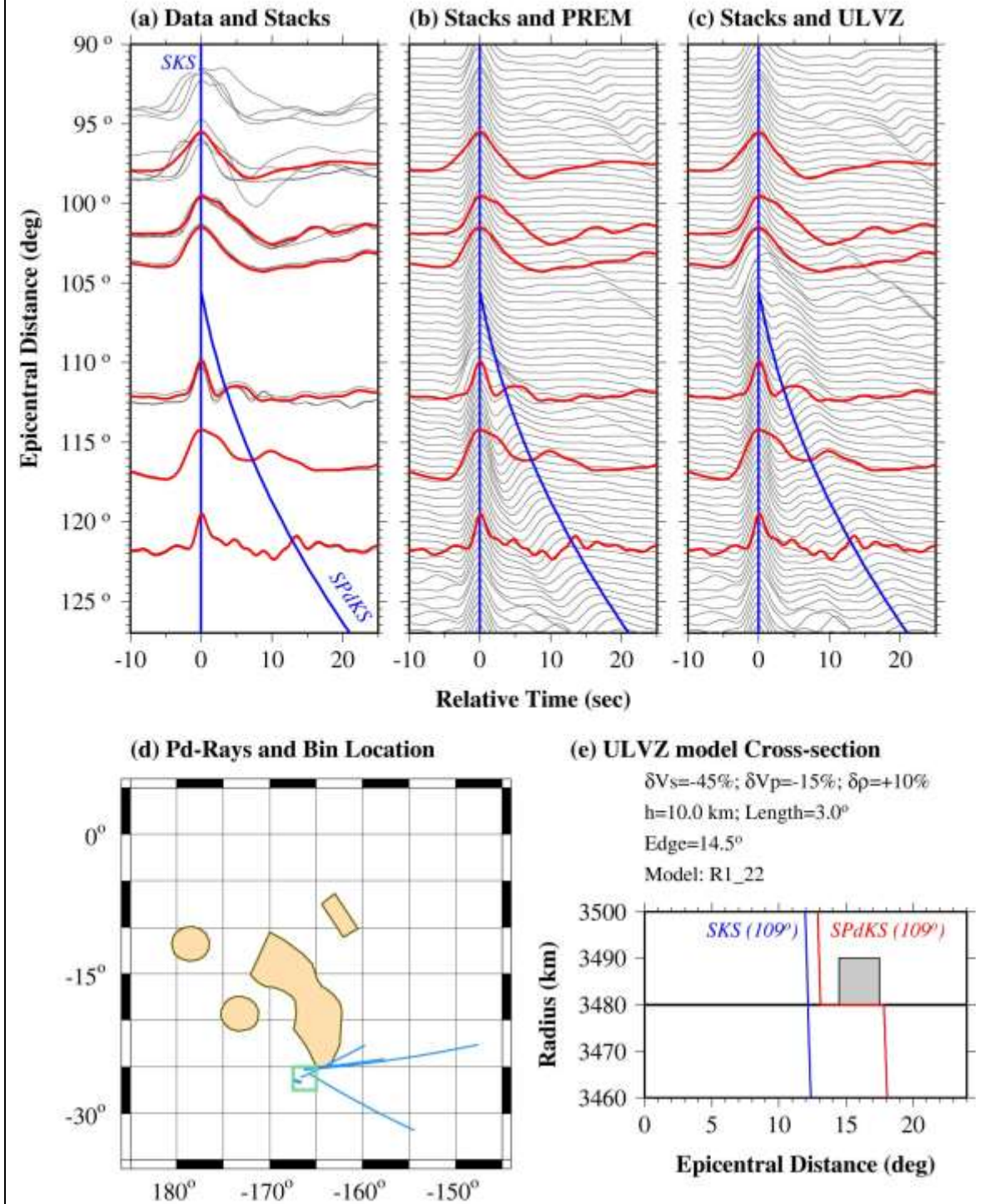
Bin Center: Lon= 191.25° Lat=-26.25°



(d) Pd-Rays and Bin Location



Bin: 1114
Bin Center: Lon= 193.75° Lat=-26.25°

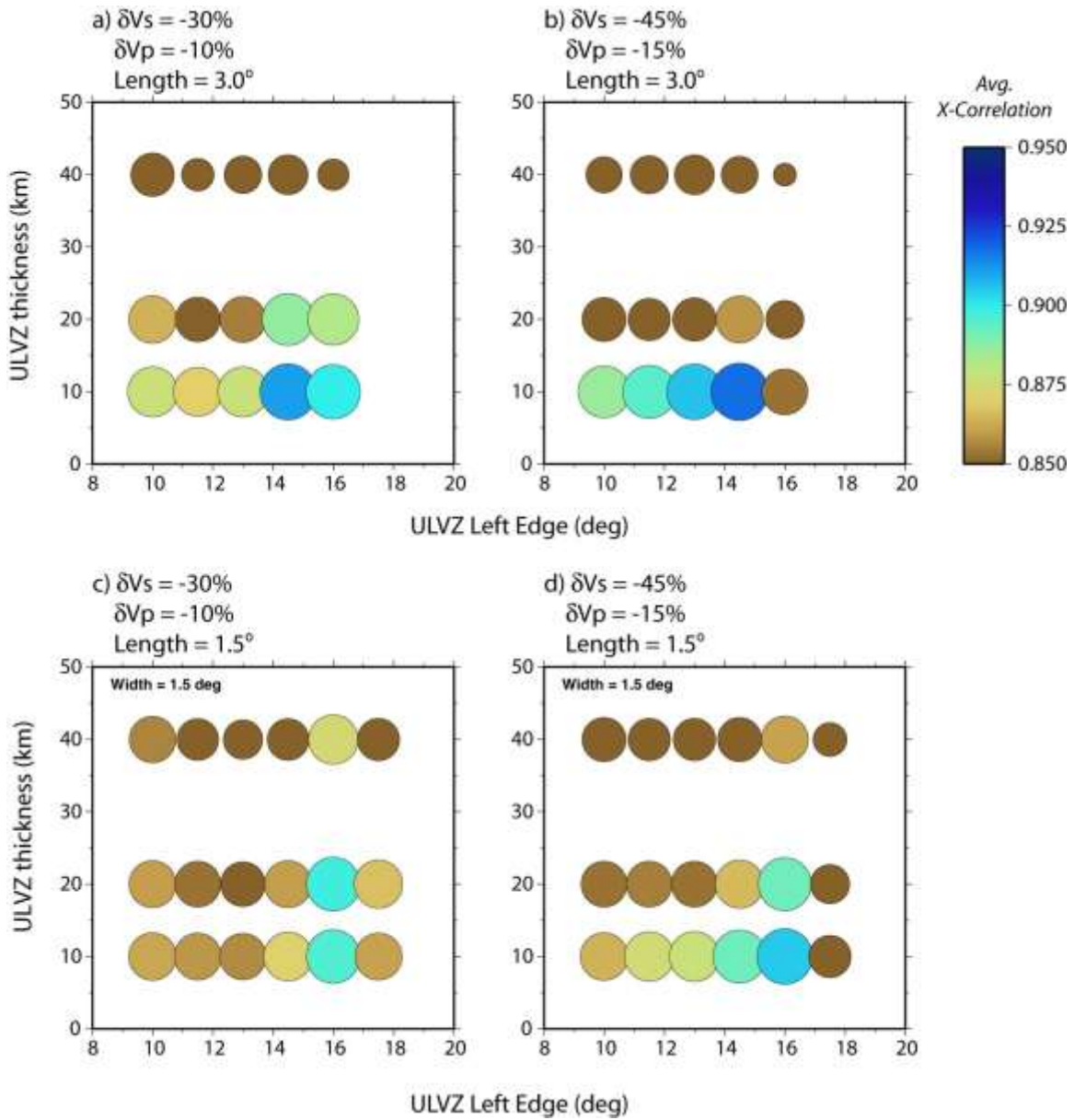


S3. Model sensitivity

Once average cross-correlations are computed for each synthetic model (for each geographic bin) we can plot the average correlations based on ULVZ parameters to determine if (a) the “answer” for best fit model actually falls within a global maximum of cross-correlations (and thus the “answer” makes sense) and (b) to get a sense of what range of model classes are also capable of explaining these data. An example is shown in the figure below. Here we look at one geographic distance bin and compare average cross-correlations for 4 groups of ULVZ models: (a) $\delta V_S = -30\%$; $\delta V_P = -10\%$; $\delta \rho = +10\%$; $length = 3.0^\circ$, (b) $\delta V_S = -45\%$; $\delta V_P = -15\%$; $\delta \rho = +10\%$; $length = 3.0^\circ$, (c) $\delta V_S = -30\%$; $\delta V_P = -10\%$; $\delta \rho = +10\%$; $length = 1.5^\circ$, (d) $\delta V_S = -45\%$; $\delta V_P = -15\%$; $\delta \rho = +10\%$; $length = 1.5^\circ$.

For the group of models examined in this example, one can see that the best-fitting model is for group b. Here the best fit model has a thickness of 10 km (with fit dramatically reduced for thicker models). One can also see how important ULVZ location is in obtaining the best fit. Notice in panel *b*, how the fit is increasingly better going from edge location = 10° to edge location = 14.5° . But going to edge location = 16° is too far, and the fit is dramatically reduced.

The figure below shows: Panels a-d show average cross-correlation results for a single geographic distance bin (Bin 0813). Each panel is with respect to a different class of ULVZ models. For example, panel (a) is for a ULVZ model with properties: $\delta V_S = -30\%$; $\delta V_P = -10\%$; $\delta \rho = +10\%$; $width = 3.0^\circ$ (models computed vary in thickness as 10, 20 or 40 km and in edge position by 10.0° , 11.5° , 13.0° , 14.5° or 16.0°). Each circle in each plot is color coded by the average cross-correlation coefficient between data in the geographic bin and the synthetic seismograms for the respective model.



S4. Comparison between PREM and ULVZ models.

The following table lists the averaged cross-correlation coefficient for the PREM model and ULVZ model shown for each data bin.

Bin Number	PREM Avg. X-Corr	ULVZ Avg. X-Corr
0409	0.910	NA
0411	0.818	NA
0412	0.887	NA
0413	0.861	NA
0414	0.873	0.871
0415	0.797	0.828
0508	0.936	NA
0509	0.843	0.893
0511	0.822	0.926
0513	0.837	0.872
0514	0.806	0.816
0609	0.808	0.807
0610	0.968	0.911
0613	0.831	0.885
0614	0.843	0.859
0615	0.823	0.823
0616	0.888	NA
0711	0.774	0.774
0712	0.856	0.909
0713	0.783	0.808
0714	0.782	0.796
0715	0.818	0.864
0716	0.912	NA
0811	0.883	0.960
0812	0.800	0.864
0813	0.821	0.919
0814	0.830	0.882
0815	0.718	0.777
0816	0.877	0.933
0911	0.763	0.906
0912	0.690	0.800
0913	0.793	0.827
0914	0.772	0.817
0916	0.916	0.930
1013	0.754	0.844
1014	0.843	0.885
1015	0.786	0.841
1016	0.808	0.826
1109	0.845	NA
1113	0.737	NA
1114	0.776	0.819

S5. Notes about the data

Bin 0409 – Not distinguishable from PREM

Bin 0411 – Not distinguishable from PREM

Bin 0412 – Not distinguishable from PREM

Bin 0413 – A couple of records are interesting; but overall not distinguishable from PREM

Bin 0414 – Data not necessarily the best ever. But, clearly not PREM. Model is consistent with Pd-inception prior to encountering ULVZ. However, is not fully constrained from these data. This bin was one of the most difficult to model. As can be seen from the table in section D3 the PREM model actually does better with the cross-correlation coefficient test than other ULVZ models. However the records at 110° would suggest a mild ULVZ is present.

Bin 0415 – Data clearly not PREM-like. Most consistent model has Pd-inception right along the leading edge of the ULVZ.

Bin 0508 – Only really long epicentral distance records in this bin. These are not distinguishable from PREM.

Bin 0509 – Records around 110° are truly remarkable. Pd-inception directly inside ULVZ. Longer distance records are potentially problematic as azimuths go in many directions.

Bin 0511 – This Bin is potentially in a very important location. However, there is only one data trace. It is impossible to tell from this trace whether or not the ULVZ extends into this space. For comparison, both PREM and ULVZ synthetics are shown in this case, but no conclusions can be drawn from this.

Bin 0513 – This bin is potentially problematic in that SPdKS could be interacting with two ULVZs. The best fit ULVZ model is shown, in which SPdKS seems to be dominantly affected by the large ULVZ. However, there is a notable gap in records around 110° which would be more enlightening.

Bin 0514 – The records here are most consistent with Pd-inception occurring prior to hitting a ULVZ. It is difficult to get those records around 110° to look the way they do without this being the case. Similarly to data in Bin 0414 the cross-correlation test suffers in this case. Note that the waveforms are very similar between Bin 0414 and Bin 0514. These data clearly indicate the presence of a ULVZ as records at 110° display a prominent SPdKS arrival which is not yet emerging in the PREM model.

Bin 0609 – Not enough data in this bin to really be confident about anything. It is included only to show that there are a couple of records here that may potentially be useful in the future.

Bin 0610 – Also not enough data in this bin to say much with confidence. Note the long epicentral distance record essentially looks like PREM.

Bin 0613 – Data consistent with Pd-inception hitting inside ULVZ.

Bin 0614 – This is one of the most difficult bins to try and match synthetics and data for. Note, there is not really a fantastic agreement for the records around 110° to 112° . This is possibly due to the SPdKS ray path interaction with multiple ULVZs. The ULVZ model shown provides the best fit of all models.

Bin 0615 – The best fit model displayed shows the ULVZ to the left of the Pd-inception points. However, the Pd-inception points appear further to the right of the preferred

ULVZ model. Note that data between 100° and 110° do not show the complexity inferred from the ULVZ model displayed. This is likely indicative of the mantle here being more PREM-like. The average correlation for the PREM model is identical to that for the ULVZ model, indicating an alternate explanation that these records may actually just fall outside of the ULVZ.

Bin 0616 – There are few data in this bin. But, those records available show a birth of SPdKS that is PREM-like.

Bin 0711 – Data are consistent with the pattern observed when Pd-inception occurs prior to the Pd path entering the ULVZ. The best-fit ULVZ model appears to overestimate the SPdKS delays and amplitude however. This may be due to either (a) a thinning of the ULVZ here (in thickness) or perhaps a slight shift in the ULVZ edge position as indicated by Pd inception point with respect to the preferred ULVZ model.

Bin 0712 – These data are highly consistent with Pd-inception right along or near the left-most edge of the ULVZ. In the ULVZ models explored in this study it is nearly impossible to generate the observed records near 108° if this is not the case.

Bin 0713 – These data support a narrower, thicker ULVZ in this region. Note the excellent agreement in waveform behavior for records at $\sim 106^\circ$.

Bin 0714 – This bin has some remarkable waveforms. These are most consistent with SPdKS directly initiating inside a ULVZ. There is one record at 106° that does not fit the mold however. With only a single record it is difficult to assess the quality of this observation. There are several records at $\sim 112^\circ$ that show three distinct arrivals. This is well fit by the ULVZ model.

Bin 0715 – There are few data in this bin. The waveform shapes are consistent with the preferred ULVZ model.

Bin 0716 - Not distinguishable from PREM.

Bin 0811 – Few data, but those that are available at $\sim 108^\circ$ are consistent with Pd-inception occurring inside a ULVZ.

Bin 0812 – One of the most intriguing bins in the data set. These waveforms are nearly impossible to explain if Pd-inception does not occur outside of the ULVZ. In support of other bins (e.g., Bins 0713, 0714, 0715) these data also suggest a relatively thick ULVZ – 15 km in this location.

Bin 0813 – Another key bin demonstrating Pd-inception prior to entering the ULVZ.

Bin 0814 – Few data, but consistent with Pd-inception inside ULVZ.

Bin 0815 – Few data. Longest distance record is most consistent with PREM. However, records at 116° show a delay with respect to the PREM model.

Bin 0816 – Few data, but data is almost identical location to Bin 0815. Exact same observations hold: longest distance record is most consistent with PREM but records at 116° show a delay with respect to the PREM model.

Bin 0911 – Only one record here, but it is notable. This record displays an uncanny similarity to the records observed in Bin 0509 and is characteristic with a direct strike on a ULVZ.

Bin 0912 – The few records in this bin around 110° are similar to those in Bin 0911 suggesting the presence of the mapped ULVZ where it is. These records may suggest the extension of this ULVZ to the southeast.

Bin 0913 – A couple very interesting records here. Clearly not PREM-like.

Bin 0914 – The data in this bin are primarily responsible for classifying the ULVZ edge here. Remarkable agreement between synths and data for distances between 105° and 112°.

Bin 0916 – Very little data to draw a conclusion from. The longest distance record appears essentially as PREM. ULVZ model is shown for reference.

Bin 1013 – This bin shows data that are incredibly distinctive of a Pd-inception occurring prior to entering the ULVZ.

Bin 1014 – Data in this bin are somewhat difficult to model exactly. Perhaps this is due to the wide variety of azimuths present. Nonetheless the model shown provides the best explanation for the distinctive Type A records near 110°.

Bin 1015 – It is unfortunate there is so little data here. Can not make any decisive conclusions about this bin.

Bin 1016 – These data are not really distinguishable from PREM. For reference sake, I include the plot of the closest ULVZ model as well.

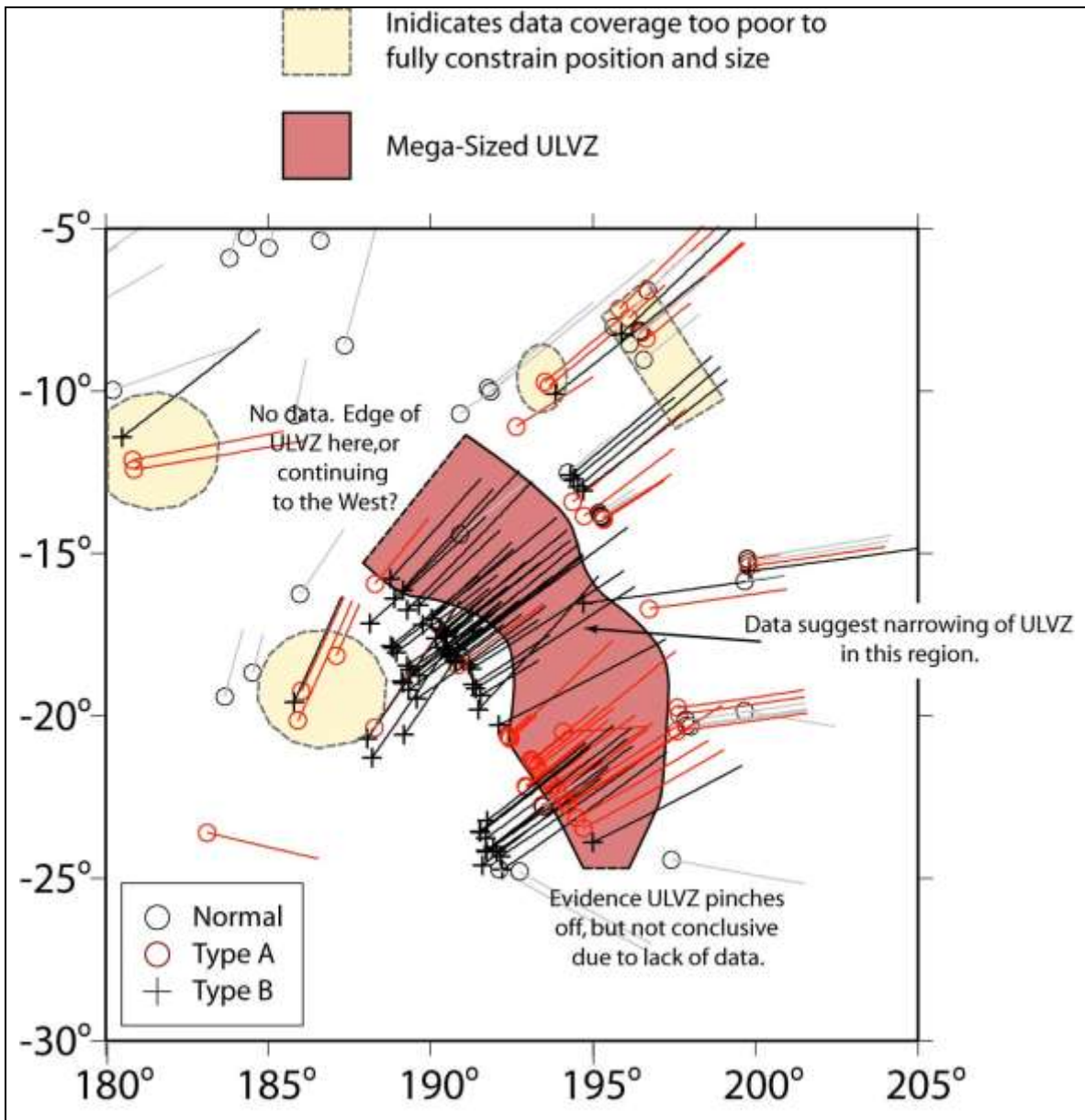
Bin 1109 – Only a couple of records here, but essentially look PREM-like.

Bin 1113 – It is a shame there are only one or two records here. The one record there is at ~114° suggests that maybe the ULVZ extends a little more to the south. But this record is not incredibly different from the PREM synths either. This bin is included primarily to show the lack of data here in the crucial area for determining the southern extent of the ULVZ.

Bin 1114 – Records near 112° suggest a deviation from the PREM model, however not quite as much as indicated by the ULVZ model. ULVZ may be pinching off here.

S6. Notes about the final ULVZ model

A detailed plot of our final ULVZ model is shown below.

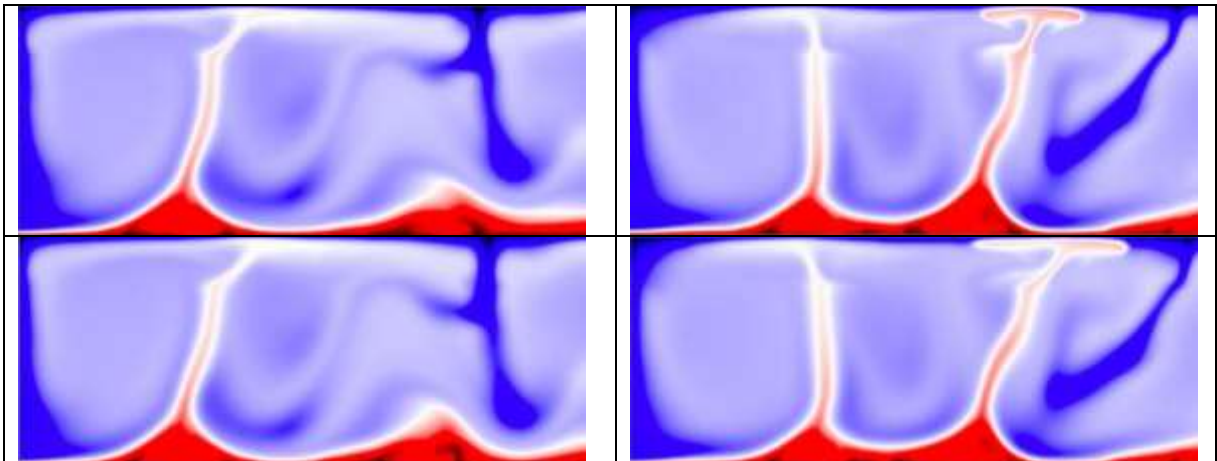


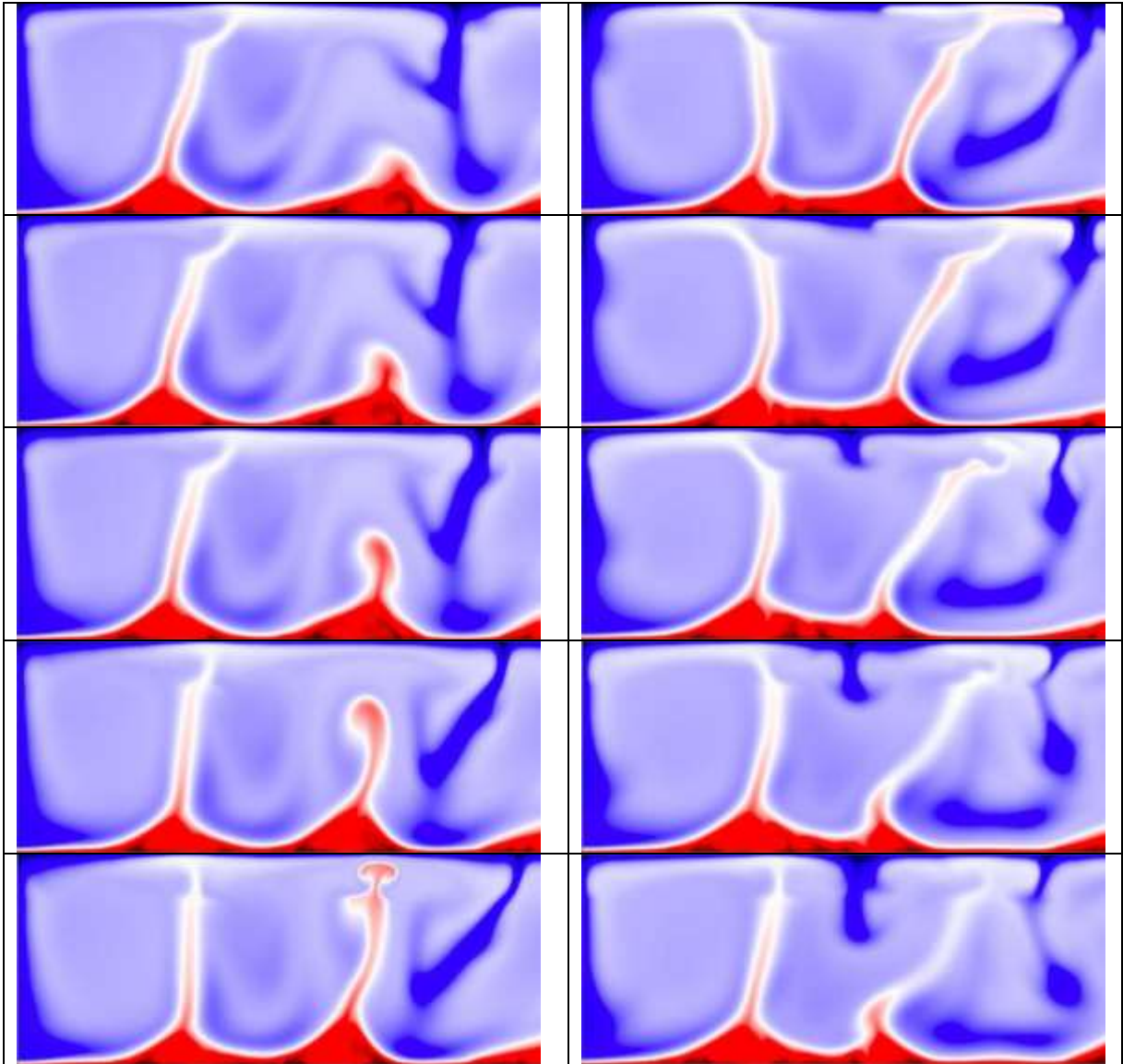
Detail on the primary ULVZ detected in this study. Pd-inception points and arcs are drawn for Normal (black circles and gray lines respectively), Type A (red circles and lines), and Type B (black crosses and lines) waveforms. The geographic extent of the Mega-Sized ULVZ is shown in dark red. Well defined boundaries are drawn with a solid black line whereas the dashed black line corresponds to boundaries that the current data distribution can not define. Yellow areas bound by dashed gray lines indicate that the data suggest the presence of a ULVZ in these areas however current data coverage is not sufficient to define the ULVZ boundaries.

Important points about the final model are:

- The large scale ULVZ imaged here is shaded in red. Key points are that the ULVZ edges on the east and west sides (lined in solid black) are well resolved. However there is not enough data to constrain the southern and northeastern boundary (dashed black line). There is some evidence this ULVZ may pinch off to the south. However, possible continuation of the ULVZ to the northwest cannot be determined due to lack of data.
- Areas outlined with dashed gray lines (filled yellow) show strong evidence for ULVZ presence. However, exact size and boundaries cannot be determined from these data.
- Type A waveforms along the NE boundary of the ULVZ (filled in red) are consistent with the model. The open red circles show the Pd-inception point based on PREM. The SKS pierce point (not shown) for those records occur in the great circle arc direction further to the southwest of the Pd-inception points. The pierce point for SPKS (also not shown), which defines the Type A records, is located in between the Pd-inception point and the SKS pierce point and is inside the ULVZ as drawn.
- There are two records showing Type A behavior at approximately -15° latitude and 200° longitude, and a single Type B record in this location as well. But, there are also 4 Normal waveforms here as well. It is possible that there is a smallish patch of ULVZ material there (possibly due west from the Type A points). But, the overall solution from our modeling indicated this location behaved most closely to PREM. The solution is dominated by the 4 records that appeared Normal.

S7. Convection calculations





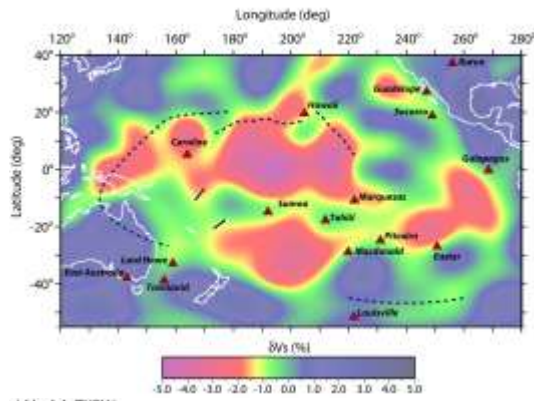
Snapshots from geodynamic calculations. Progressive time steps are drawn starting from the upper left corner and progressing down the first column and then going down the second column. Color represents blue: background mantle, red: compositional reservoirs, and black: ULVZ material. Shown is the merger of two compositional reservoirs giving rise to a large-scale ULVZ in the center of the merged reservoir. This figure shows results of geodynamic simulations with three distinct provinces: (1) background mantle, (2) compositional reservoirs, and (3) dense ULVZ material (McNamara et al., 2010).

S8. S-wave tomography models

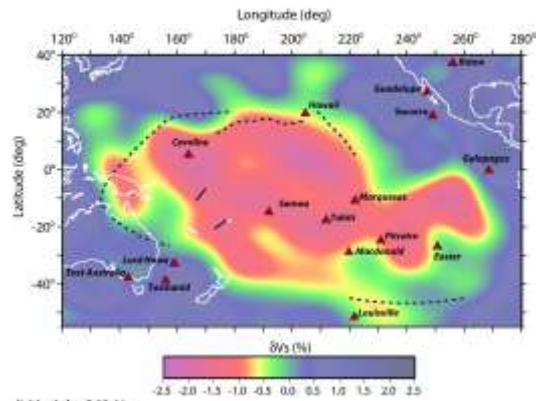
Figure S15 displays a collection of *S*-wave tomography models. Note that many of these models (panels *a*, *b*, *c*, *e*, and *g*) suggest *S*-wave velocities near the Samoa hot spot (and thus the mega-sized ULVZ) that are consistent with the hot spot lying near an interior boundary of the LLSVP. Although, not all models are consistent with this picture (panels

d and f), a mean of *S*-wave models (Becker and Boschi, 2002) is suggestive of a hole in the middle of the LLSVP (panel g).

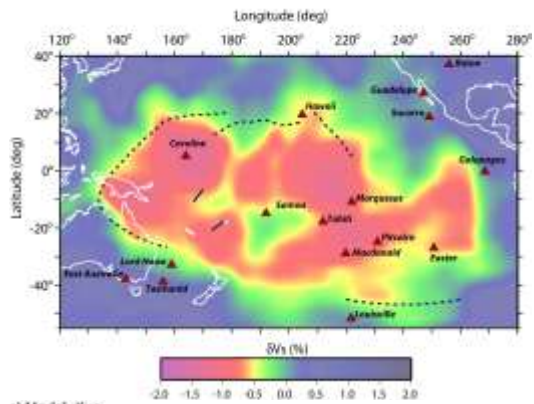
a) Model: saw24b16



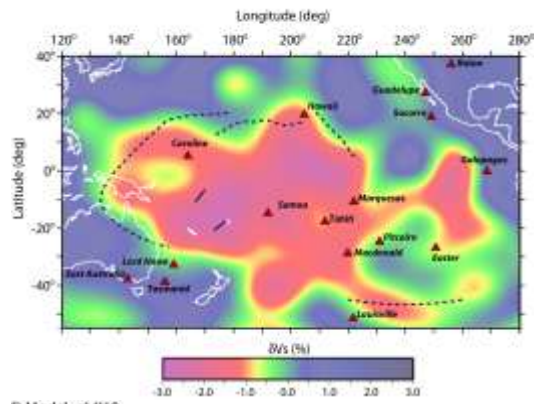
b) Model: s20rts



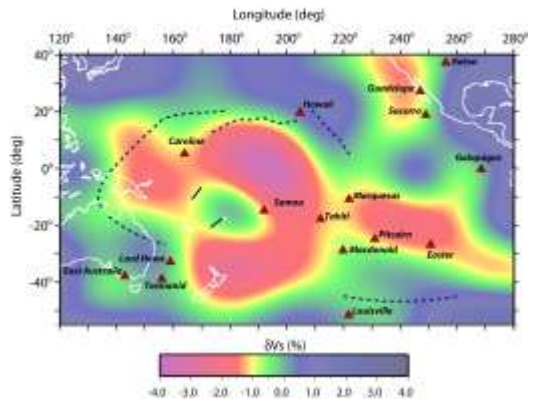
c) Model: TXBW



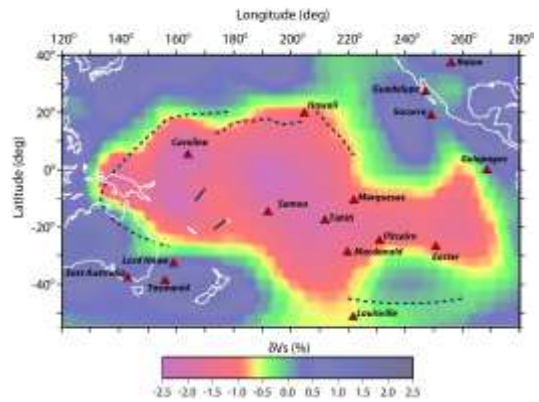
d) Model: s362d1

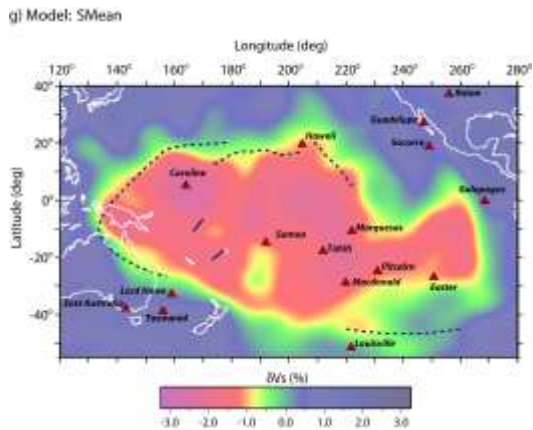


e) Model: Kuo



f) Model: s14118





S-wave tomography models. Models are: (a) saw24b16 (Méglin and Romanowicz, 2000), (b) s20rts (Ritsema and van Heijst, 2000), (c) TXBW (Grand, 2002), (d) s362d1 (Gu et al., 2001), (e) Kuo (Kuo et al., 2000), (f) s14118 (Masters et al., 2000), and (g) SMean (Becker and Boschi, 2002). Red triangles show hot spot surface locations (Steinberger, 2000).

S9. References

- Becker, T.W., Boschi, L., 2002. A comparison of tomographic and geodynamic mantle models. *Geochemistry Geophysics Geosystems* 3. doi:10.129/2001GC000168.
- Grand, S.P., 2002. Mantle shear-wave tomography and the fate of subducted slabs. *Philosophical Transactions of the Royal Society London A* 360, 2475-2491. doi:10.1098/rsta.2002.1077.
- Gu, Y.J., Dziewonski, A.M., Su, W., Ekström, G., 2001. Models of the mantle shear velocity and discontinuities in the pattern of lateral heterogeneities. *Journal of Geophysical Research* 106, 11169-111,199.
- Kuo, B.-Y., Garnero, E.J., Lay, T., 2000. Tomographic inversion of S-SKS times for shear velocity heterogeneity in D^{''}: Degree 12 and hybrid models. *Journal of Geophysical Research* 105, 28,139-128,157.
- Masters, G., Laske, G., Bolton, H., Dziewonski, A.M., 2000. The relative behavior of shear velocity, bulk sound speed, and compressional velocity in the mantle: implications for chemical and thermal structure, *Earth's Deep Interior: Mineral Physics and Tomography From the Atomic to the Global Scale*. American Geophysical Union, Washington, D. C., pp. 63-87.
- McNamara, A.K., Garnero, E.J., Rost, S., 2010. Tracking deep mantle reservoirs with ultra-low velocity zones. *Earth and Planetary Science Letters* 299, 1-9. doi:10.1016/j.epsl.2010.07.042.
- Méglin, C., Romanowicz, B., 2000. The three-dimensional shear velocity structure of the mantle from the inversion of body, surface and higher-mode waveforms. *Geophysical Journal International* 143, 709-728.
- Ritsema, J., van Heijst, H.-J., 2000. Seismic imaging of structural heterogeneity in Earth's mantle: Evidence for large-scale mantle flow. *Science Progress* 83, 243-259.
- Steinberger, B., 2000. Plumes in a convecting mantle: Models and observations for individual hotspots. *Journal of Geophysical Research* 105, 11,127-111,152.